Survey of Constraints on the Proton Finite Size

— Zemach Radius from (Muonic) Hydrogen —

Franziska Hagelstein (JGU Mainz & PSI Villigen)

in collaboration with

V. Lensky, V. Pascalutsa (JGU) and V. Sharkovska (PSI, UZH)

WHY MUONIC ATOMS?

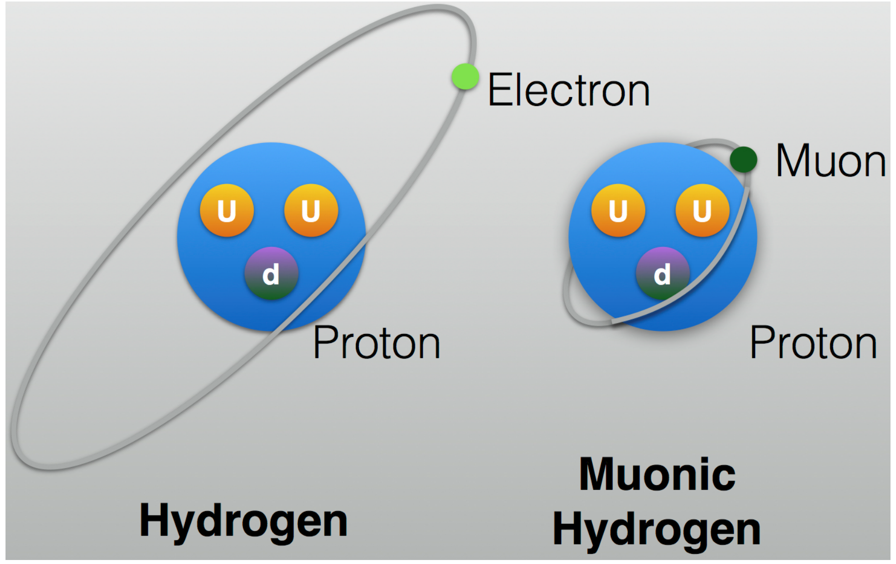

WHY MUONIC ATOMS?

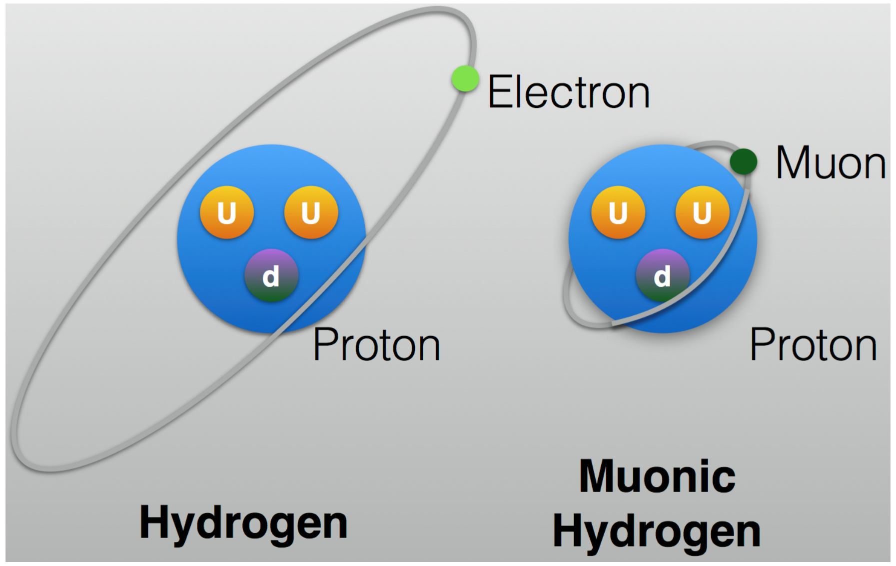

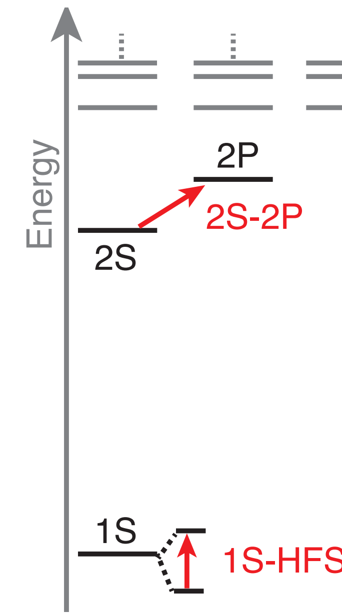

Lamb shift
μH, μD, μ^3He$^+$, μ^4He$^+$
⇒ Charge radii

Hyperfine splitting (HFS)
μH, μ^3He$^+$
⇒ Zemach radii, magnetic properties

- **Lamb shift:**

$\boxed{\text{wave function at the origin}}$

$$\Delta E_{nl}(\mathrm{LO{+}NLO}) = \delta_{l0}\,\frac{2\pi Z\alpha}{3}\,\frac{1}{\pi(an)^3}\left[R_E^2 - \frac{Z\alpha m_r}{2}R^3_{E(2)}\right]$$

- **HFS:**

$$\Delta E_{nS}(\mathrm{LO}+\mathrm{NLO}) = E_F(nS)\,[1 - 2\,Z\alpha m_r\,R_Z]$$

Fermi - Energy:

$$E_F(nS) = \frac{8}{3}\frac{Z\alpha}{a^3}\frac{1+\kappa}{mM}\frac{1}{n^3}$$

with Bohr radius $a = 1/(Z\alpha m_r)$

WHY MUONIC ATOMS?

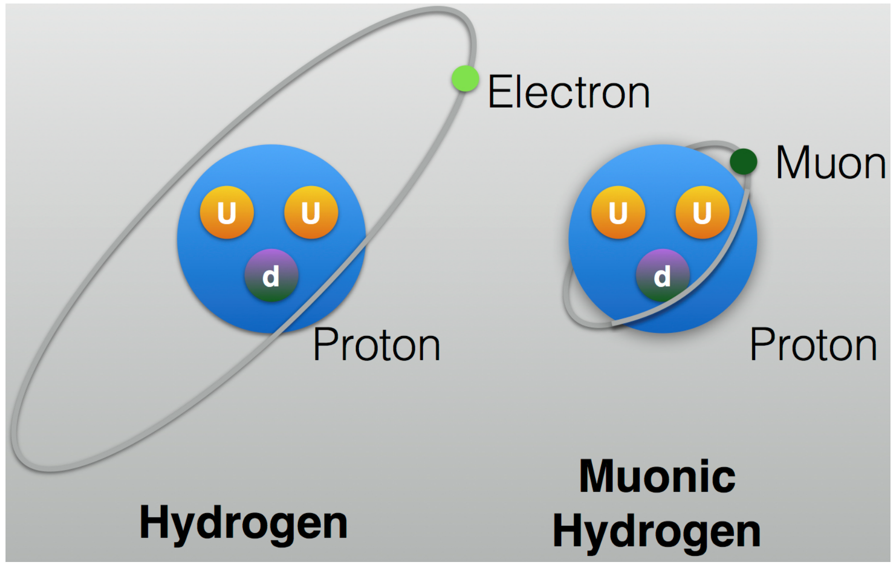

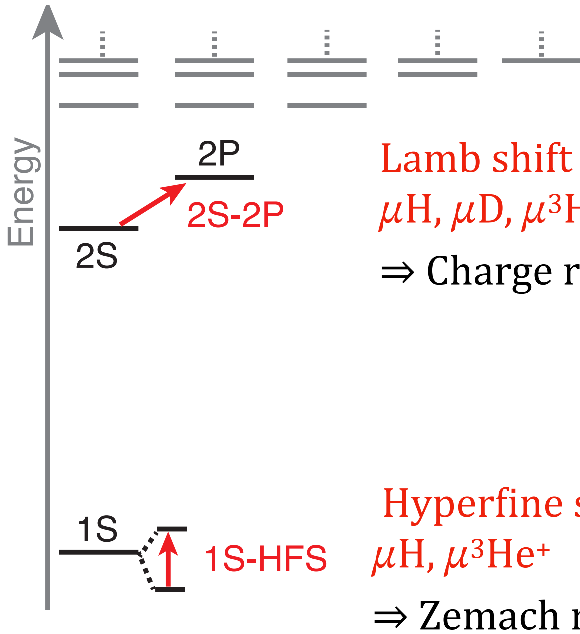

Lamb shift
μH, μD, μ^3He$^+$, μ^4He$^+$
⇒ Charge radii

Hyperfine splitting (HFS)
μH, μ^3He$^+$
⇒ Zemach radii, magnetic properties

- **Lamb shift:**

wave function at the origin

charge radius

Friar radius or 3rd Zemach moment

$$\Delta E_{nl}(\text{LO+NLO}) = \delta_{l0}\,\frac{2\pi Z\alpha}{3}\,\frac{1}{\pi(an)^3}\left[R_E^2 - \frac{Z\alpha m_r}{2}R^3_{E(2)}\right]$$

- **HFS:**

$$\Delta E_{nS}(\text{LO}+\text{NLO}) = E_F(nS)\,[1-2\,Z\alpha m_r\,R_Z]$$

Zemach radius

Fermi - Energy:

$$E_F(nS) = \frac{8}{3}\frac{Z\alpha}{a^3}\frac{1+\kappa}{mM}\frac{1}{n^3}$$

with Bohr radius $a = 1/(Z\alpha m_r)$

WHY MUONIC ATOMS?

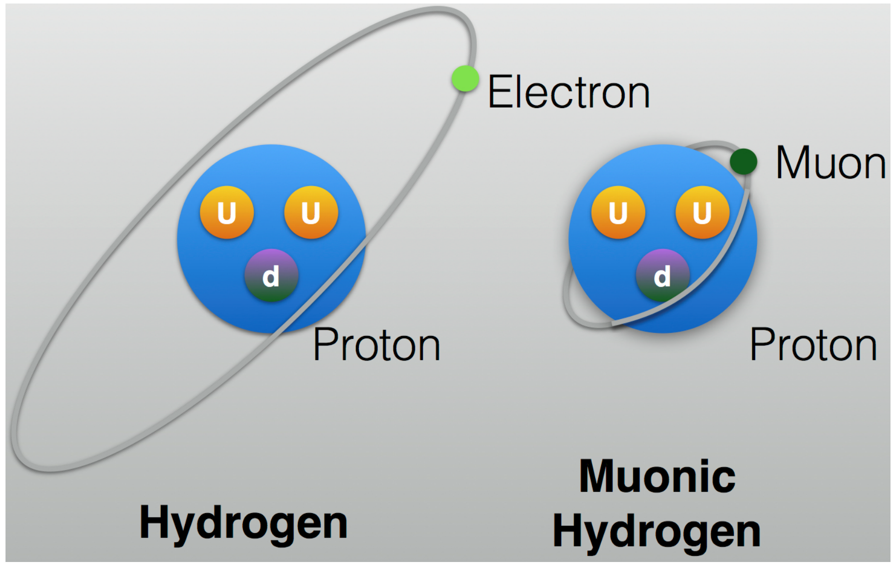

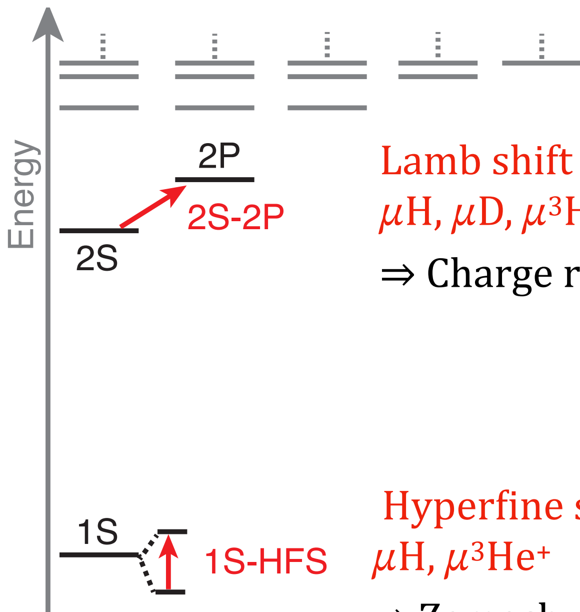

Lamb shift
μH, μD, μ^3He⁺, μ^4He⁺
⇒ Charge radii

Hyperfine splitting (HFS)
μH, μ^3He⁺
⇒ Zemach radii, magnetic properties

- **Lamb shift:**

wave function at the origin

charge radius

Friar radius or 3rd Zemach moment

$$\Delta E_{nl}(\text{LO+NLO}) = \delta_{l0}\,\frac{2\pi Z\alpha}{3}\,\frac{1}{\pi(an)^3}\left[R_E^2 - \frac{Z\alpha m_r}{2} R^3_{E(2)}\right]$$

NLO becomes appreciable in μH

- **HFS:**

$$\Delta E_{nS}(\text{LO}+\text{NLO}) = E_F(nS)\,[1 - 2\,Z\alpha m_r\,R_Z]$$

Zemach radius

Fermi - Energy:

$$E_F(nS) = \frac{8}{3}\frac{Z\alpha}{a^3}\frac{1+\kappa}{mM}\frac{1}{n^3}$$

with Bohr radius $a = 1/(Z\alpha m_r)$

— Proton Charge Radius —

STATUS PROTON CHARGE RADIUS

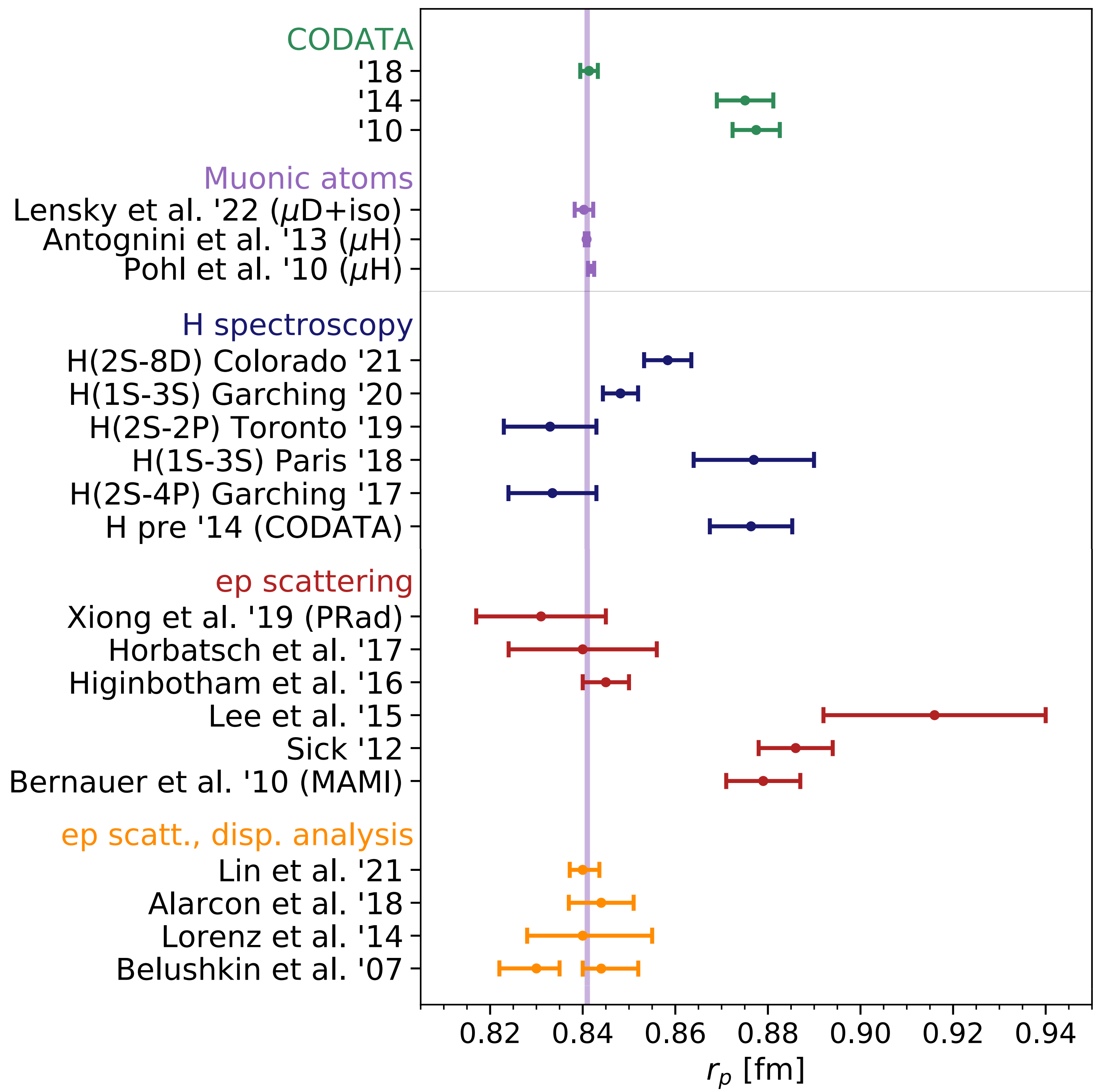

- Complementary experimental approaches:

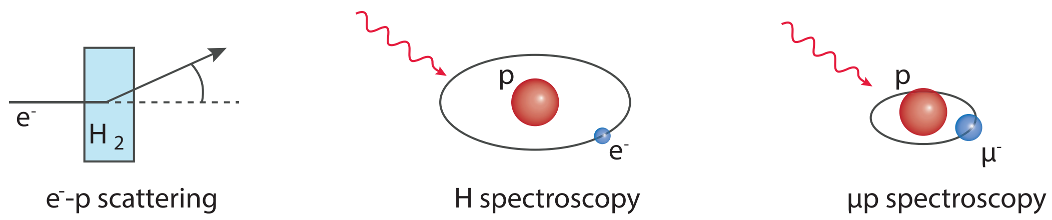

STATUS PROTON CHARGE RADIUS

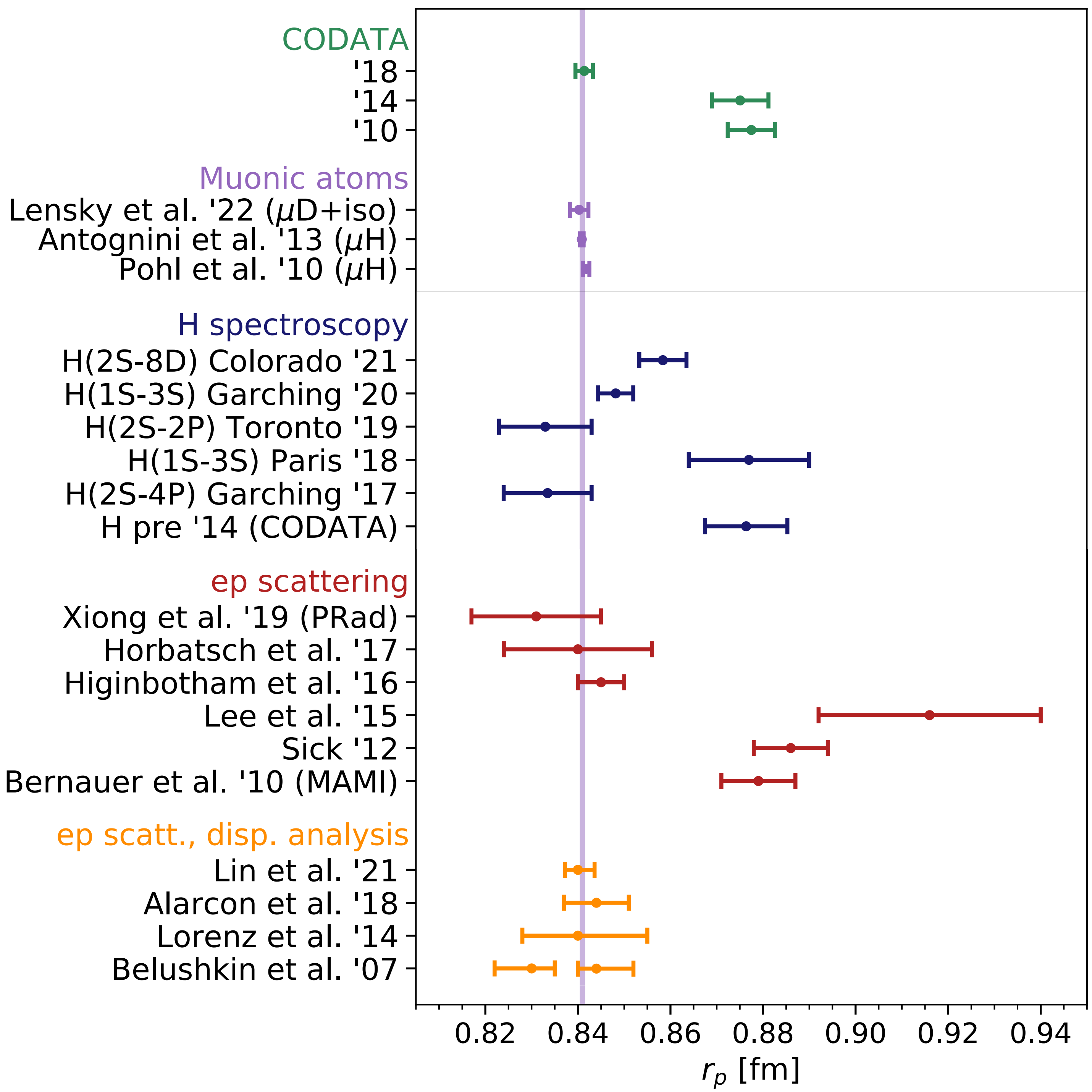

- Complementary experimental approaches:

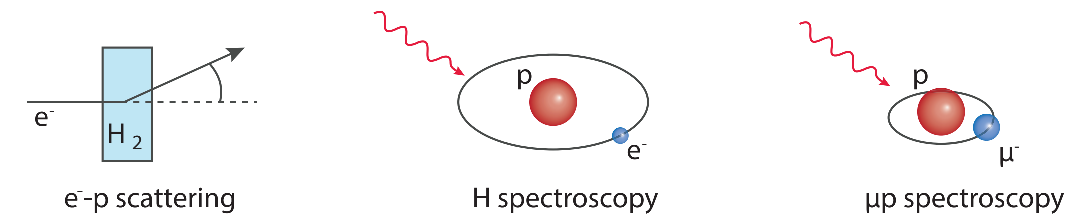

- Muonic atoms allow for PRECISE extractions of nuclear charge radii
- CODATA since 2018 included the μH result for r_p

STATUS PROTON CHARGE RADIUS

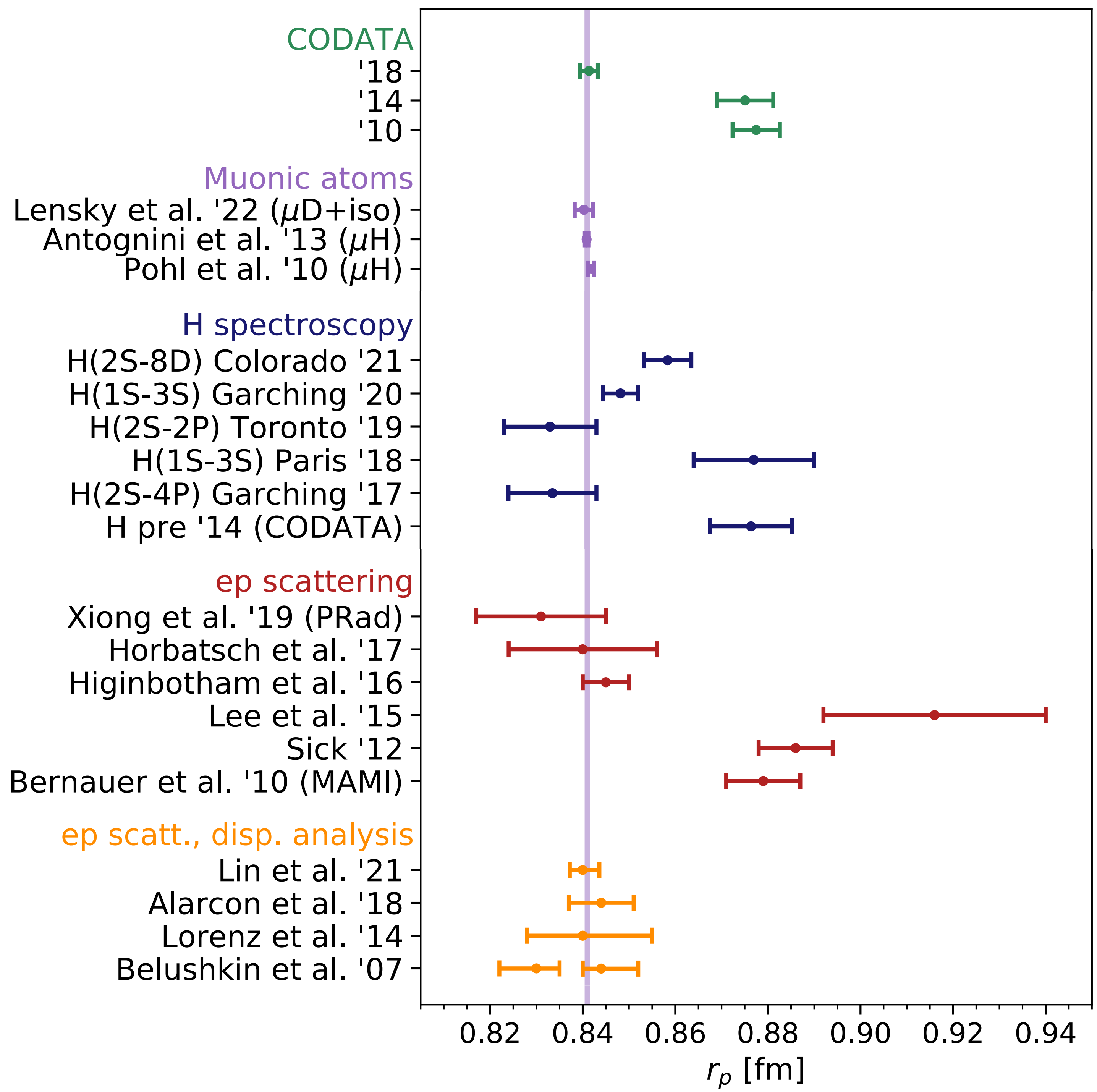

- Complementary experimental approaches:

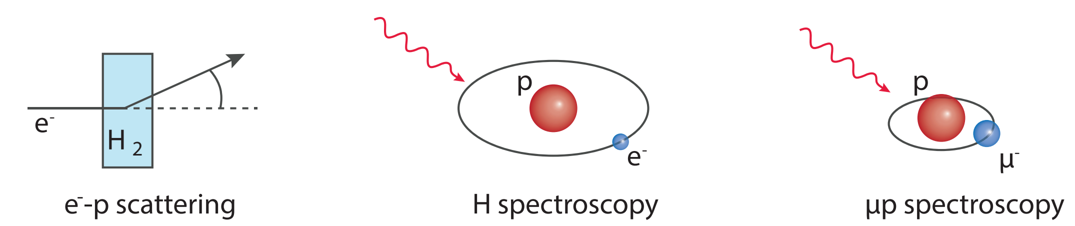

- Muonic atoms allow for PRECISE extractions of nuclear charge radii
- CODATA since 2018 included the μH result for r_p
- Still open issues: H(2S-8D), H(1S-3S) @ Paris
- Important question:

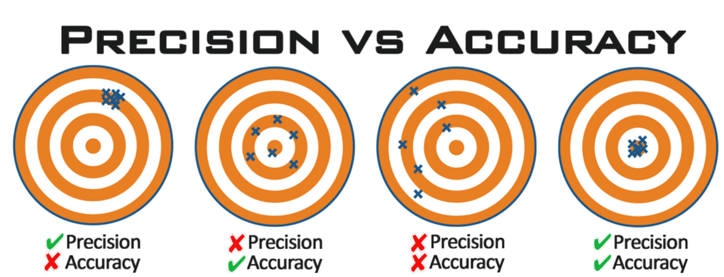

STATUS PROTON CHARGE RADIUS

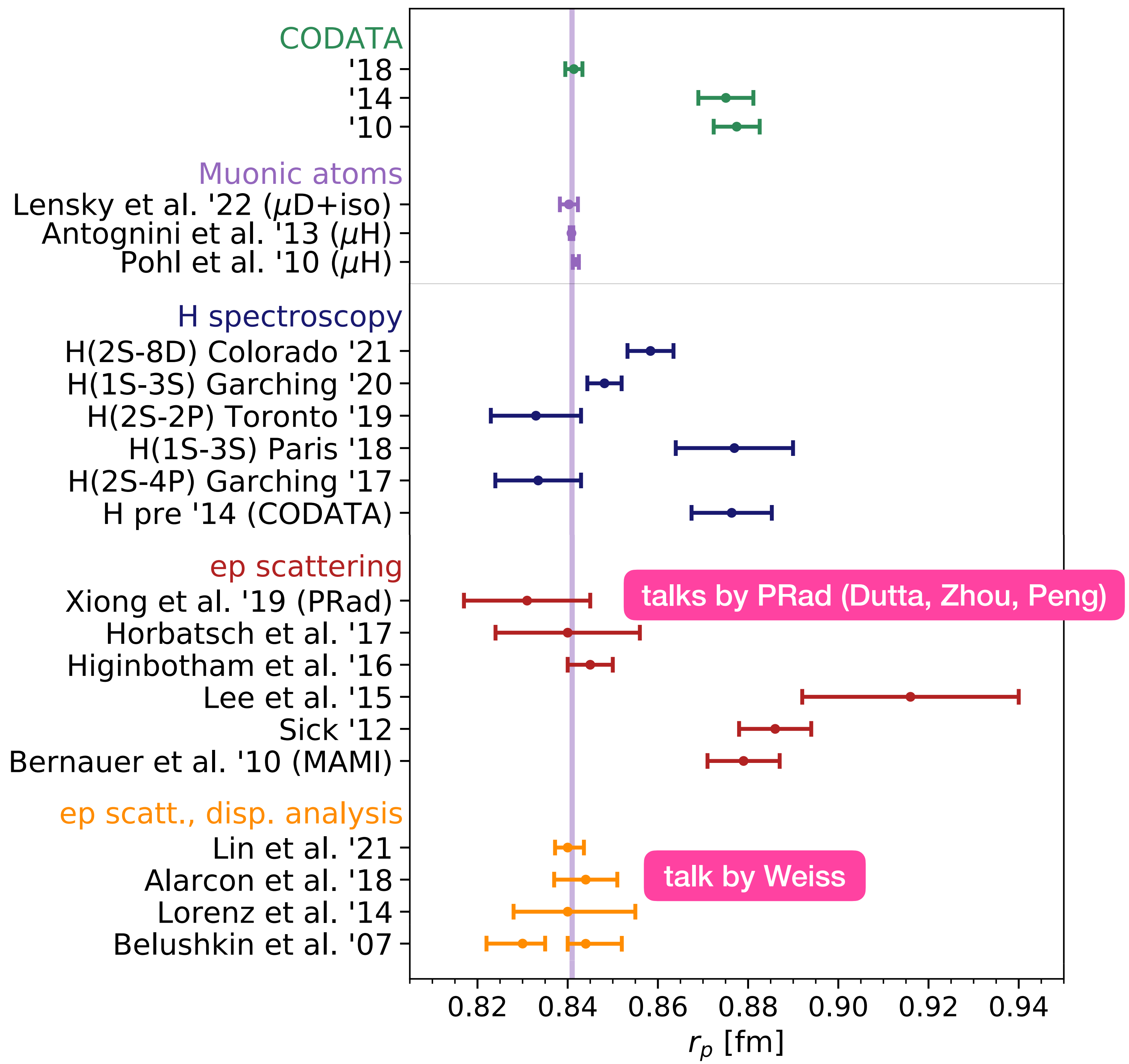

- Complementary experimental approaches:

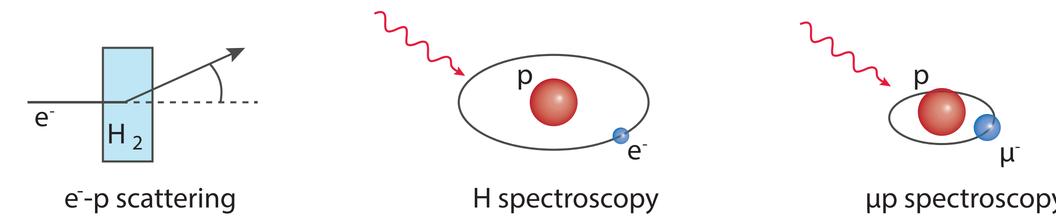

- Muonic atoms allow for PRECISE extractions of nuclear charge radii
- CODATA since 2018 included the μH result for r_p
- Still open issues: H(2S-8D), H(1S-3S) @ Paris
- Important question:

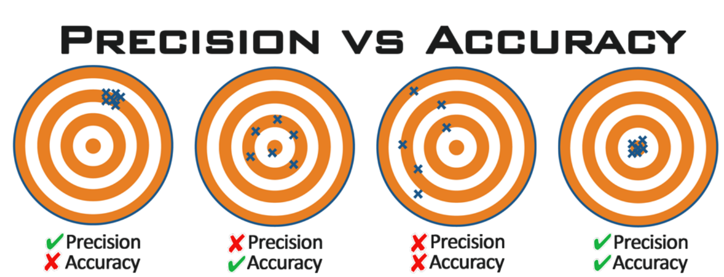

ELECTRIC SACHS FORM FACTOR

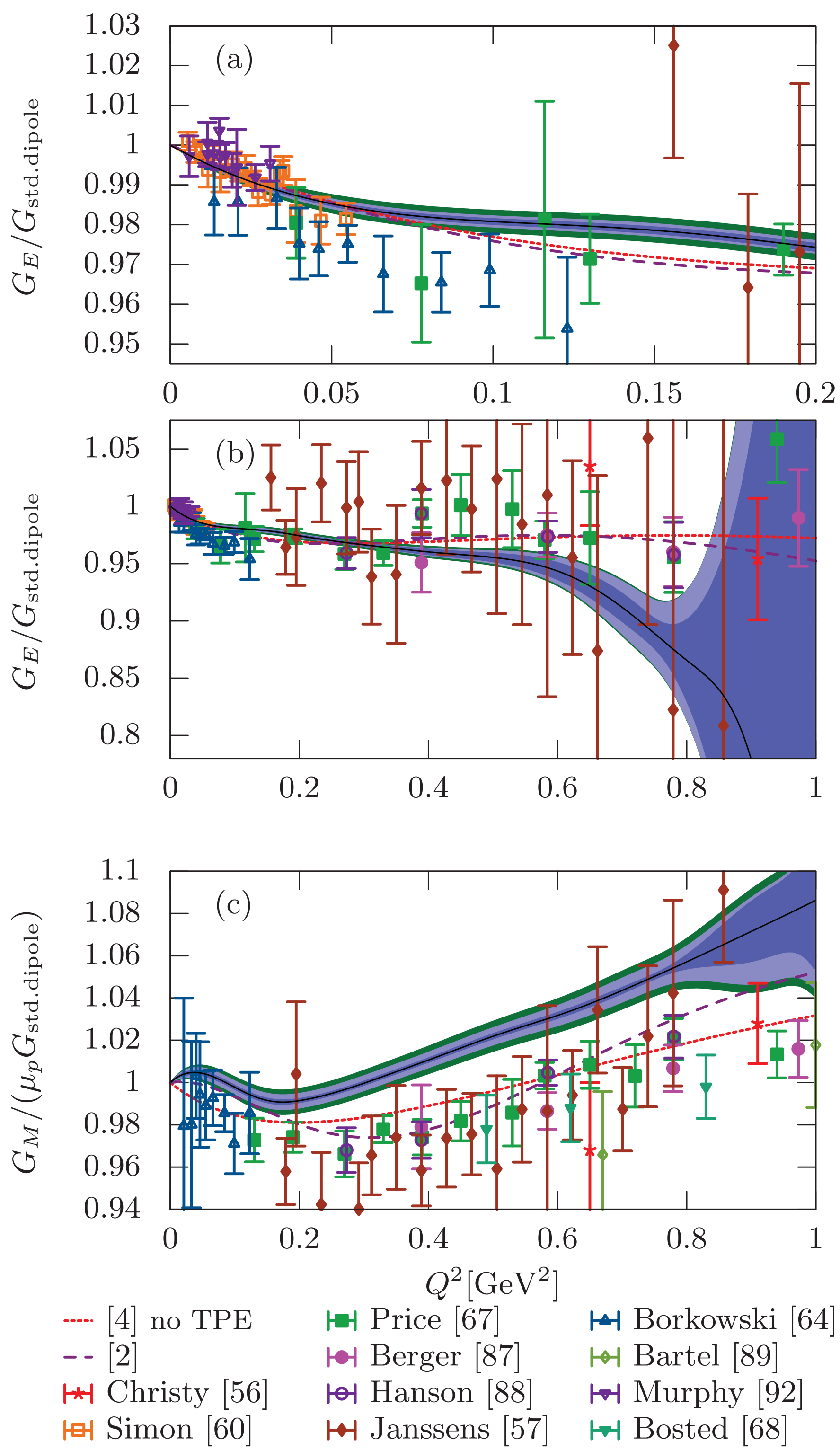

J. C. Bernauer *et al.*, Phys. Rev. C **90**, 015206 (2014) talk by Schlimme

- Measured in lepton-proton scattering

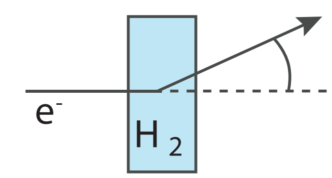

e^--p scattering

- Form factors (FF): Fourier transforms of charge and magnetization distributions

$$\rho(r) = \int \frac{\mathrm{d}\boldsymbol{q}}{(2\pi)^3} G(\boldsymbol{q}^2) e^{-i\boldsymbol{q}\boldsymbol{r}}$$

- Root-mean-square (rms) charge radius:

$$R_E = \sqrt{\langle r^2 \rangle_E}$$

$$\langle r^2 \rangle_E \equiv \int \mathrm{d}\boldsymbol{r}\, r^2 \rho_E(\boldsymbol{r}) = -6 \frac{\mathrm{d}}{\mathrm{d}Q^2} G_E(Q^2)\Big|_{Q^2=0}$$

talk by Pascalutsa

SYSTEMATICS OF THE CHARGE RADIUS EXTRACTION

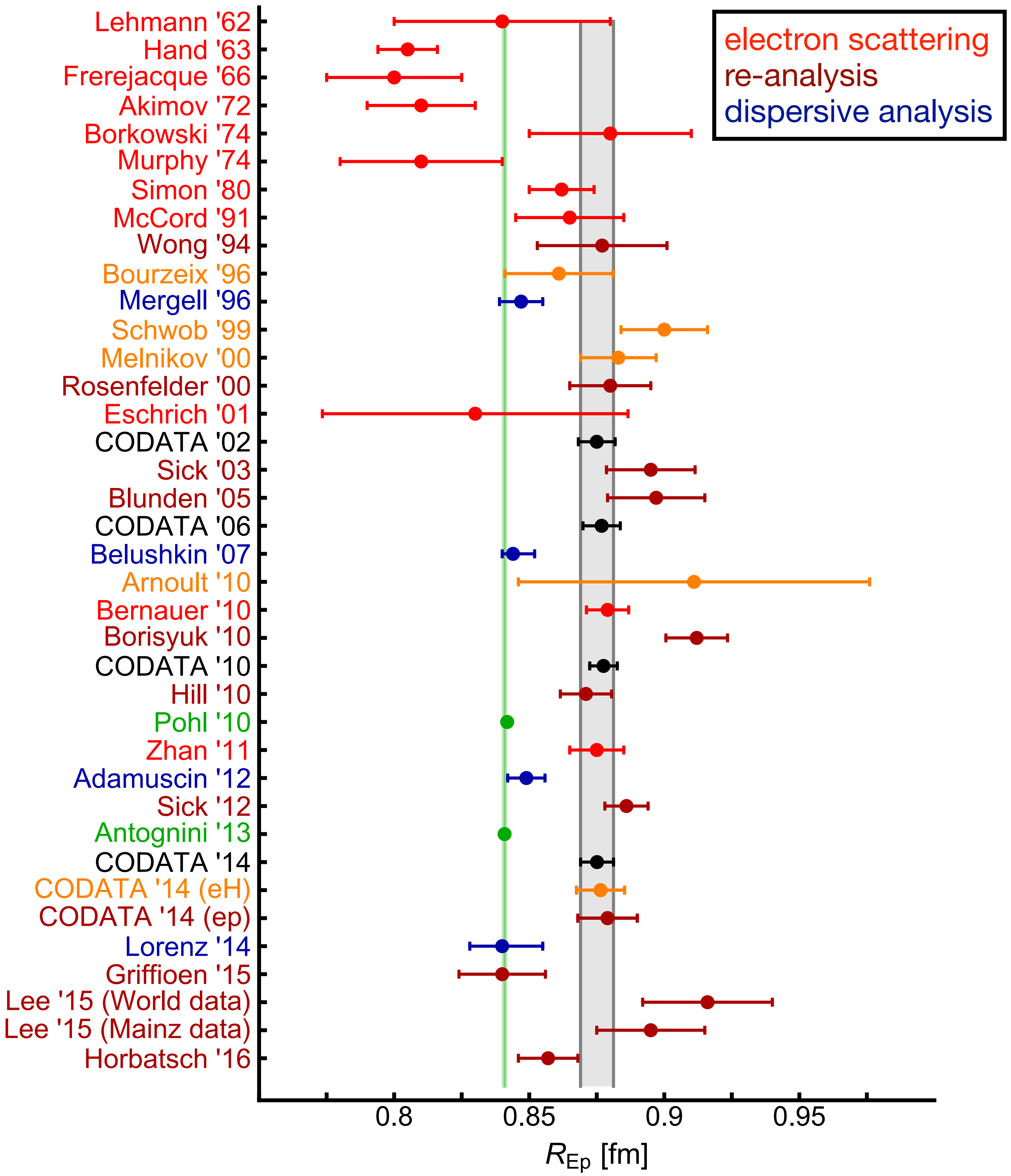

SYSTEMATICS OF THE CHARGE RADIUS EXTRACTION

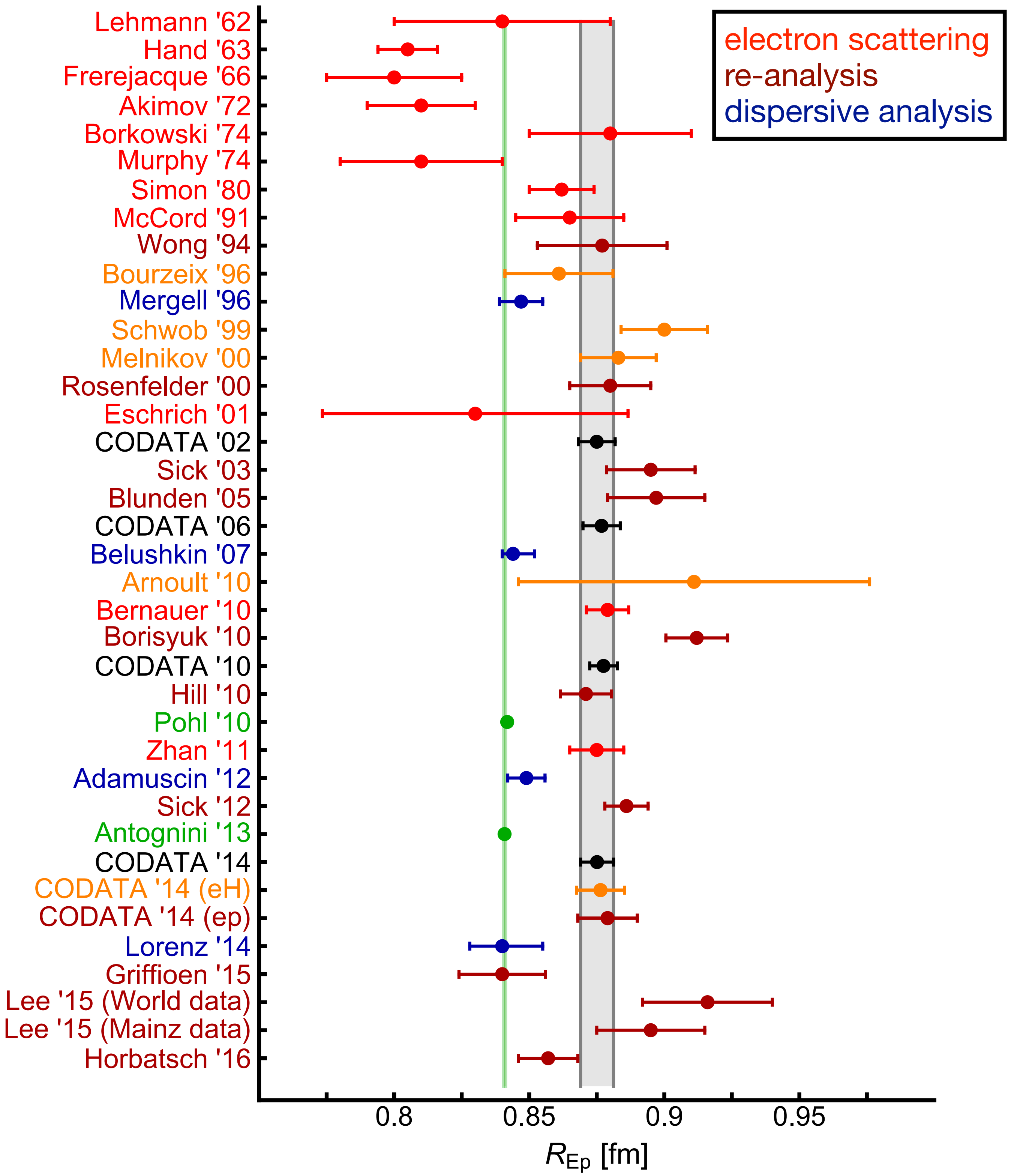

Data still not consistent...

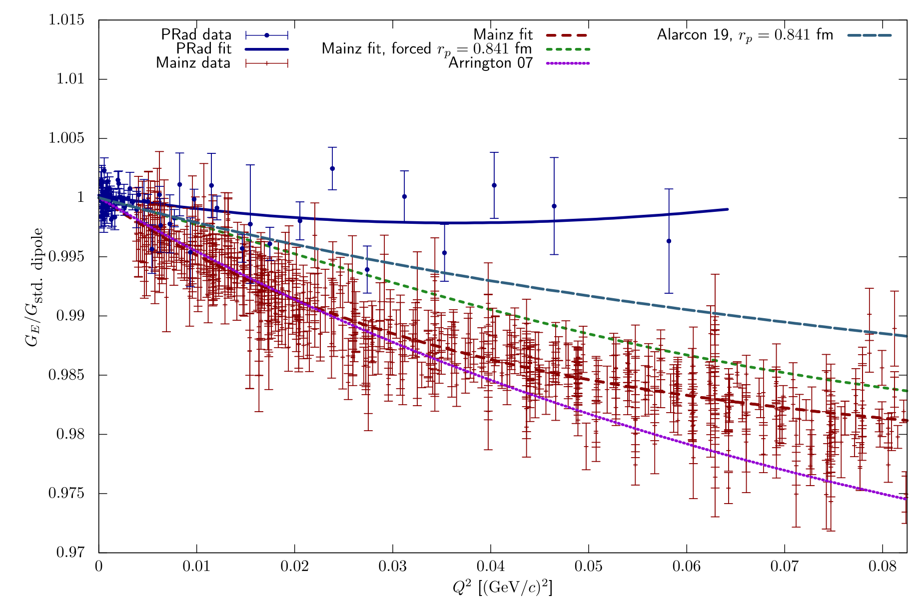

talk by Pascalutsa

SYSTEMATICS OF THE CHARGE RADIUS EXTRACTION

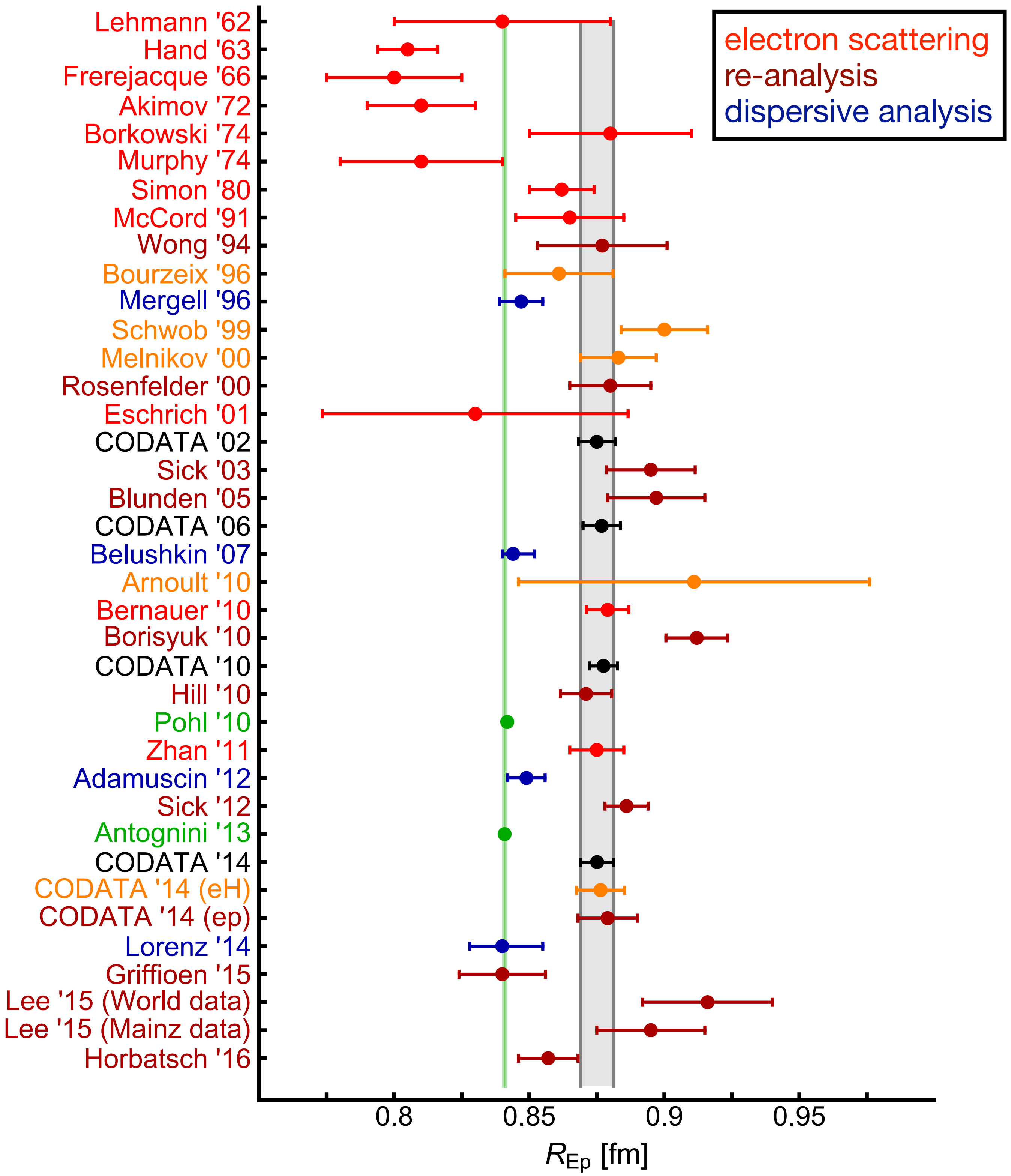

Data still not consistent...

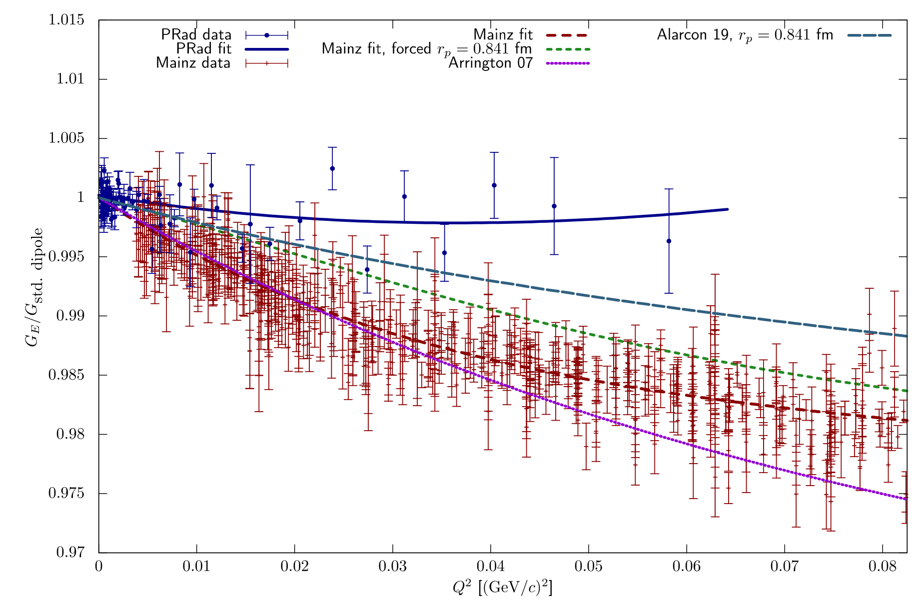

- Need to know radiative corrections to lepton-proton scattering talk by Signer

talk by Pascalutsa

SYSTEMATICS OF THE CHARGE RADIUS EXTRACTION

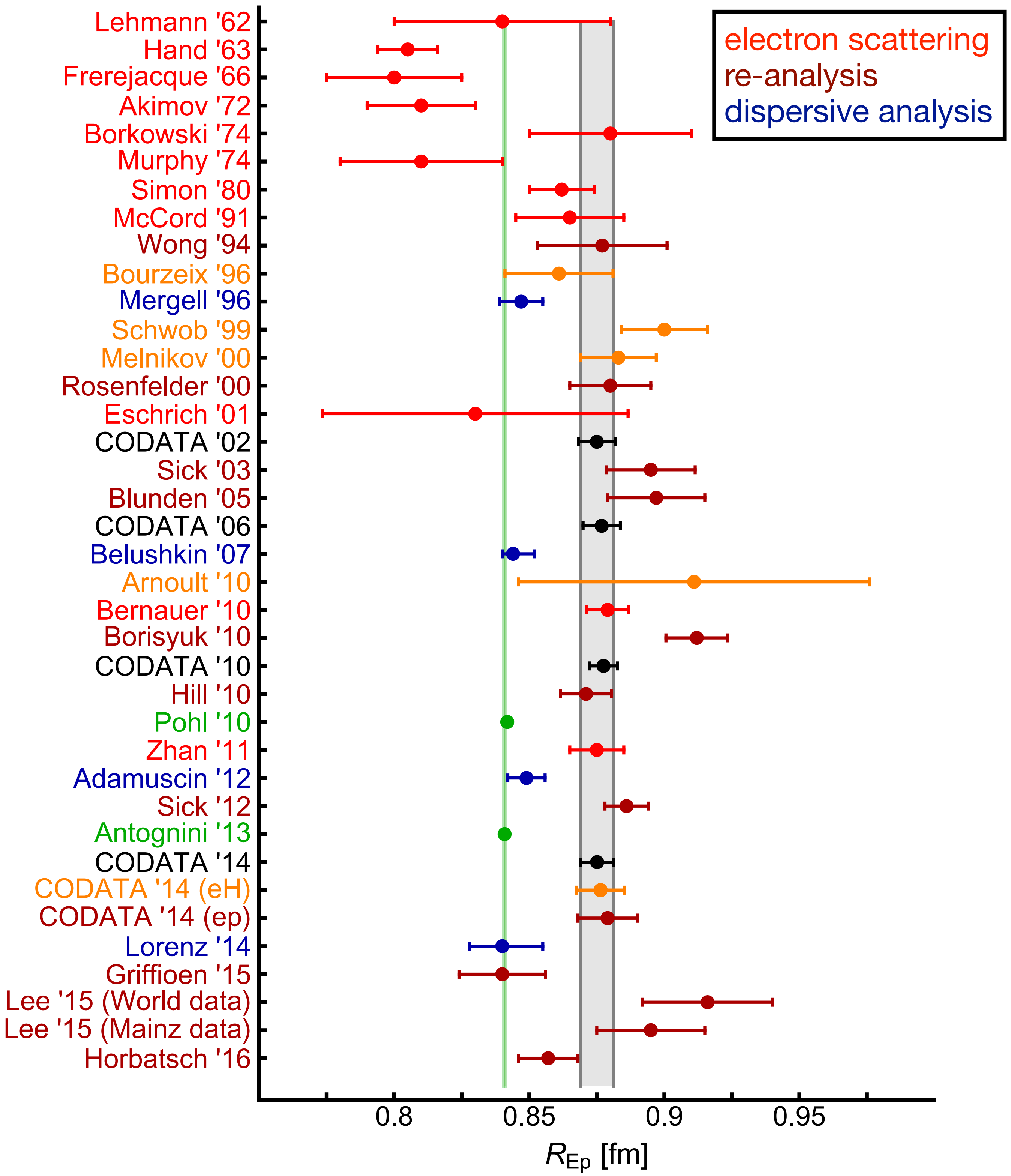

Data still not consistent...

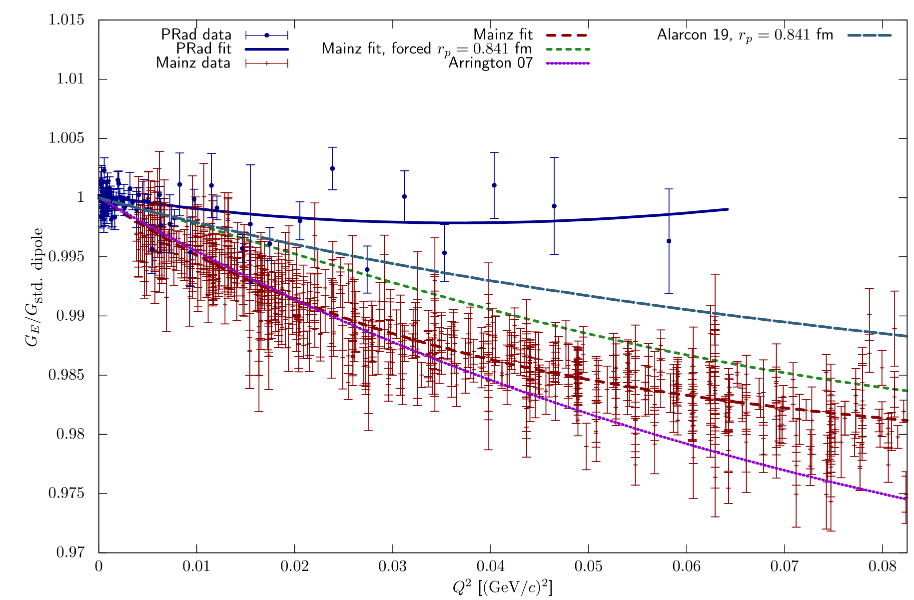

- Need to know radiative corrections to lepton-proton scattering talk by Signer
- Dispersive form factor analysis historically always gave small proton charge radius

talk by Pascalutsa

SYSTEMATICS OF THE CHARGE RADIUS EXTRACTION

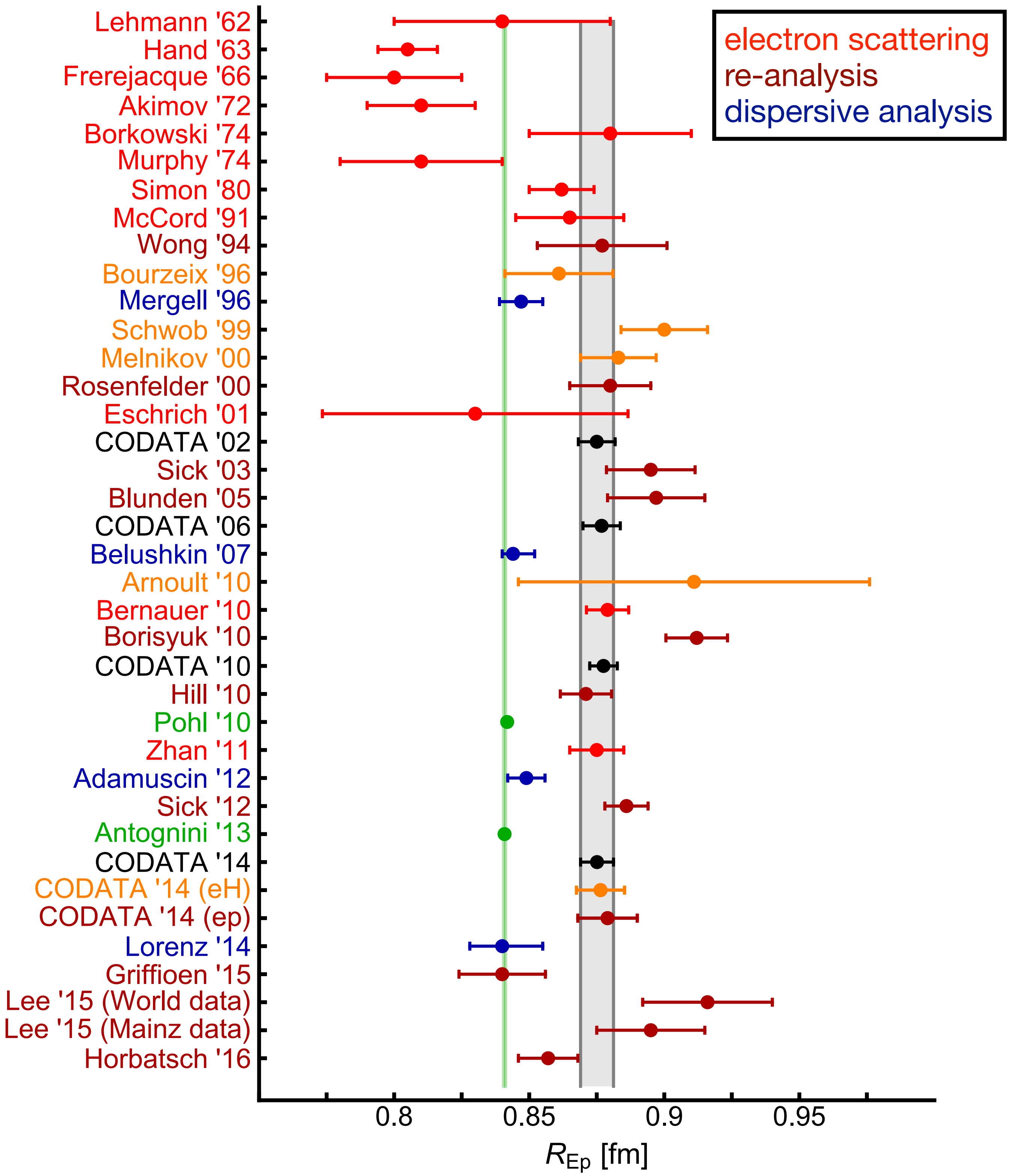

Data still not consistent...

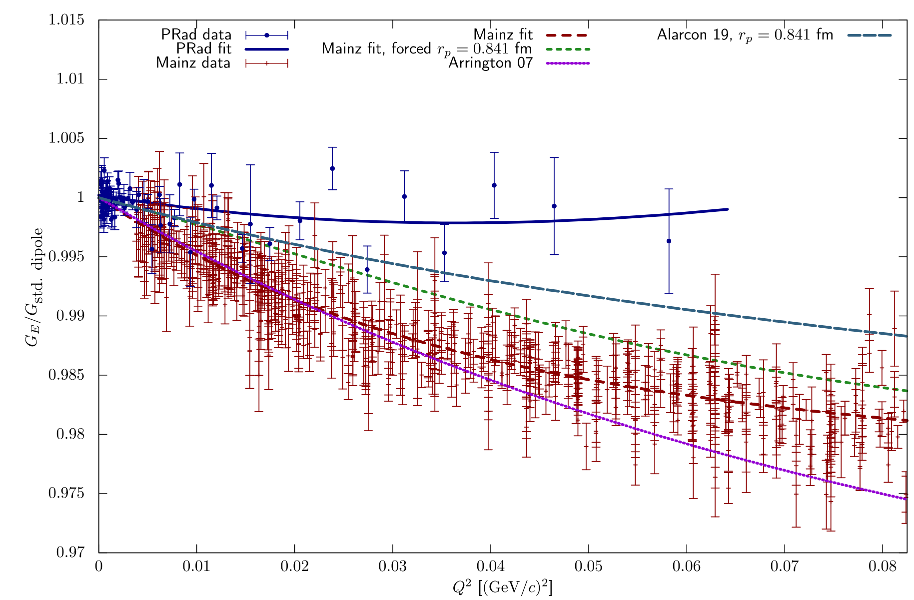

- Need to know radiative corrections to lepton-proton scattering talk by Signer
- Dispersive form factor analysis historically always gave small proton charge radius
- Fits of scattering data suffer from model / extrapolation uncertainty

SYSTEMATICS OF THE CHARGE RADIUS EXTRACTION

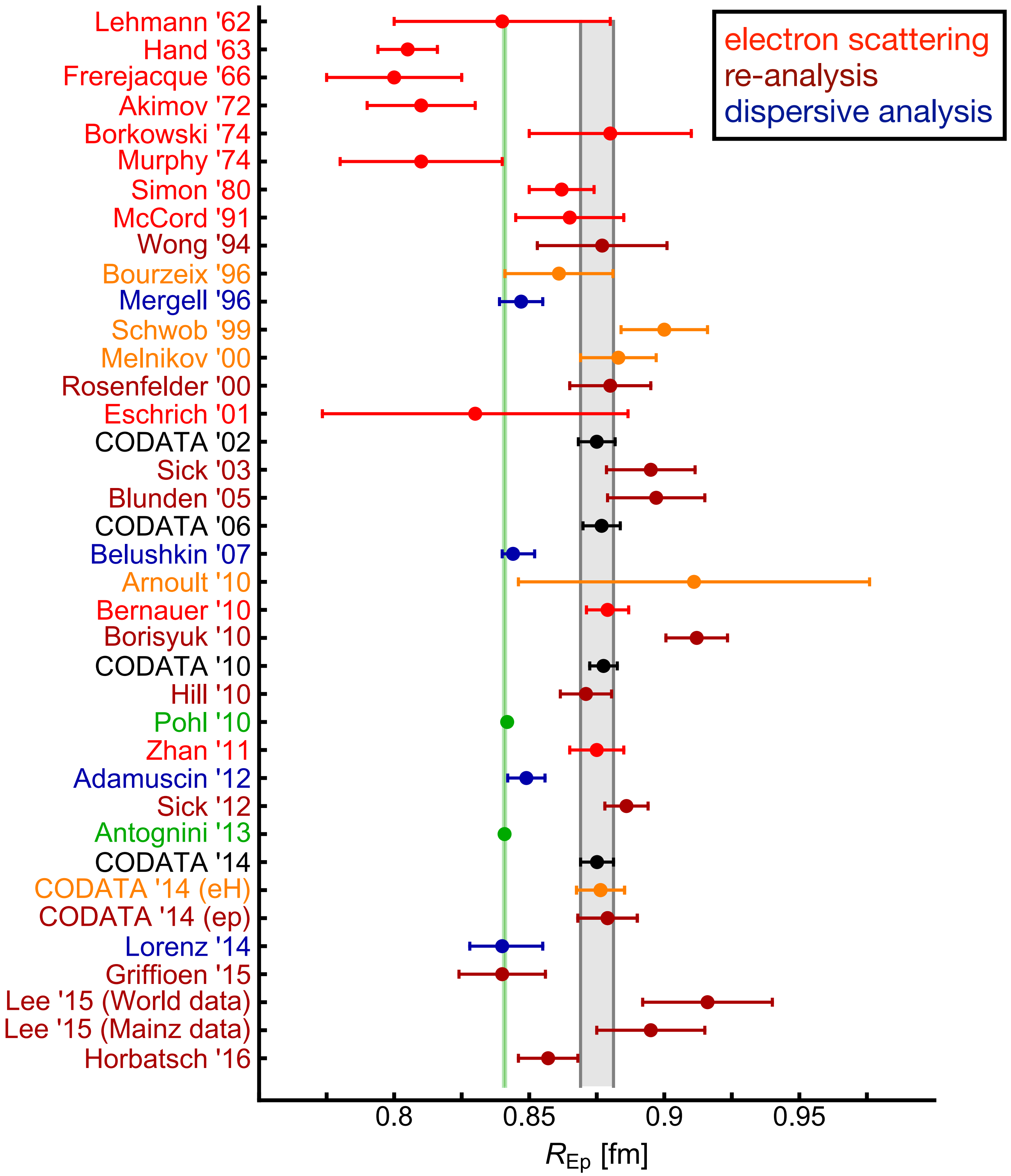

Data still not consistent...

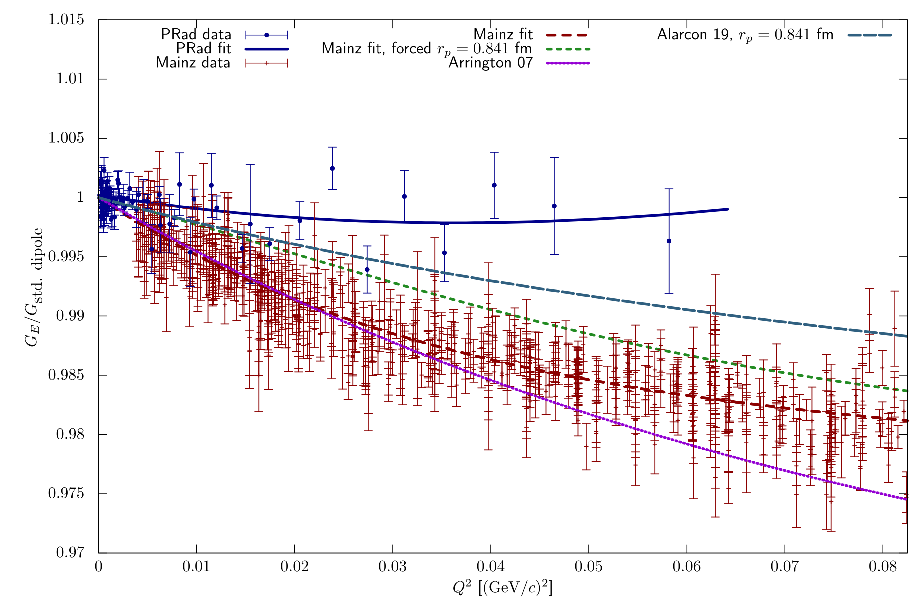

- Need to know radiative corrections to lepton-proton scattering talk by Signer
- Dispersive form factor analysis historically always gave small proton charge radius
- Fits of scattering data suffer from model / extrapolation uncertainty
- Strict lower bound on proton radius ?

talk by Pascalutsa

LOWER BOUND ON CHARGE RADIUS

$$\boxed{R_E^2(Q^2) = -\frac{6}{Q^2}\log G_E(Q^2) \xrightarrow{Q^2=0} R_E^2}$$ is a lower bound $\boxed{R_E^2(Q^2) \leq R_E^2}$ for $Q^2 \geq 0$

FH and V. Pascalutsa, Phys. Lett. B **797** (2019)

- $R_E^2(Q^2)$ is monotonically increasing towards $Q^2=0$
- Lower bound follows from finite Q^2 data, no extrapolation of FF data required

LOWER BOUND ON CHARGE RADIUS

$$\boxed{R_E^2(Q^2) = -\frac{6}{Q^2}\log G_E(Q^2) \xrightarrow{Q^2=0} R_E^2}$$ is a lower bound $\boxed{R_E^2(Q^2) \leq R_E^2}$ for $Q^2 \geq 0$

FH and V. Pascalutsa, Phys. Lett. B **797** (2019)

- $R_E^2(Q^2)$ is monotonically increasing towards $Q^2=0$
- Lower bound follows from finite Q^2 data, no extrapolation of FF data required

tentative evaluation: lower bound from ISR and Bernauer data

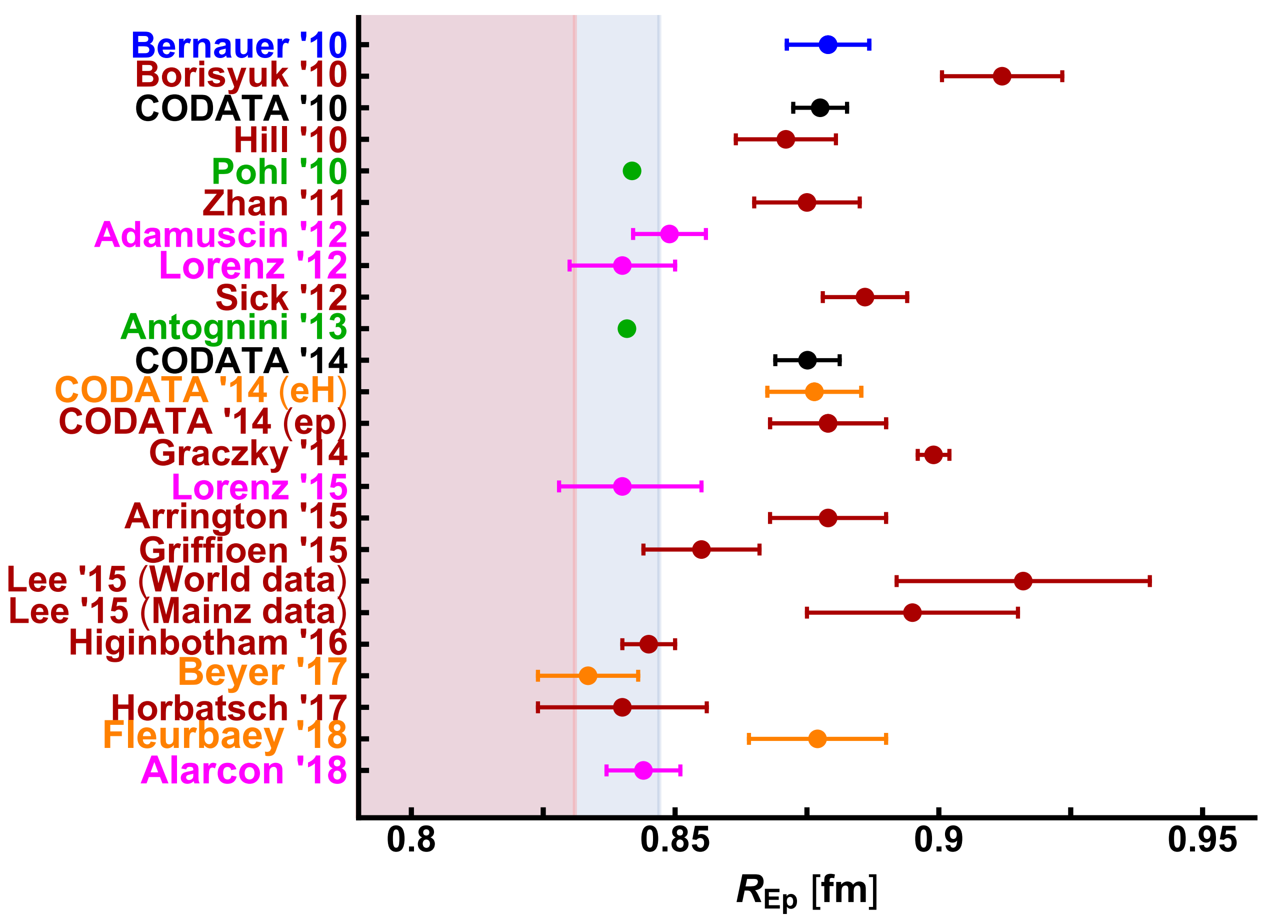

talk by Pascalutsa

LOWER BOUND ON CHARGE RADIUS

$$\boxed{R_E^2(Q^2) = -\frac{6}{Q^2}\log G_E(Q^2) \xrightarrow{Q^2=0} R_E^2}$$ is a lower bound $\boxed{R_E^2(Q^2) \leq R_E^2}$ for $Q^2 \geq 0$

FH and V. Pascalutsa, Phys. Lett. B **797** (2019)

- $R_E^2(Q^2)$ is monotonically increasing towards $Q^2=0$
- Lower bound follows from finite Q^2 data, no extrapolation of FF data required

tentative evaluation: lower bound from ISR and Bernauer data

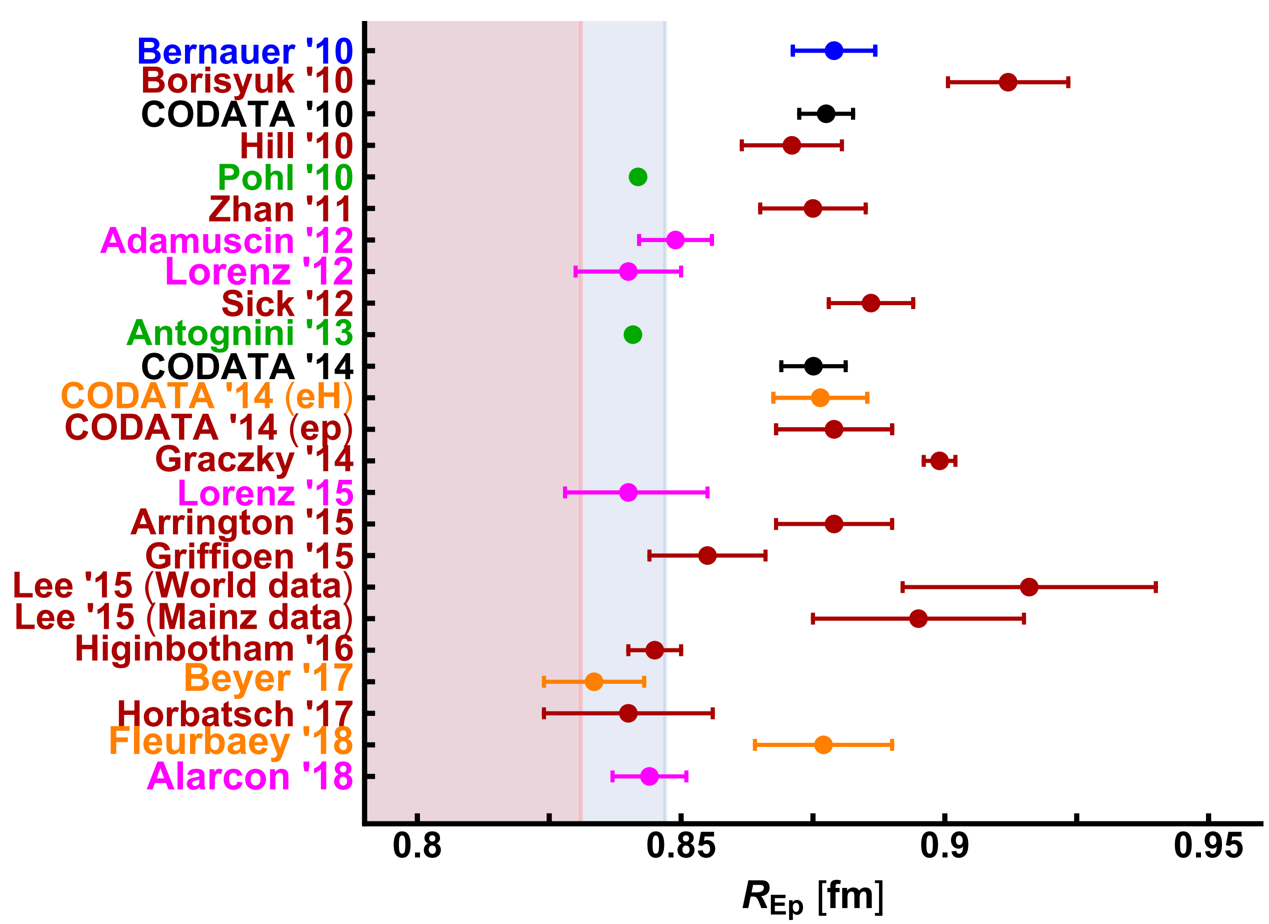

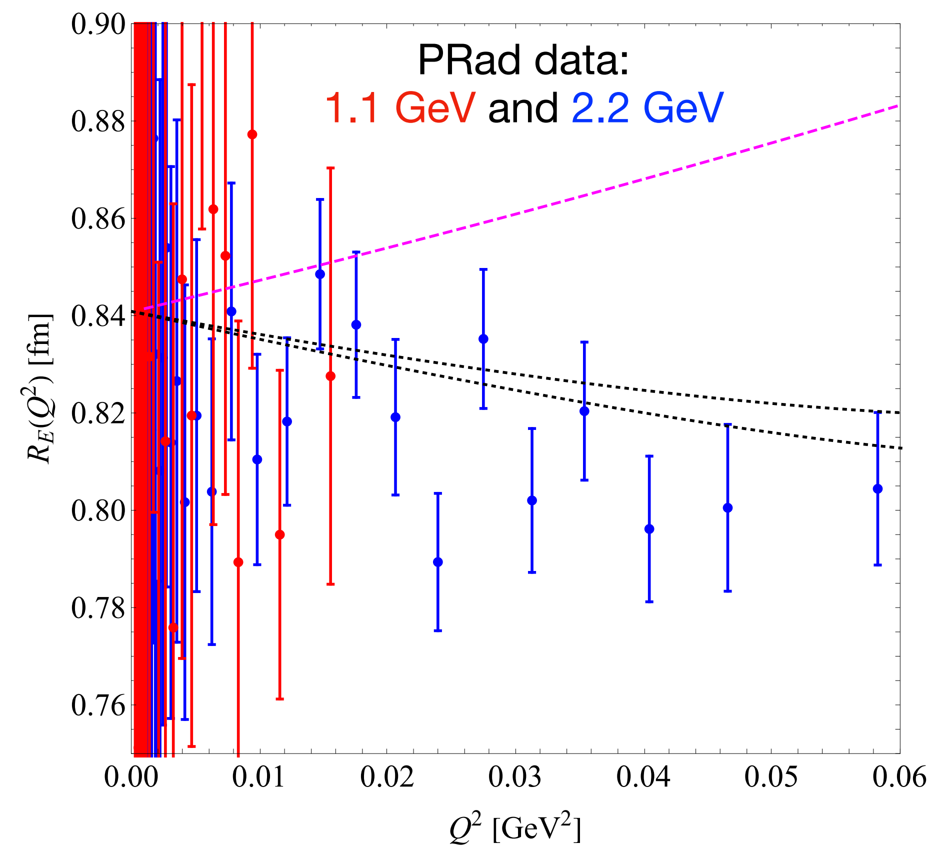

M. Horbatsch, Phys. Lett. B **804** (2020) 135373 talk by Pachucki

Comprehensive theory of the Lamb shift in light muonic atoms

K. Pachucki,[1] V. Lensky,[2] F. Hagelstein,[2,3] S. S. Li Muli,[2] S. Bacca,[2,4] and R. Pohl[5]
[1] *Faculty of Physics, University of Warsaw, Pasteura 5, 02-093 Warsaw, Poland*
[2] *Institut für Kernphysik, Johannes Gutenberg-Universität Mainz, 55128 Mainz, Germany*
[3] *Paul Scherrer Institut, CH-5232 Villigen PSI, Switzerland*
[4] *Helmholtz-Institut Mainz, Johannes Gutenberg Universität Mainz, 55099 Mainz, Germany*
[5] *Institut für Physik, Johannes Gutenberg-Universität Mainz, 55099 Mainz, Germany*

(Dated: May 19, 2023) Rev. Mod. Phys. **96** (2024) 1, 015001

E_{QED}	point nucleus	206.034 4(3)	228.774 0(3)	1644.348(8)	1668.491(7)
$\mathcal{C}\, r_C^2$	finite size	$-5.225\,9\, r_p^2$	$-6.107\,4\, r_d^2$	$-103.383\, r_h^2$	$-106.209\, r_\alpha^2$
E_{NS}	nuclear structure	0.028 9(25)	1.750 3(200)	15.499(378)	9.276(433)
$E_L(\text{exp})$	experiment[a]	202.370 6(23)	202.878 5(34)	1258.598(48)	1378.521(48)
r_C	this work	0.840 60(39)	2.127 58(78)	1.970 07(94)	1.678 6(12)
r_C	previous[a]	0.840 87(39)	2.125 62(78)	1.970 07(94)	1.678 24(83)

talk by Pachucki

Comprehensive theory of the Lamb shift in light muonic atoms

K. Pachucki,[1] V. Lensky,[2] F. Hagelstein,[2,3] S. S. Li Muli,[2] S. Bacca,[2,4] and R. Pohl[5]
[1] *Faculty of Physics, University of Warsaw, Pasteura 5, 02-093 Warsaw, Poland*
[2] *Institut für Kernphysik, Johannes Gutenberg-Universität Mainz, 55128 Mainz, Germany*
[3] *Paul Scherrer Institut, CH-5232 Villigen PSI, Switzerland*
[4] *Helmholtz-Institut Mainz, Johannes Gutenberg Universität Mainz, 55099 Mainz, Germany*
[5] *Institut für Physik, Johannes Gutenberg-Universität Mainz, 55099 Mainz, Germany*

(Dated: May 19, 2023) Rev. Mod. Phys. **96** (2024) 1, 015001

E_{QED}	point nucleus	206.034 4(3)	228.774 0(3)	1644.348(8)	1668.491(7)
$\mathcal{C}\,r_C^2$	finite size	$-5.225\,9\,r_p^2$	$-6.107\,4\,r_d^2$	$-103.383\,r_h^2$	$-106.209\,r_\alpha^2$
E_{NS}	nuclear structure	0.028 9(25)	1.750 3(200)	15.499(378)	9.276(433)
$E_L(\mathrm{exp})$	experiment[a]	202.370 6(23)	202.878 5(34)	1258.598(48)	1378.521(48)
r_C	this work	0.840 60(39)	2.127 58(78)	1.970 07(94)	1.678 6(12)
r_C	previous[a]	0.840 87(39)	2.125 62(78)	1.970 07(94)	1.678 24(83)

μH: present accuracy comparable with experimental precision

μD, μ^3He^+, μ^4He^+: present accuracy factor 5-10 worse than experimental precision

Comprehensive theory of the Lamb shift in light muonic atoms

K. Pachucki,[1] V. Lensky,[2] F. Hagelstein,[2,3] S. S. Li Muli,[2] S. Bacca,[2,4] and R. Pohl[5]
[1] *Faculty of Physics, University of Warsaw, Pasteura 5, 02-093 Warsaw, Poland*
[2] *Institut für Kernphysik, Johannes Gutenberg-Universität Mainz, 55128 Mainz, Germany*
[3] *Paul Scherrer Institut, CH-5232 Villigen PSI, Switzerland*
[4] *Helmholtz-Institut Mainz, Johannes Gutenberg Universität Mainz, 55099 Mainz, Germany*
[5] *Institut für Physik, Johannes Gutenberg-Universität Mainz, 55099 Mainz, Germany*

(Dated: May 19, 2023) Rev. Mod. Phys. **96** (2024) 1, 015001

E_{QED}	point nucleus	206.034 4(3)	228.774 0(3)	1644.348(8)	1668.491(7)
$\mathcal{C}\, r_C^2$	finite size	$-5.225\,9\, r_p^2$	$-6.107\,4\, r_d^2$	$-103.383\, r_h^2$	$-106.209\, r_\alpha^2$
E_{NS}	nuclear structure	0.028 9(25)	1.750 3(200)	15.499(378)	9.276(433)
$E_L(\text{exp})$	experiment[a]	202.370 6(23)	202.878 5(34)	1258.598(48)	1378.521(48)
r_C	this work	0.840 60(39)	2.127 58(78)	1.970 07(94)	1.678 6(12)
r_C	previous[a]	0.840 87(39)	2.125 62(78)	1.970 07(94)	1.678 24(83)

μH: present accuracy comparable with experimental precision

μD, μ^{3}He$^+$, μ^{4}He$^+$: present accuracy factor 5-10 worse than experimental precision

- Experiments will improve by up to a factor of 5
- Theoretical improvement needed for nuclear/nucleon 2- and 3-photon exchange

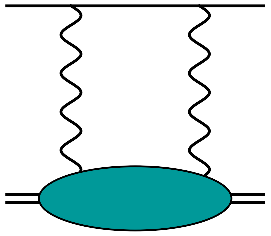

2γ EFFECT IN THE LAMB SHIFT

wave function at the origin

$$\Delta E(nS) = 8\pi\alpha m\,\phi_n^2\,\frac{1}{i}\int_{-\infty}^{\infty}\frac{\mathrm{d}\nu}{2\pi}\int\frac{\mathrm{d}\mathbf{q}}{(2\pi)^3}\,\frac{\left(Q^2-2\nu^2\right)T_1(\nu,Q^2)-\left(Q^2+\nu^2\right)T_2(\nu,Q^2)}{Q^4(Q^4-4m^2\nu^2)}$$

dispersion relation & optical theorem:

$$T_1(\nu,Q^2) = T_1(0,Q^2) + \frac{32\pi Z^2\alpha M\nu^2}{Q^4}\int_0^1 \mathrm{d}x\,\frac{x f_1(x,Q^2)}{1-x^2(\nu/\nu_{\mathrm{el}})^2-i0^+}$$

$$T_2(\nu,Q^2) = \frac{16\pi Z^2\alpha M}{Q^2}\int_0^1 \mathrm{d}x\,\frac{f_2(x,Q^2)}{1-x^2(\nu/\nu_{\mathrm{el}})^2-i0^+}$$

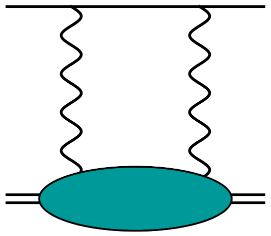

2γ EFFECT IN THE LAMB SHIFT

wave function at the origin

$$\Delta E(nS) = 8\pi\alpha m\,\phi_n^2\,\frac{1}{i}\int_{-\infty}^{\infty}\frac{\mathrm{d}\nu}{2\pi}\int\frac{\mathrm{d}\mathbf{q}}{(2\pi)^3}\,\frac{\left(Q^2-2\nu^2\right)T_1(\nu,Q^2)-\left(Q^2+\nu^2\right)T_2(\nu,Q^2)}{Q^4(Q^4-4m^2\nu^2)}$$

dispersion relation & optical theorem:

$$T_1(\nu,Q^2) = \boxed{T_1(0,Q^2)} + \frac{32\pi Z^2\alpha M\nu^2}{Q^4}\int_0^1 \mathrm{d}x\,\frac{x f_1(x,Q^2)}{1-x^2(\nu/\nu_{\mathrm{el}})^2-i0^+}$$

$$T_2(\nu,Q^2) = \frac{16\pi Z^2\alpha M}{Q^2}\int_0^1 \mathrm{d}x\,\frac{f_2(x,Q^2)}{1-x^2(\nu/\nu_{\mathrm{el}})^2-i0^+}$$

- Caution: in the data-driven dispersive approach the $T_1(0,Q^2)$ subtraction function is modelled!

low-energy expansion:

$$\lim_{Q^2\to 0}\overline{T}_1(0,Q^2)/Q^2 = 4\pi\beta_{M1}$$

modelled Q^2 behavior:

$$\overline{T}_1(0,Q^2) = 4\pi\beta_{M1}\,Q^2/\left(1+Q^2/\Lambda^2\right)^4$$

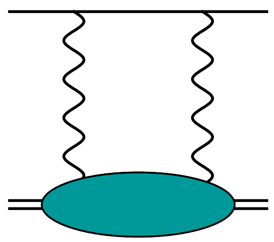

2γ EFFECT IN THE LAMB SHIFT

wave function at the origin

$$\boxed{\Delta E(nS) = 8\pi\alpha m\, \phi_n^2\, \frac{1}{i}\int_{-\infty}^{\infty}\frac{\mathrm{d}\nu}{2\pi}\int\frac{\mathrm{d}\mathbf{q}}{(2\pi)^3}\,\frac{\left(Q^2-2\nu^2\right)T_1(\nu,Q^2)-\left(Q^2+\nu^2\right)T_2(\nu,Q^2)}{Q^4(Q^4-4m^2\nu^2)}}$$

dispersion relation & optical theorem:

$$T_1(\nu,Q^2) = \boxed{T_1(0,Q^2)} + \frac{32\pi Z^2\alpha M\nu^2}{Q^4}\int_0^1 \mathrm{d}x\,\frac{x f_1(x,Q^2)}{1-x^2(\nu/\nu_{\mathrm{el}})^2-i0^+}$$

$$T_2(\nu,Q^2) = \frac{16\pi Z^2\alpha M}{Q^2}\int_0^1 \mathrm{d}x\,\frac{f_2(x,Q^2)}{1-x^2(\nu/\nu_{\mathrm{el}})^2-i0^+}$$

- Caution: in the data-driven dispersive approach the $T_1(0,Q^2)$ subtraction function is modelled!

low-energy expansion:

$$\lim_{Q^2\to 0}\overline{T}_1(0,Q^2)/Q^2 = 4\pi\beta_{M1}$$

modelled Q^2 behavior:

$$\overline{T}_1(0,Q^2) = 4\pi\beta_{M1}\,Q^2/\left(1+Q^2/\Lambda^2\right)^4$$

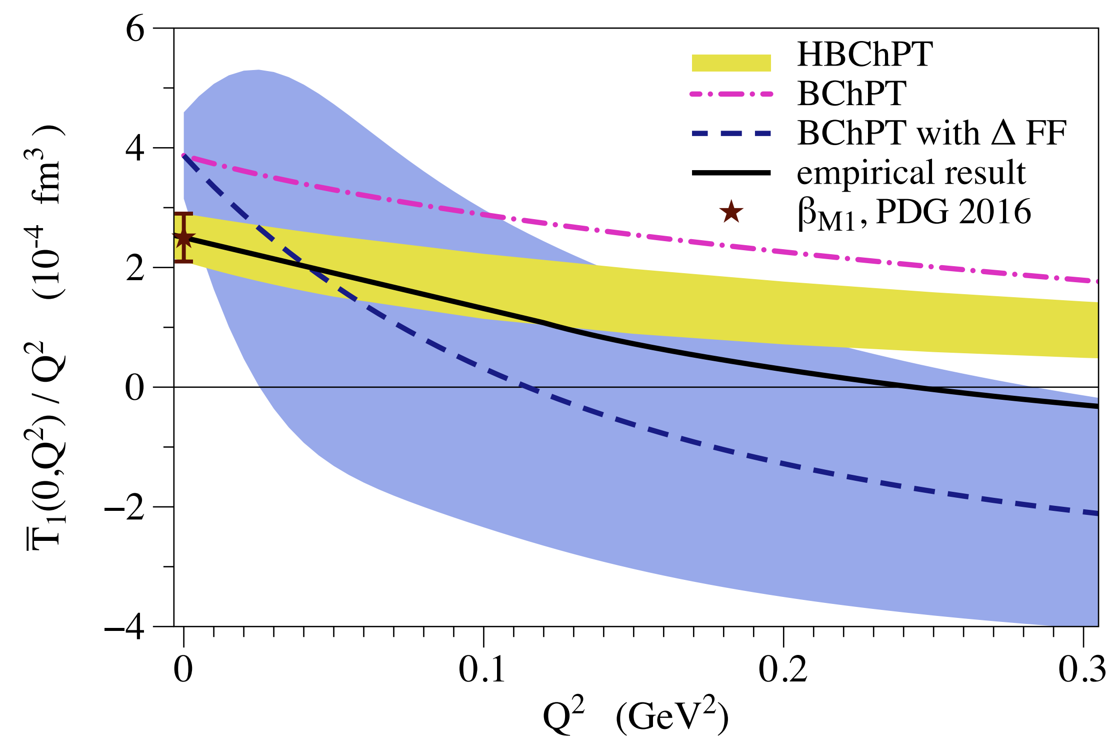

POLARIZABILITY EFFECT IN μH LAMB SHIFT

Table 1 Forward 2γ-exchange contributions to the $2S$-shift in μH, in units of μeV.

Reference	$E_{2S}^{(\mathrm{subt})}$	$E_{2S}^{(\mathrm{inel})}$	$E_{2S}^{(\mathrm{pol})}$	$E_{2S}^{(\mathrm{el})}$	$E_{2S}^{\langle 2\gamma\rangle}$
DATA-DRIVEN					
(73) Pachucki '99	1.9	−13.9	−12(2)	−23.2(1.0)	−35.2(2.2)
(74) Martynenko '06	2.3	−16.1	−13.8(2.9)		
(75) Carlson *et al.* '11	5.3(1.9)	−12.7(5)	−7.4(2.0)		
(76) Birse and McGovern '12	4.2(1.0)	−12.7(5)	−8.5(1.1)	−24.7(1.6)	−33(2)
(77) Gorchtein et al.'13 [a]	−2.3(4.6)	−13.0(6)	−15.3(4.6)	−24.5(1.2)	−39.8(4.8)
(78) Hill and Paz '16					−30(13)
(79) Tomalak'18	2.3(1.3)		−10.3(1.4)	−18.6(1.6)	−29.0(2.1)
LEADING-ORDER BχPT					
(80) Alarcòn *et al.* '14			$-9.6^{+1.4}_{-2.9}$		
(81) Lensky *et al.* '17 [b]	$3.5^{+0.5}_{-1.9}$	−12.1(1.8)	$-8.6^{+1.3}_{-5.2}$		
LATTICE QCD					
(82) Fu *et al.* '22					−37.4(4.9)

[a] Adjusted values due to a different decomposition into the elastic and polarizability contributions.
[b] Partially includes the $\Delta(1232)$-isobar contribution.

POLARIZABILITY EFFECT IN μH LAMB SHIFT

$\propto \alpha_{E1}$

Assuming ChPT is working, it should be best applicable to atomic systems, where the energies are very small !

Table 1 Forward 2γ-exchange contributions to the $2S$-shift in μH, in units of μeV.

Reference	$E_{2S}^{(\text{subt})}$	$E_{2S}^{(\text{inel})}$	$E_{2S}^{(\text{pol})}$	$E_{2S}^{(\text{el})}$	$E_{2S}^{\langle 2\gamma\rangle}$
DATA-DRIVEN					
(73) Pachucki '99	1.9	−13.9	−12(2)	−23.2(1.0)	−35.2(2.2)
(74) Martynenko '06	2.3	−16.1	−13.8(2.9)		
(75) Carlson *et al.* '11	5.3(1.9)	−12.7(5)	−7.4(2.0)		
(76) Birse and McGovern '12	4.2(1.0)	−12.7(5)	−8.5(1.1)	−24.7(1.6)	−33(2)
(77) Gorchtein et al.'13 [a]	−2.3(4.6)	−13.0(6)	−15.3(4.6)	−24.5(1.2)	−39.8(4.8)
(78) Hill and Paz '16					−30(13)
(79) Tomalak'18	2.3(1.3)		−10.3(1.4)	−18.6(1.6)	−29.0(2.1)
LEADING-ORDER BχPT					
(80) Alarcòn *et al.* '14			$-9.6^{+1.4}_{-2.9}$		
(81) Lensky *et al.* '17 [b]	$3.5^{+0.5}_{-1.9}$	−12.1(1.8)	$-8.6^{+1.3}_{-5.2}$		
LATTICE QCD					
(82) Fu *et al.* '22					−37.4(4.9)

[a] Adjusted values due to a different decomposition into the elastic and polarizability contributions.
[b] Partially includes the $\Delta(1232)$-isobar contribution.

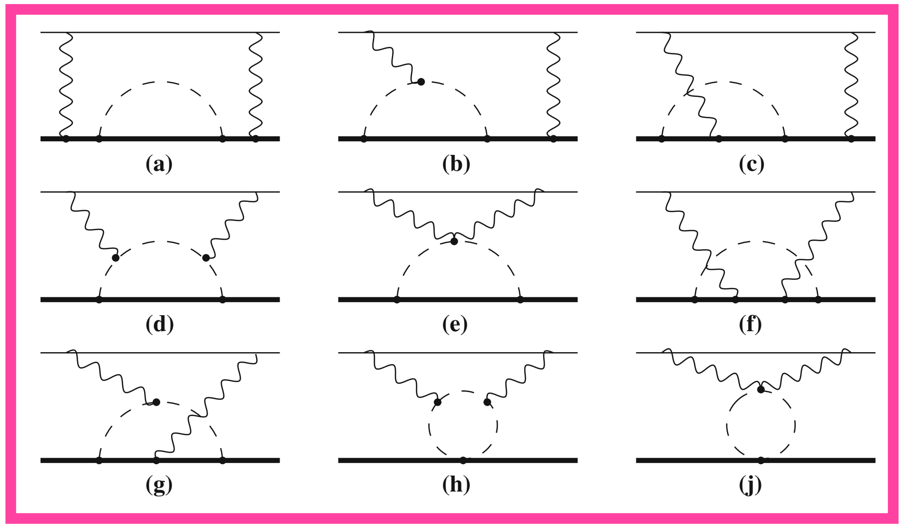

POLARIZABILITY EFFECT IN μH LAMB SHIFT

$\propto \beta_{M1}$ $\propto \alpha_{E1}$

Table 1 Forward 2γ-exchange contributions to the $2S$-shift in μH, in units of μeV.

Reference	$E_{2S}^{(\mathrm{subt})}$	$E_{2S}^{(\mathrm{inel})}$	$E_{2S}^{(\mathrm{pol})}$	$E_{2S}^{(\mathrm{el})}$	$E_{2S}^{\langle 2\gamma \rangle}$
DATA-DRIVEN					
(73) Pachucki '99	1.9	−13.9	−12(2)	−23.2(1.0)	−35.2(2.2)
(74) Martynenko '06	2.3	−16.1	−13.8(2.9)		
(75) Carlson *et al.* '11	5.3(1.9)	−12.7(5)	−7.4(2.0)		
(76) Birse and McGovern '12	4.2(1.0)	−12.7(5)	−8.5(1.1)	−24.7(1.6)	−33(2)
(77) Gorchtein et al.'13 [a]	−2.3(4.6)	−13.0(6)	−15.3(4.6)	−24.5(1.2)	−39.8(4.8)
(78) Hill and Paz '16					−30(13)
(79) Tomalak'18	2.3(1.3)		−10.3(1.4)	−18.6(1.6)	−29.0(2.1)
LEADING-ORDER BχPT					
(80) Alarcòn *et al.* '14			$-9.6^{+1.4}_{-2.9}$		
(81) Lensky *et al.* '17 [b]	$3.5^{+0.5}_{-1.9}$	−12.1(1.8)	$-8.6^{+1.3}_{-5.2}$		
LATTICE QCD					
(82) Fu *et al.* '22					−37.4(4.9)

[a] Adjusted values due to a different decomposition into the elastic and polarizability contributions.
[b] Partially includes the $\Delta(1232)$-isobar contribution.

Assuming ChPT
is working, it should be best
applicable to atomic systems,
where the energies are very
small !

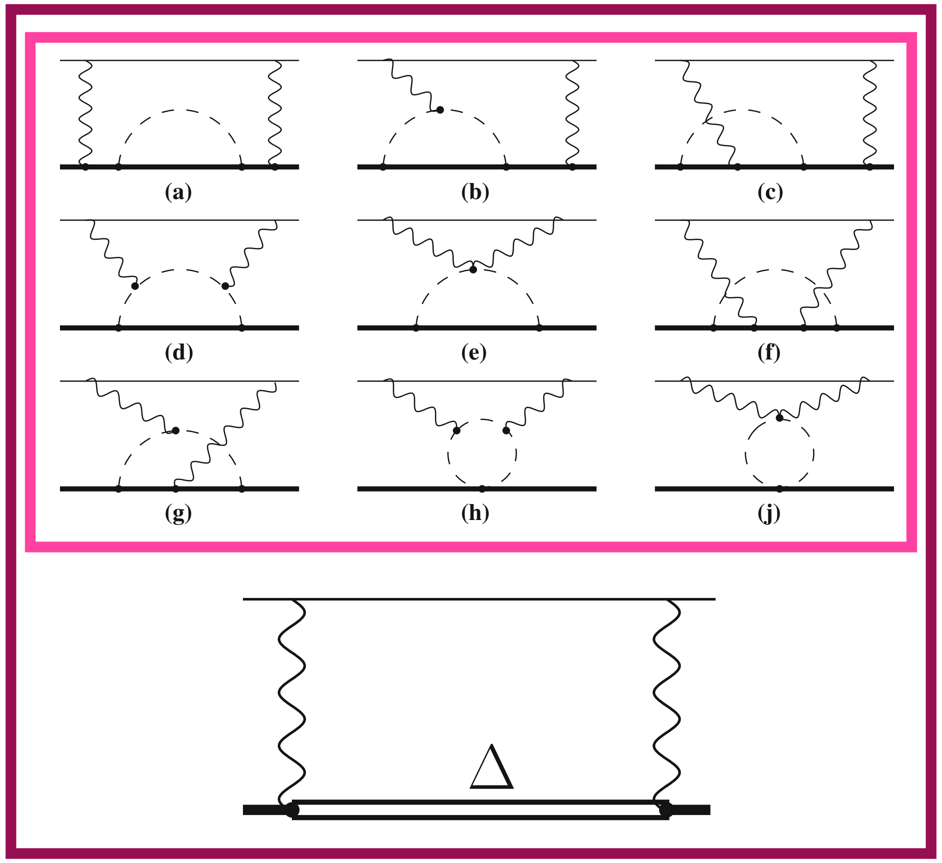

EUCLIDEAN SUBTRACTION FUNCTION

- Once-subtracted dispersion relation for $\overline{T}_1(\nu, Q^2)$ with subtraction at $\nu_s = iQ$
- Dominant part of polarizability contribution:

$$\Delta E_{nS}^{\prime\,(\mathrm{subt})} = \frac{2\alpha m}{\pi}\phi_n^2 \int_0^\infty \frac{\mathrm{d}Q}{Q^3}\frac{2+v_l}{(1+v_l)^2}\,\overline{T}_1(iQ, Q^2) \text{ with } v_l = \sqrt{1+4m^2/Q^2}$$

EUCLIDEAN SUBTRACTION FUNCTION

- Once-subtracted dispersion relation for $\overline{T}_1(\nu, Q^2)$ with subtraction at $\nu_s = iQ$
- Dominant part of polarizability contribution:

$$\Delta E_{nS}^{\prime\,\mathrm{(subt)}} = \frac{2\alpha m}{\pi}\phi_n^2 \int_0^\infty \frac{\mathrm{d}Q}{Q^3}\frac{2+v_l}{(1+v_l)^2}\,\overline{T}_1(iQ, Q^2) \text{ with } v_l = \sqrt{1+4m^2/Q^2}$$

- Inelastic contribution for $\nu_s = iQ$ is order of magnitude smaller than for $\nu_s = 0$

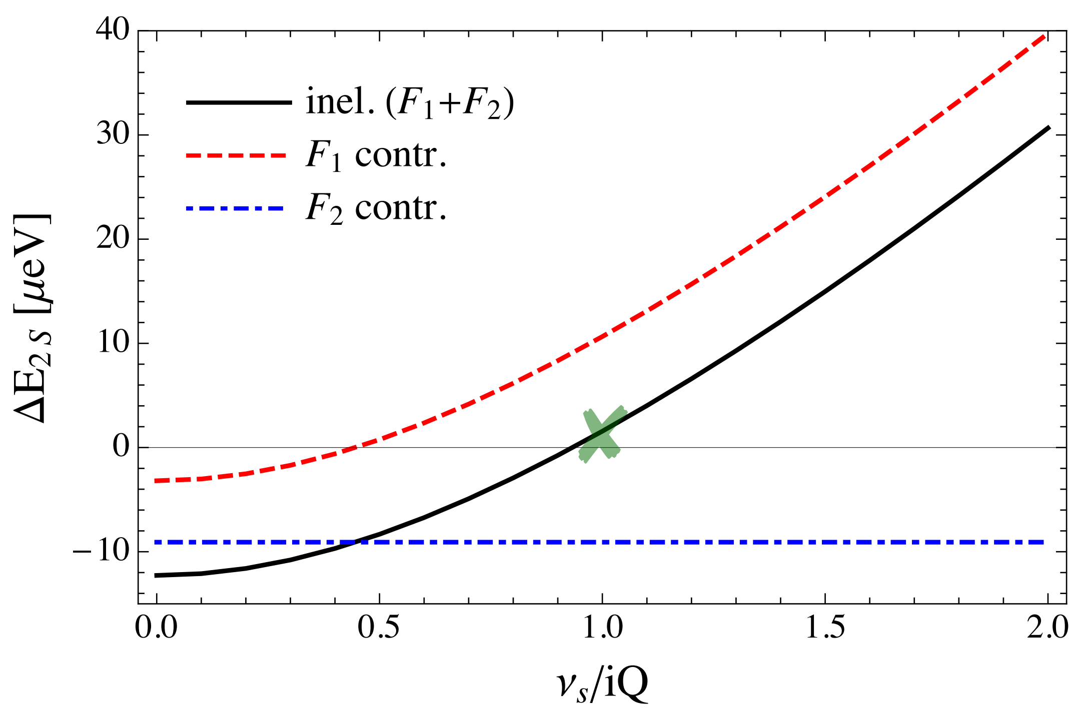

FH, V. Pascalutsa, Nucl. Phys. A **1016** (2021) 122323

based on Bosted-Christy parametrization:

$$\Delta E_{2S}^{\mathrm{(inel)}}(\nu_s = 0) \simeq -12.3\,\mu\mathrm{eV}$$

$$\Delta E_{2S}^{\prime\,\mathrm{(inel)}}(\nu_s = iQ) \simeq 1.6\,\mu\mathrm{eV}$$

EUCLIDEAN SUBTRACTION FUNCTION

- Once-subtracted dispersion relation for $\overline{T}_1(\nu, Q^2)$ with subtraction at $\nu_s = iQ$
- Dominant part of polarizability contribution:

$$\Delta E_{nS}^{\prime\,(\text{subt})} = \frac{2\alpha m}{\pi}\phi_n^2 \int_0^\infty \frac{\mathrm{d}Q}{Q^3}\frac{2+v_l}{(1+v_l)^2}\,\overline{T}_1(iQ, Q^2) \text{ with } v_l = \sqrt{1+4m^2/Q^2}$$

- Inelastic contribution for $\nu_s = iQ$ is order of magnitude smaller than for $\nu_s = 0$
- Prospects for future lattice QCD LQCD talk by Fu and EFT calculations

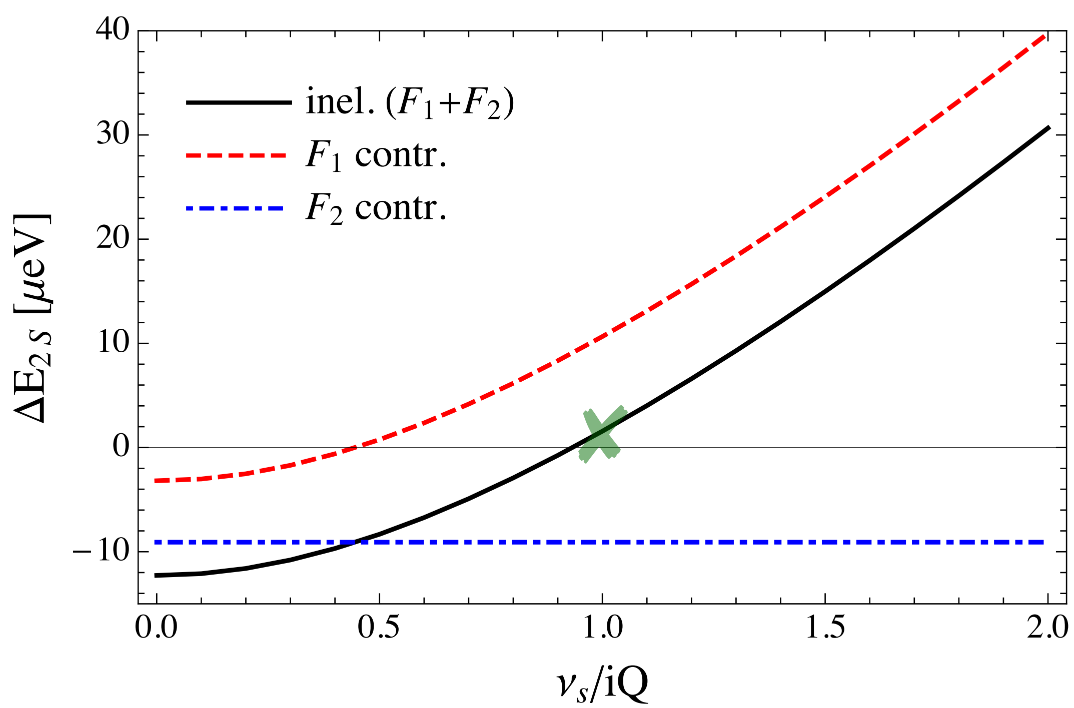

FH, V. Pascalutsa, Nucl. Phys. A **1016** (2021) 122323

based on Bosted-Christy parametrization:

$$\Delta E_{2S}^{(\text{inel})}(\nu_s = 0) \simeq -12.3\,\mu\text{eV}$$

$$\Delta E_{2S}^{\prime\,(\text{inel})}(\nu_s = iQ) \simeq 1.6\,\mu\text{eV}$$

— Proton Zemach Radius —

HYPERFINE SPLITTING IN μH

$$\Delta E_{\mathrm{HFS}}(nS) = \left[1 + \Delta_{\mathrm{QED}} + \Delta_{\mathrm{weak}} + \Delta_{\mathrm{structure}}\right] E_F(nS)$$

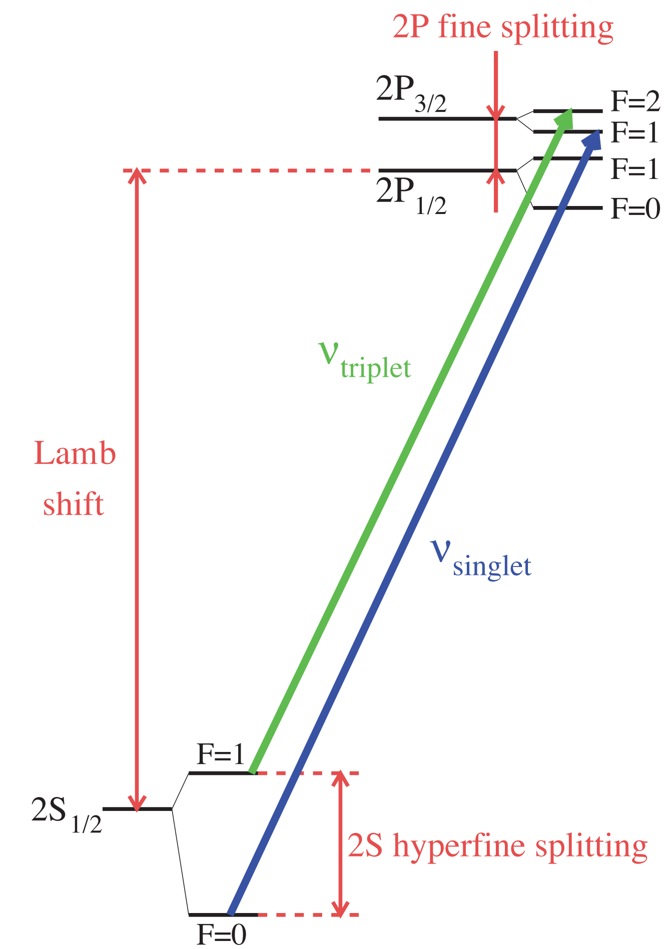

⏰ Measurements of the μH ground-state HFS planned by the CREMA and FAMU Collaborations

HYPERFINE SPLITTING IN μH

$$\Delta E_{\mathrm{HFS}}(nS) = \left[1 + \Delta_{\mathrm{QED}} + \Delta_{\mathrm{weak}} + \Delta_{\mathrm{structure}}\right] E_F(nS)$$

with $\Delta_{\mathrm{structure}} = \Delta_Z + \Delta_{\mathrm{recoil}} + \Delta_{\mathrm{pol}}$

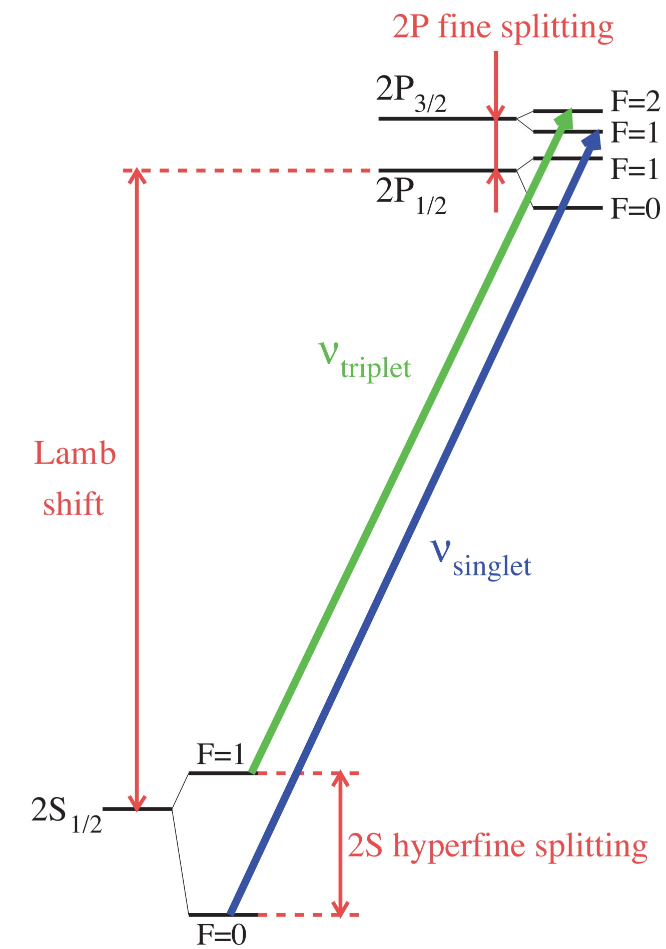

⏰ Measurements of the μH ground-state HFS planned by the CREMA and FAMU Collaborations

- Very precise input for the 2γ effect needed to find the μH ground-state HFS transition in experiment

HYPERFINE SPLITTING IN μH

$$\Delta E_{\mathrm{HFS}}(nS) = \left[1 + \Delta_{\mathrm{QED}} + \Delta_{\mathrm{weak}} + \Delta_{\mathrm{structure}}\right] E_F(nS)$$

with $\Delta_{\mathrm{structure}} = \boxed{\Delta_Z} + \Delta_{\mathrm{recoil}} + \Delta_{\mathrm{pol}}$

Zemach radius:

$$\Delta_Z = \frac{8Z\alpha m_r}{\pi} \int_0^\infty \frac{\mathrm{d}Q}{Q^2} \left[\frac{G_E(Q^2) G_M(Q^2)}{1+\kappa} - 1\right] \equiv -2Z\alpha m_r R_Z$$

experimental value: $R_Z = 1.082(37)\,\mathrm{fm}$

A. Antognini, et al., Science **339** (2013) 417–420

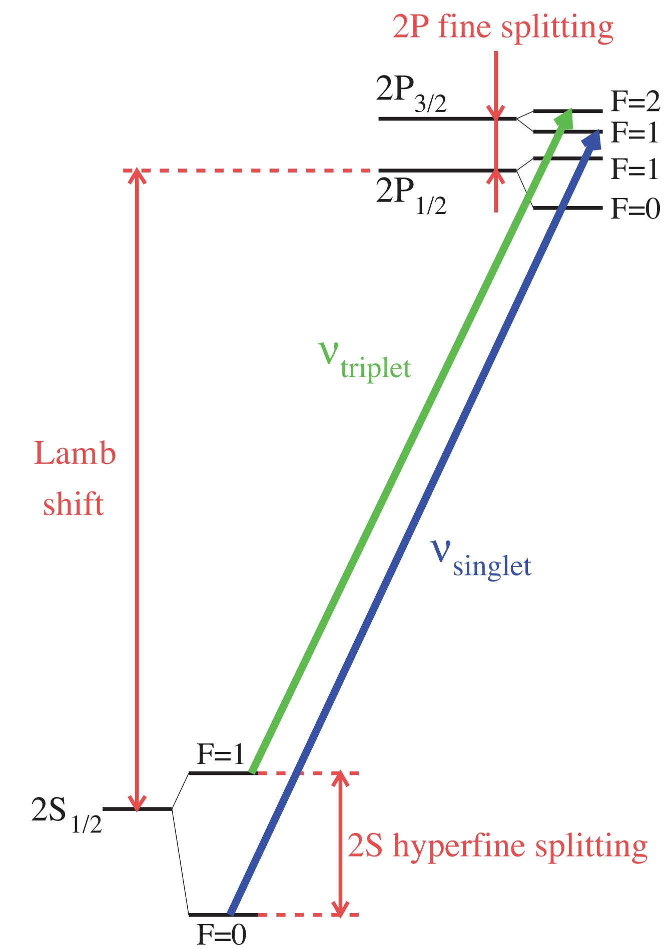

⏰ Measurements of the μH ground-state HFS planned by the CREMA and FAMU Collaborations

- Very precise input for the 2γ effect needed to find the μH ground-state HFS transition in experiment
- Zemach radius can help to pin down the magnetic properties of the proton

2γ EFFECT IN THE μH HFS

Table 1 Forward 2γ-exchange contribution to the HFS in μH.

Reference	Δ_Z [ppm]	Δ_{recoil} [ppm]	Δ_{pol} [ppm]	Δ_1 [ppm]	Δ_2 [ppm]	$E^{\langle 2\gamma\rangle}_{1S\text{-hfs}}$ [meV]
DATA-DRIVEN						
Pachucki '96 (1)	−8025	1666	0(658)			−1.160
Faustov et al. '01 (9)[a]	−7180		410(80)	468	−58	
Faustov et al. '06 (10)[b]			470(104)	518	−48	
Carlson et al. '11 (11)[c]	−7703	931	351(114)	370(112)	−19(19)	−1.171(39)
Tomalak '18 (12)[d]	−7333(48)	846(6)	364(89)	429(84)	−65(20)	−1.117(19)
HEAVY-BARYON χPT						
Peset et al. '17 (13)						−1.161(20)
LEADING-ORDER χPT						
Hagelstein et al. '16 (14)			37(95)	29(90)	9(29)	
+ Δ(1232) EXCIT.						
Hagelstein et al. '18 (15)			−13	84	−97	

[a] Adjusted values: Δ_{pol} and Δ_1 corrected by −46 ppm as described in Ref. 16.
[b] Different convention was used to calculate the Pauli form factor contribution to Δ_1, which is equivalent to the approximate formula in the limit of $m = 0$ used for H in Ref. 11.
[c] Elastic form factors from Ref. 17 and updated error analysis from Ref. 16. Note that this result already includes radiative corrections for the Zemach-radius contribution, $(1+\delta_Z^{\text{rad}})\Delta_Z$ with $\delta_Z^{\text{rad}} \sim 0.0153$ (18, 19), as well as higher-order recoil corrections with the proton anomalous magnetic moment, cf. (11, Eq. 22) and (18).
[d] Uses r_p from μH (20) as input.

2γ EFFECT IN THE μH HFS

Table 1 Forward 2γ-exchange contribution to the HFS in μH.

Reference	Δ_Z [ppm]	Δ_{recoil} [ppm]	Δ_{pol} [ppm]	Δ_1 [ppm]	Δ_2 [ppm]	$E^{\langle 2\gamma \rangle}_{1S\text{-hfs}}$ [meV]
DATA-DRIVEN						
Pachucki '96 (1)	−8025	1666	0(658)			−1.160
Faustov et al. '01 (9)[a]	−7180		410(80)	468	−58	
Faustov et al. '06 (10)[b]			470(104)	518	−48	
Carlson et al. '11 (11)[c]	−7703	931	351(114)	370(112)	−19(19)	−1.171(39)
Tomalak '18 (12)[d]	−7333(48)	846(6)	364(89)	429(84)	−65(20)	−1.117(19)
HEAVY-BARYON χPT						
Peset et al. '17 (13)						−1.161(20)
LEADING-ORDER χPT						
Hagelstein et al. '16 (14)			37(95)	29(90)	9(29)	
+ Δ(1232) EXCIT.						
Hagelstein et al. '18 (15)			−13	84	−97	

[a] Adjusted values: Δ_{pol} and Δ_1 corrected by −46 ppm as described in Ref. 16.
[b] Different convention was used to calculate the Pauli form factor contribution to Δ_1, which is equivalent to the approximate formula in the limit of $m = 0$ used for H in Ref. 11.
[c] Elastic form factors from Ref. 17 and updated error analysis from Ref. 16. Note that this result already includes radiative corrections for the Zemach-radius contribution, $(1+\delta_Z^{\rm rad})\Delta_Z$ with $\delta_Z^{\rm rad} \sim 0.0153$ (18, 19), as well as higher-order recoil corrections with the proton anomalous magnetic moment, cf. (11, Eq. 22) and (18).
[d] Uses r_p from μH (20) as input.

Assuming ChPT is working, it should be best applicable to atomic systems, where the energies are very small !

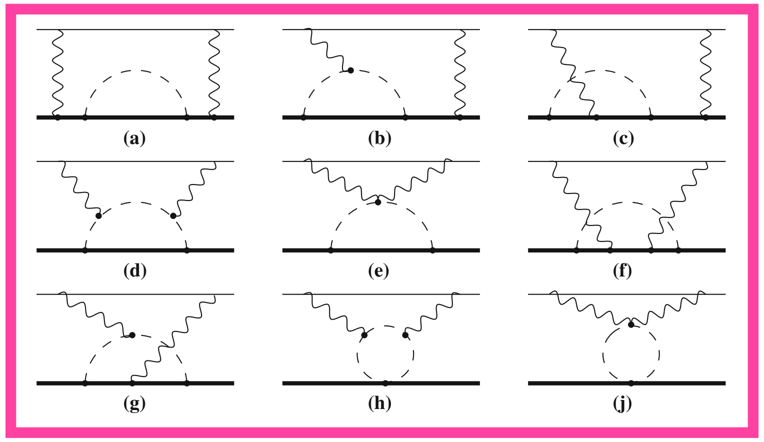

2γ EFFECT IN THE μH HFS

Table 1 Forward 2γ-exchange contribution to the HFS in μH.

Reference	Δ_Z [ppm]	Δ_{recoil} [ppm]	Δ_{pol} [ppm]	Δ_1 [ppm]	Δ_2 [ppm]	$E^{\langle 2\gamma\rangle}_{1S\text{-hfs}}$ [meV]
DATA-DRIVEN						
Pachucki '96 (1)	−8025	1666	0(658)			−1.160
Faustov et al. '01 (9)[a]	−7180		410(80)	468	−58	
Faustov et al. '06 (10)[b]			470(104)	518	−48	
Carlson et al. '11 (11)[c]	−7703	931	351(114)	370(112)	−19(19)	−1.171(39)
Tomalak '18 (12)[d]	−7333(48)	846(6)	364(89)	429(84)	−65(20)	−1.117(19)
HEAVY-BARYON χPT						
Peset et al. '17 (13)						−1.161(20)
LEADING-ORDER χPT						
Hagelstein et al. '16 (14)			37(95)	29(90)	9(29)	
+ $\Delta(1232)$ EXCIT.						
Hagelstein et al. '18 (15)			−13	84	−97	

[a]Adjusted values: Δ_{pol} and Δ_1 corrected by −46 ppm as described in Ref. 16.
[b]Different convention was used to calculate the Pauli form factor contribution to Δ_1, which is equivalent to the approximate formula in the limit of $m = 0$ used for H in Ref. 11.
[c]Elastic form factors from Ref. 17 and updated error analysis from Ref. 16. Note that this result already includes radiative corrections for the Zemach-radius contribution, $(1+\delta_Z^{\text{rad}})\Delta_Z$ with $\delta_Z^{\text{rad}} \sim 0.0153$ (18, 19), as well as higher-order recoil corrections with the proton anomalous magnetic moment, cf. (11, Eq. 22) and (18).
[d]Uses r_p from μH (20) as input.

Assuming ChPT is working, it should be best applicable to atomic systems, where the energies are very small !

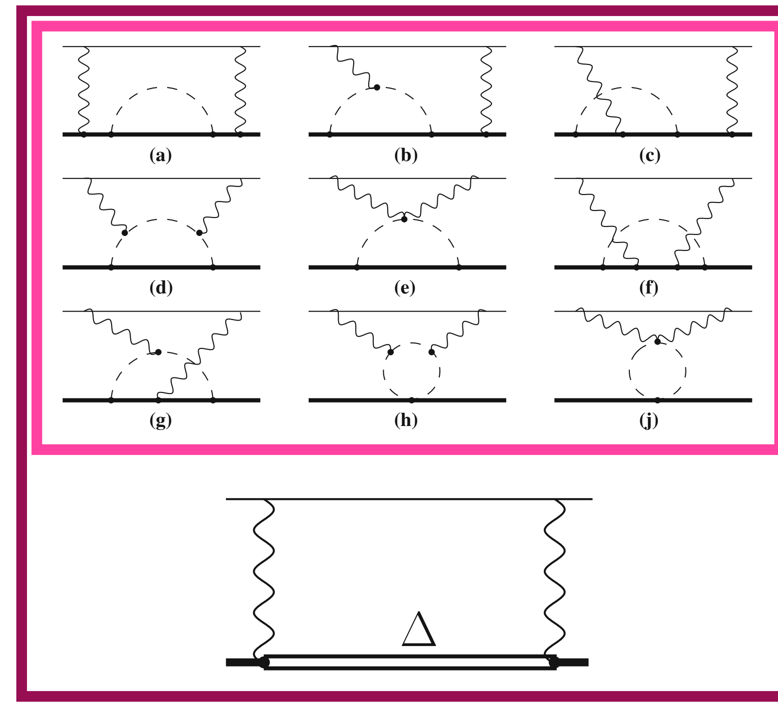

POLARIZABILITY EFFECT IN HFS

- Polarizability effect on the HFS is completely constrained by empirical information

$$\Delta_{\text{pol.}} = \Delta_1 + \Delta_2 = \frac{\alpha m}{2\pi(1+\kappa)M}\left(\delta_1 + \delta_2\right)$$

$$\delta_1 = 2\int_0^\infty \frac{\mathrm{d}Q}{Q}\left\{\frac{5+4v_l}{(v_l+1)^2}\left[4I_1(Q^2)+F_2^2(Q^2)\right] - \frac{32M^4}{Q^4}\int_0^{x_0}\mathrm{d}x\, x^2 g_1(x,Q^2)\frac{1}{(v_l+v_x)(1+v_x)(1+v_l)}\left(4+\frac{1}{1+v_x}+\frac{1}{v_l+1}\right)\right\}$$

$$\delta_2 = 96M^2\int_0^\infty \frac{\mathrm{d}Q}{Q^3}\int_0^{x_0}\mathrm{d}x\, g_2(x,Q^2)\left(\frac{1}{v_l+v_x}-\frac{1}{v_l+1}\right)$$

with $v_l = \sqrt{1+\frac{1}{\tau_l}}$, $v_x = \sqrt{1+x^2\tau^{-1}}$, $\tau_l = \frac{Q^2}{4m^2}$ and $\tau = \frac{Q^2}{4M^2}$

POLARIZABILITY EFFECT IN HFS

- Polarizability effect on the HFS is completely constrained by empirical information

$$\Delta_{\text{pol.}} = \Delta_1 + \Delta_2 = \frac{\alpha m}{2\pi(1+\kappa)M}(\delta_1 + \delta_2)$$

$$\delta_1 = 2\int_0^\infty \frac{\mathrm{d}Q}{Q}\left\{\frac{5+4v_l}{(v_l+1)^2}\left[4I_1(Q^2)+F_2^2(Q^2)\right] - \frac{32M^4}{Q^4}\int_0^{x_0}\mathrm{d}x\, x^2 g_1(x,Q^2)\frac{1}{(v_l+v_x)(1+v_x)(1+v_l)}\left(4+\frac{1}{1+v_x}+\frac{1}{v_l+1}\right)\right\}$$

$$\delta_2 = 96M^2\int_0^\infty \frac{\mathrm{d}Q}{Q^3}\int_0^{x_0}\mathrm{d}x\, g_2(x,Q^2)\left(\frac{1}{v_l+v_x}-\frac{1}{v_l+1}\right)$$

with $v_l = \sqrt{1+\frac{1}{\tau_l}}$, $v_x = \sqrt{1+x^2\tau^{-1}}$, $\tau_l = \frac{Q^2}{4m^2}$ and $\tau = \frac{Q^2}{4M^2}$

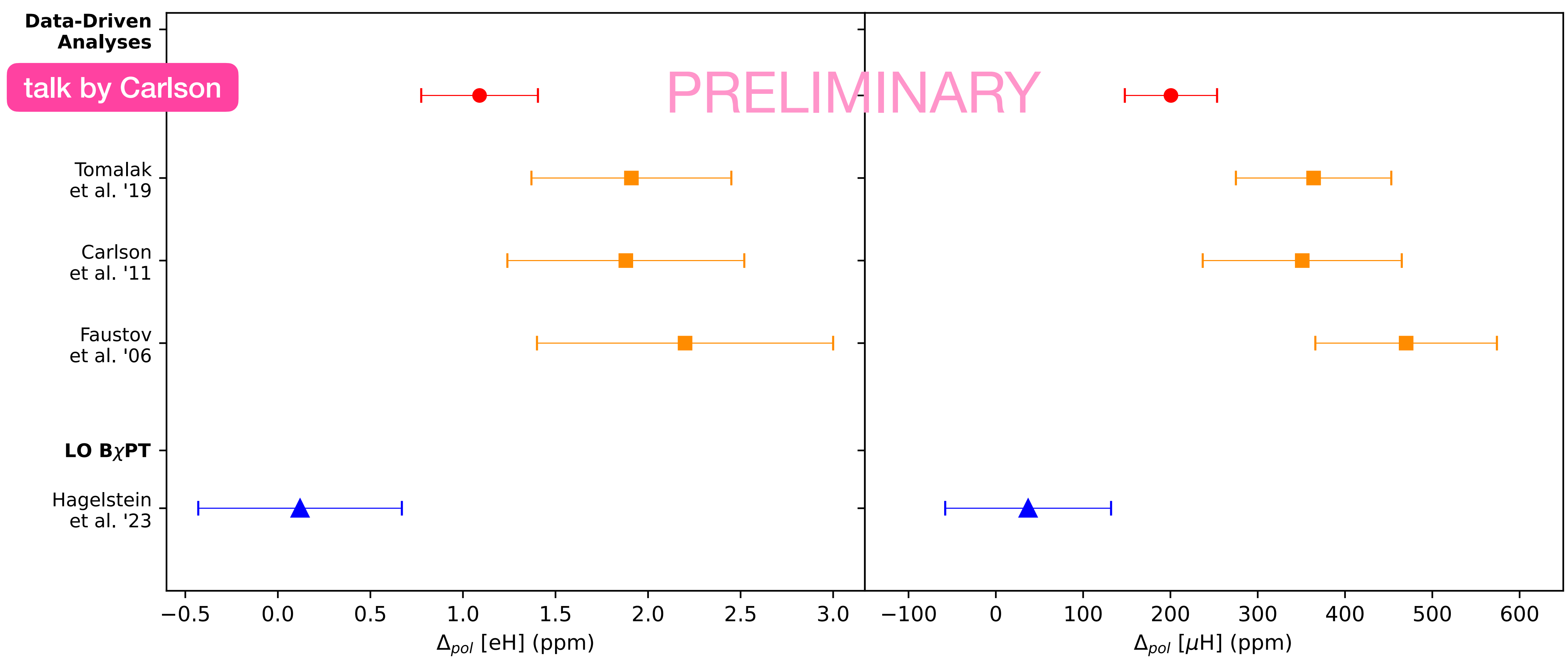

POLARIZABILITY EFFECT FROM BCHPT

- Low-Q region is very important!
- LO BChPT result is compatible with zero
  - Contributions from σ_{LT} and σ_{TT} are sizeable and largely cancel each other

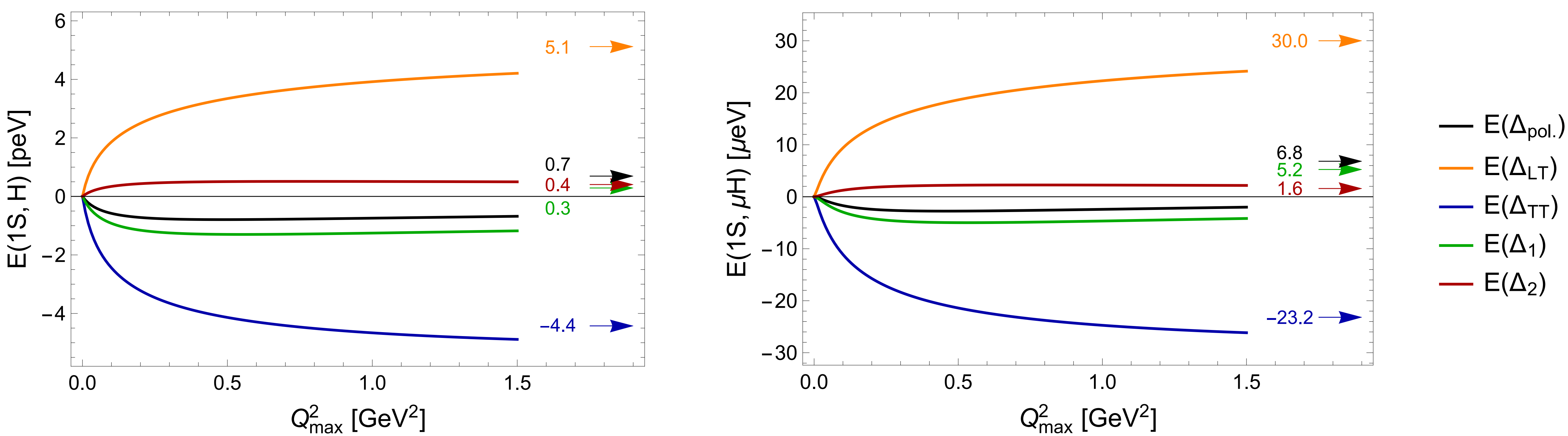

PROTON ZEMACH RADIUS

- BChPT polarizability prediction implies smaller Zemach radius (smaller, just like r_p)

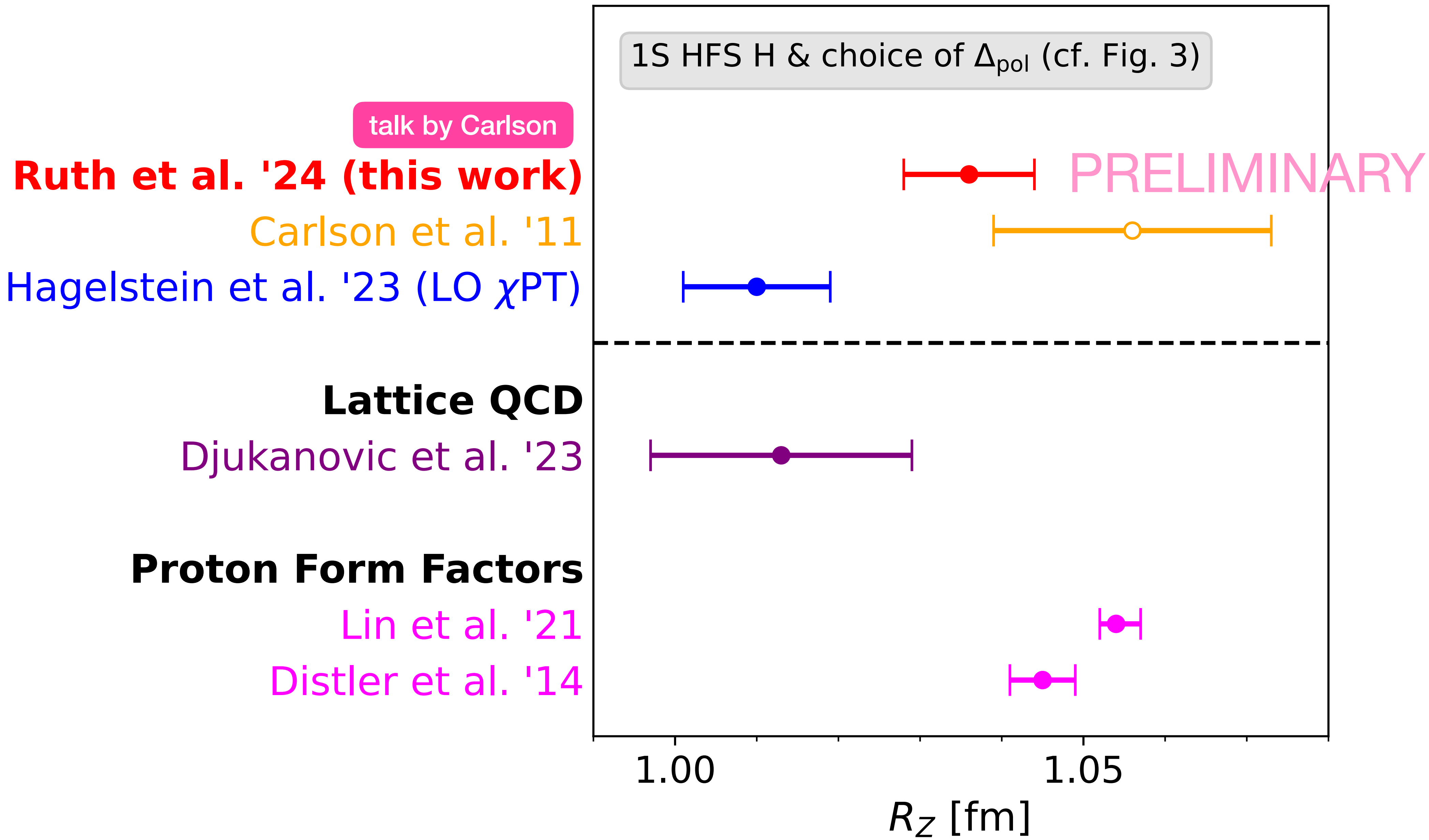

CORRELATION OF PROTON RADII

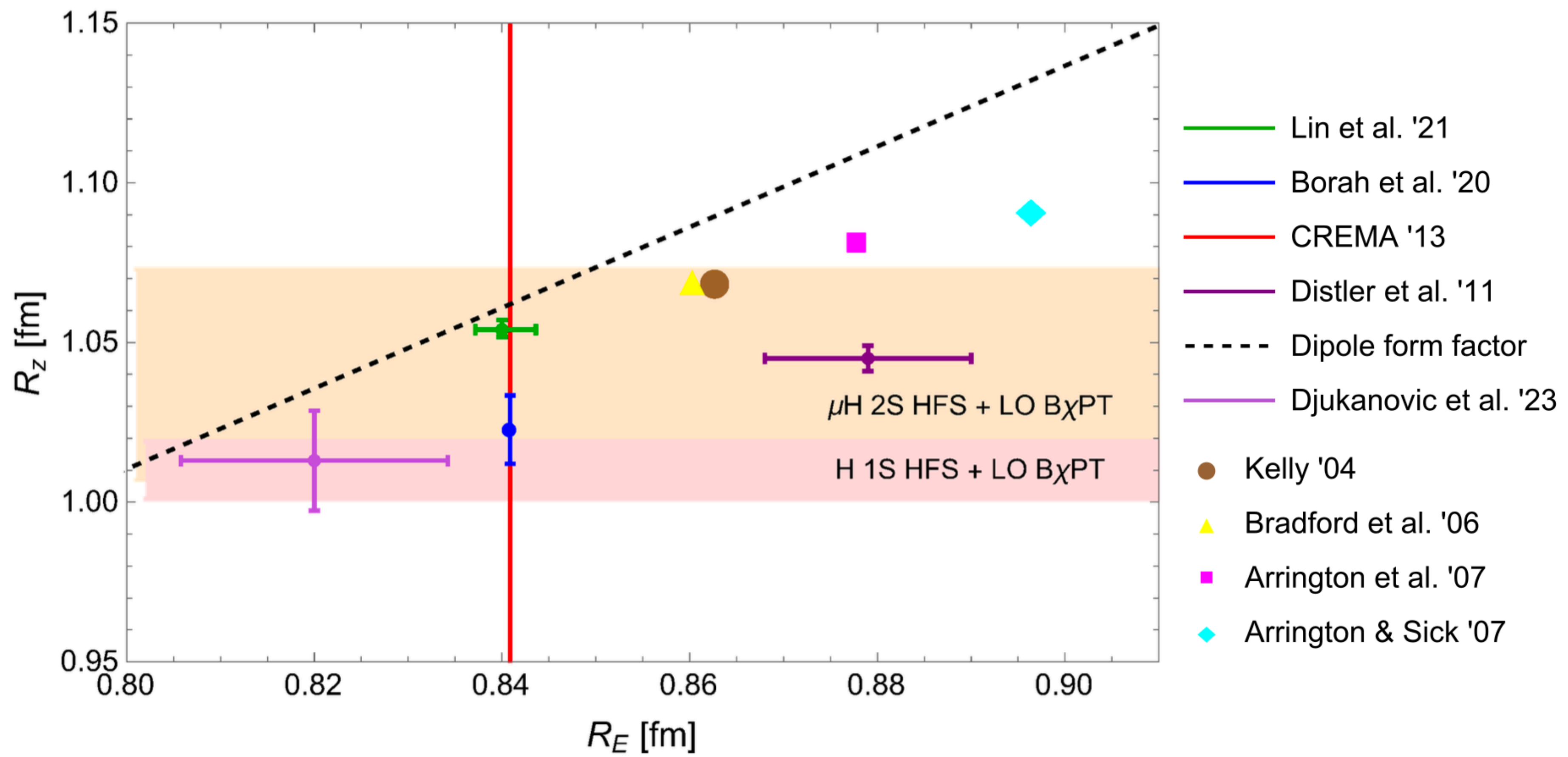

CORRELATION OF PROTON RADII

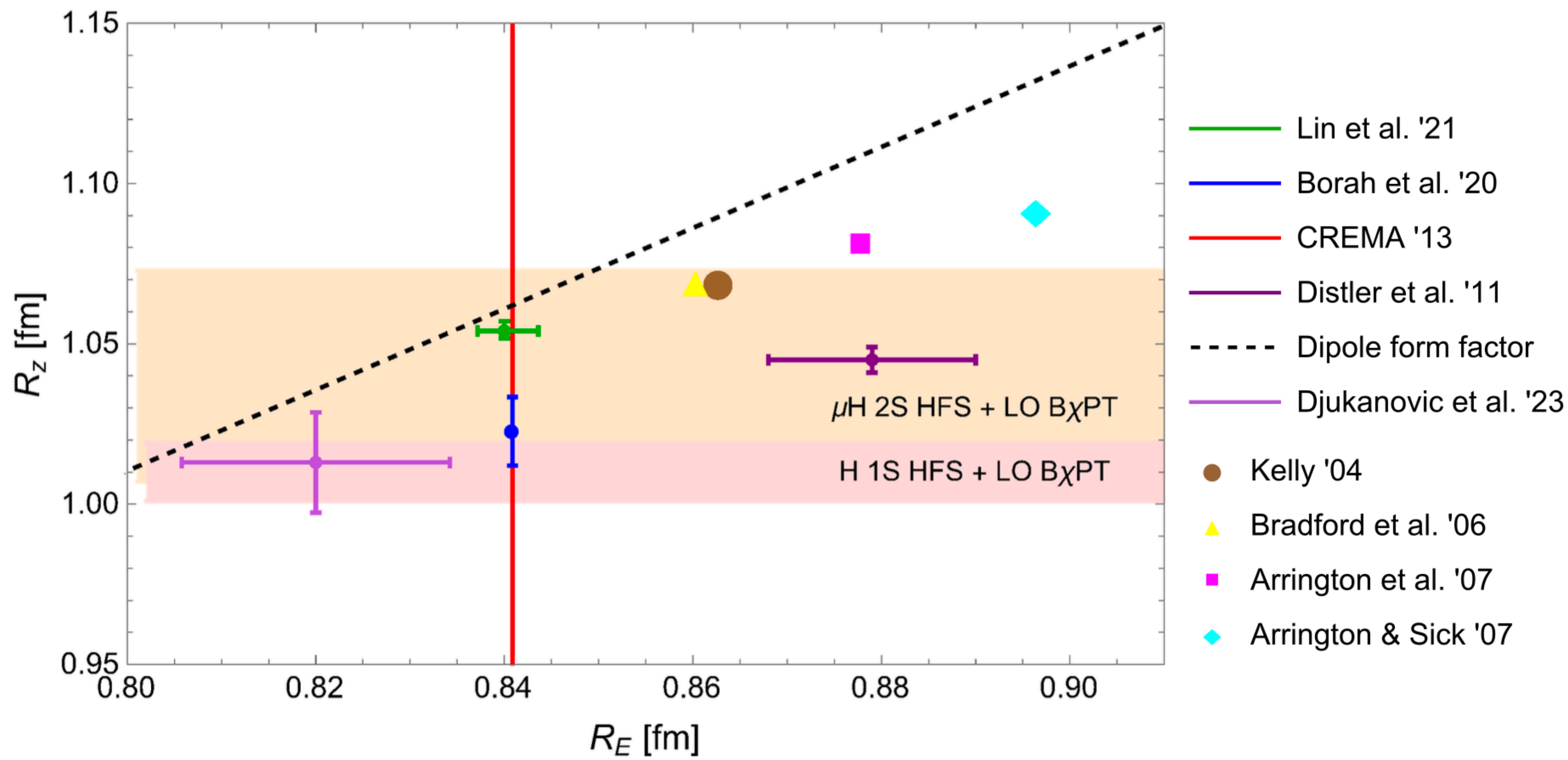

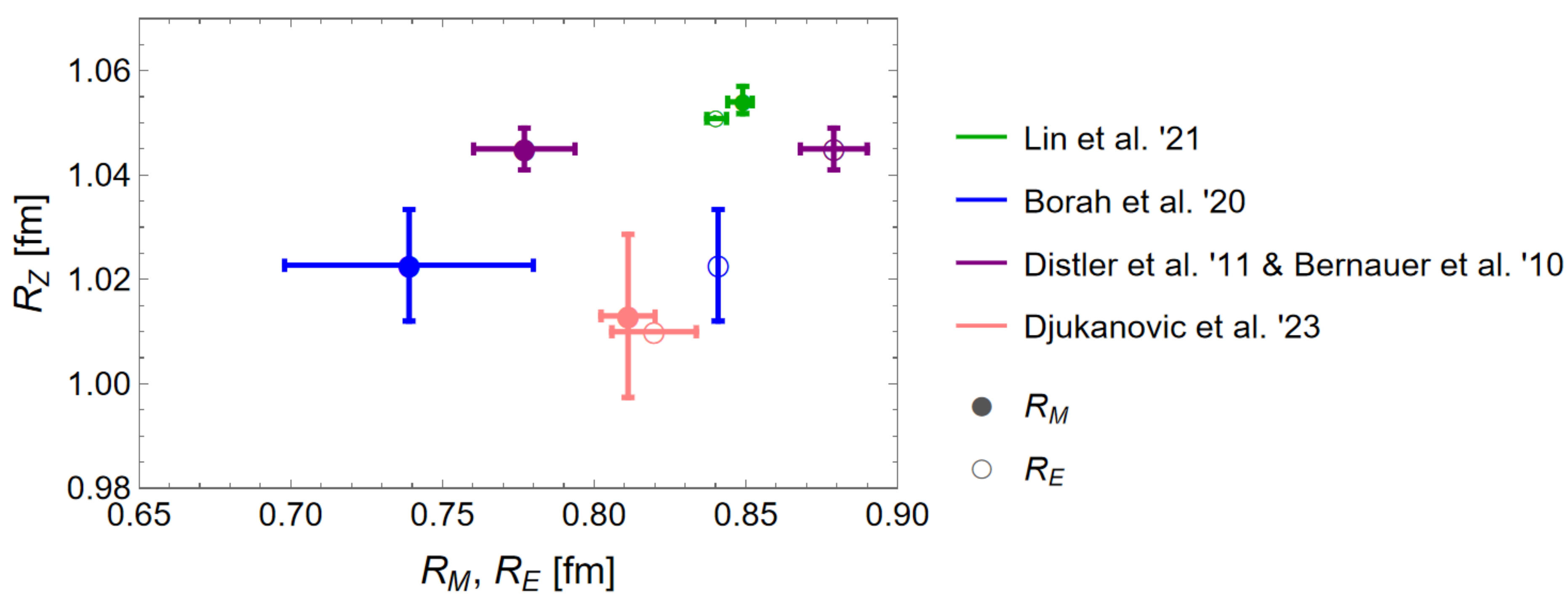

— Proton Magnetic Radius —

MAGNETIC RADIUS FROM INELASTIC SCATTERING

- Burkhardt-Cottingham sum rule relates elastic form factors to the zeroth moment of an inelastic spin structure function:

$$I_2(Q^2) = \frac{2M^2}{Q^2}\int_0^{x_0} \mathrm{d}x\, g_2(x,Q^2) = \frac{1}{4}F_2(Q^2)G_M(Q^2)$$

- Constrain the magnetic radius through inelastic scattering:

$$R_M = \left[\frac{1}{1+2\kappa}\left(-\frac{24 I_2'(0)}{1+\kappa} - \frac{3\kappa}{2M^2} + \langle r^2\rangle_E\right)\right]^{1/2}$$

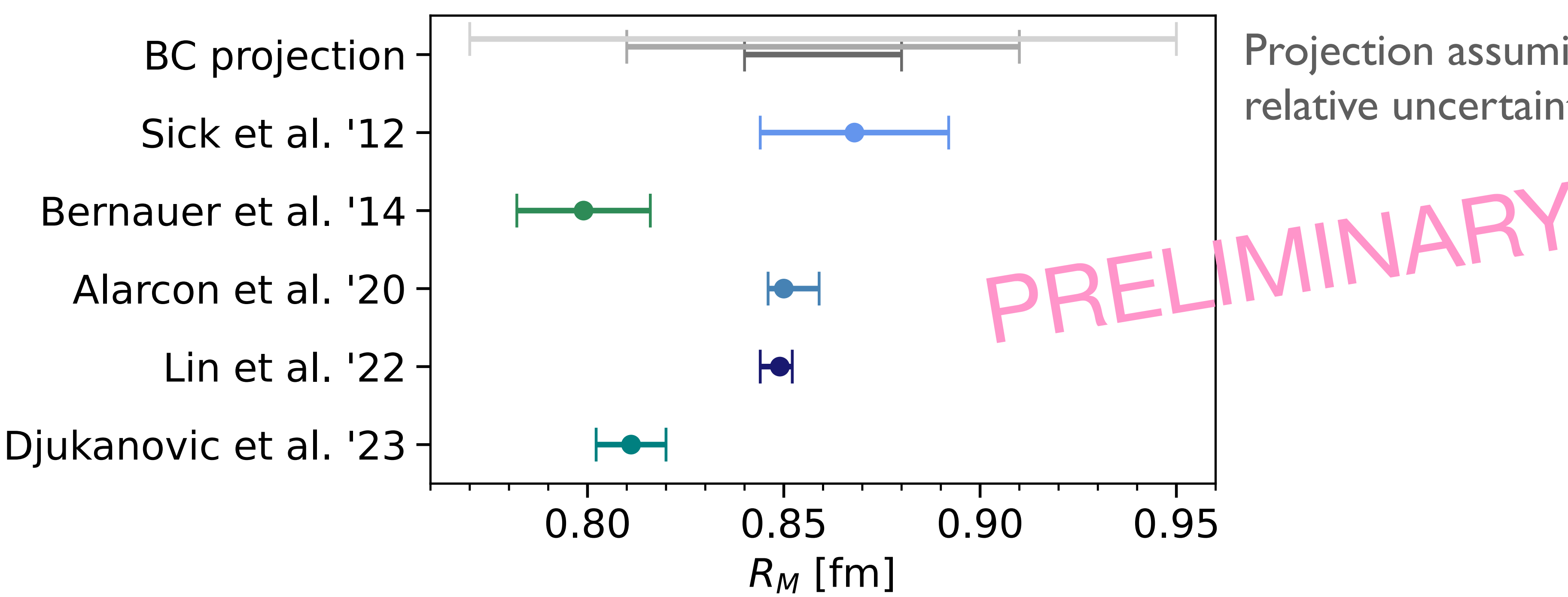

Projection assuming 25 %, 15 % and 5 % relative uncertainty for $I_2'(0)$

LOWER BOUND ON PROTON MAGNETIC RADIUS

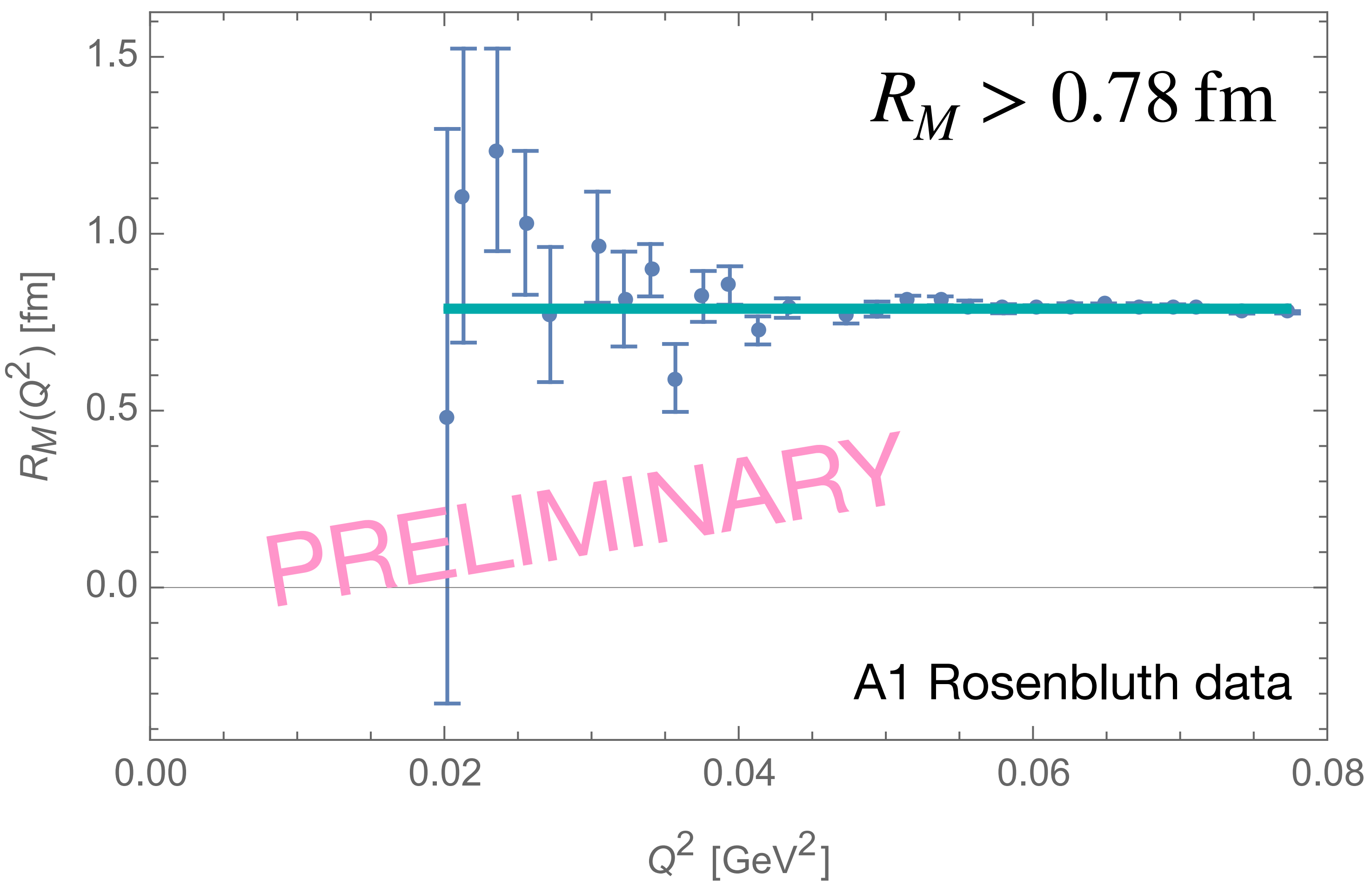

LOWER BOUND ON PROTON MAGNETIC RADIUS

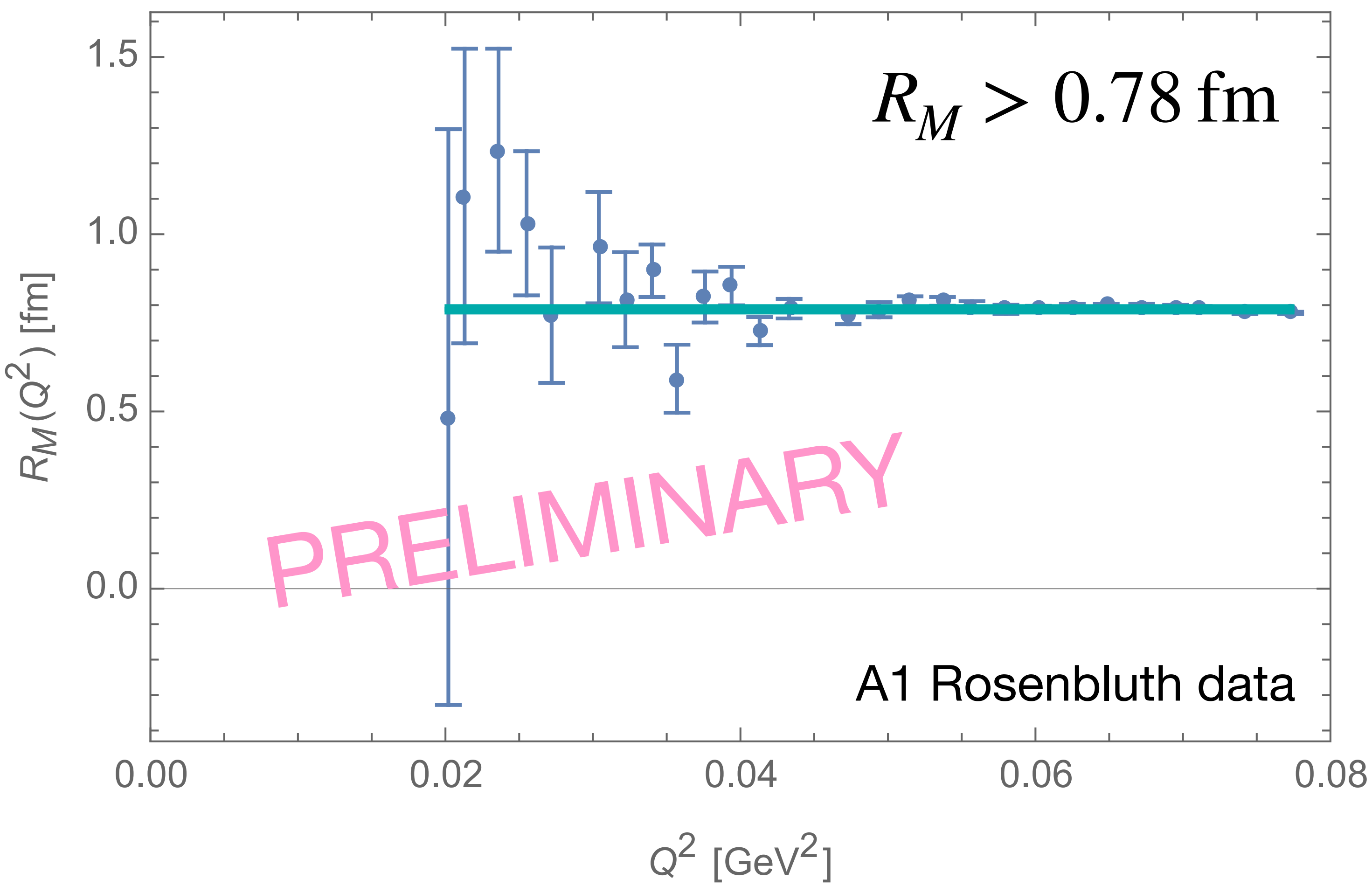

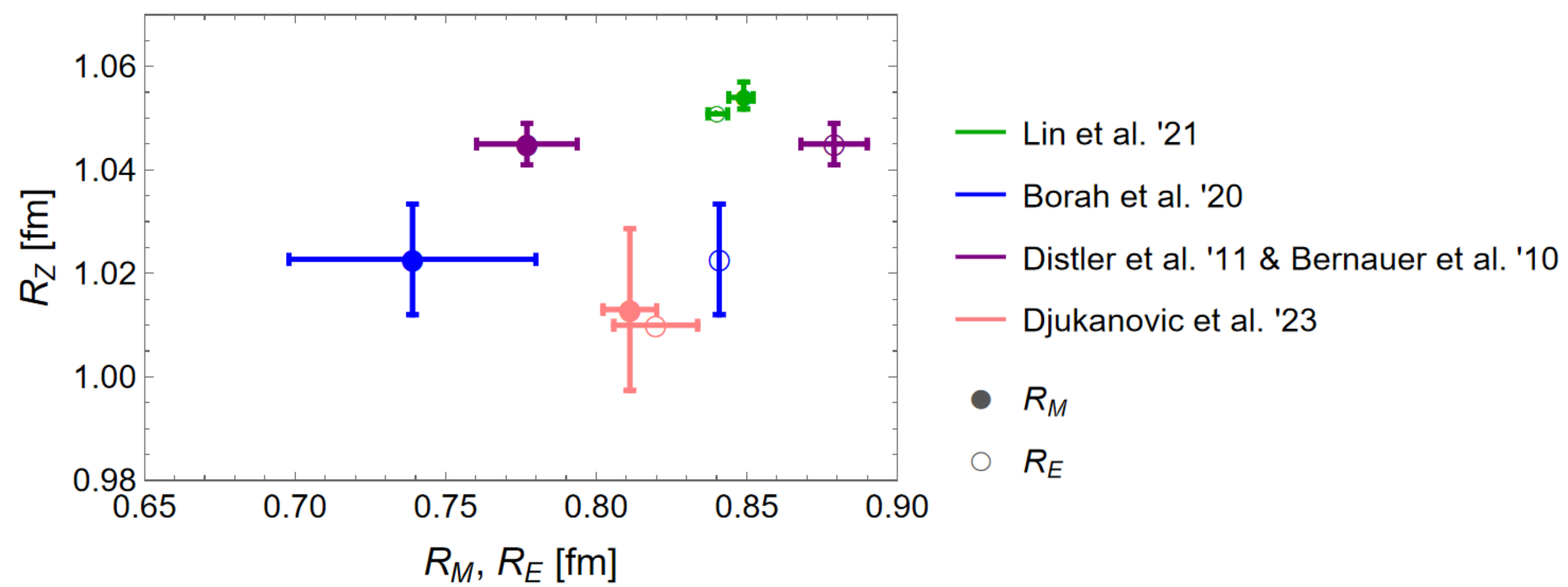

— Proton Friar Radius —

CORRELATION OF CHARGE AND FRIAR RADII

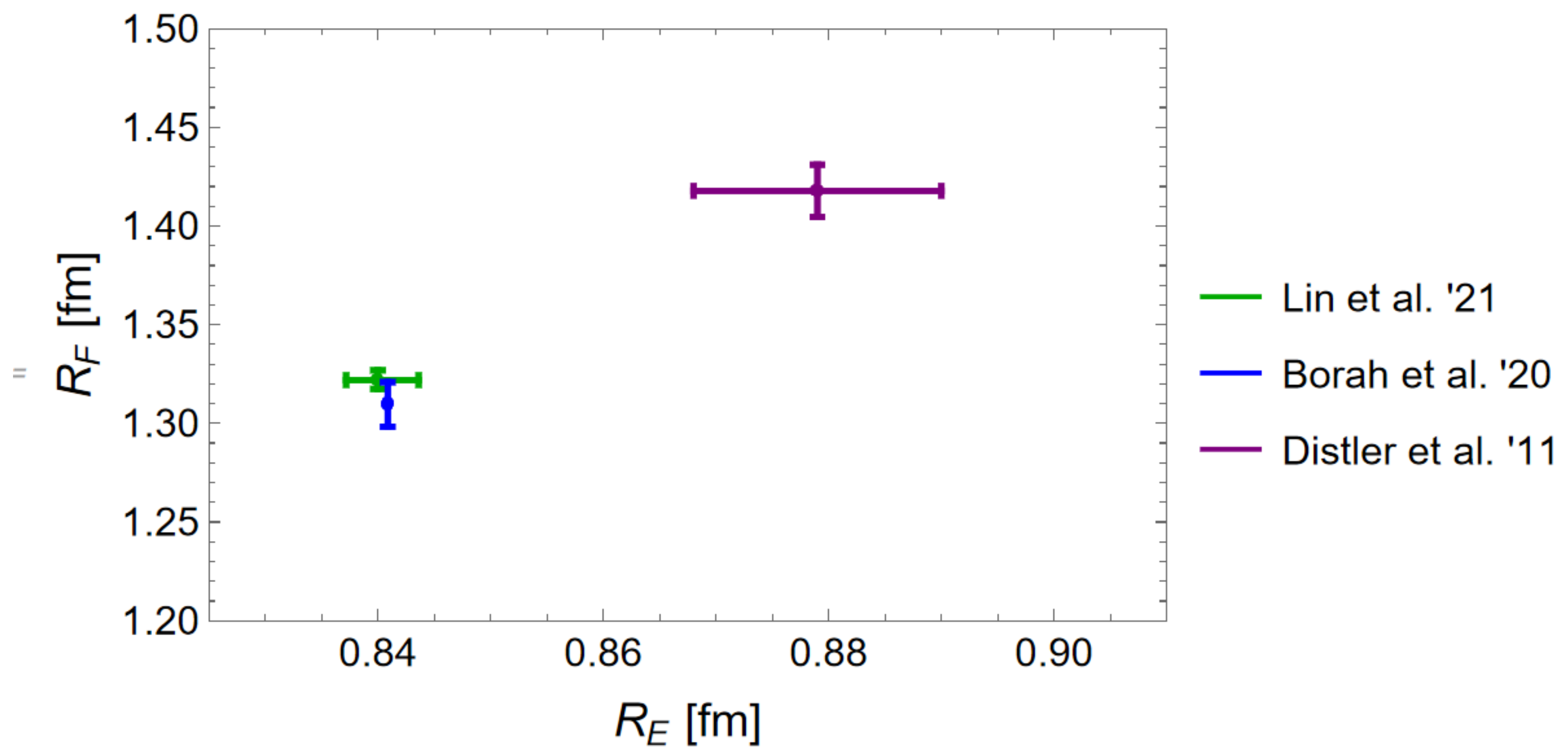

Friar radius or 3rd Zemach moment

$$R_F = \sqrt[3]{\langle r^3 \rangle_{E(2)}},$$

$$\langle r^3 \rangle_{E(2)} \equiv \int \mathrm{d}\boldsymbol{r}\, r^3\, \varrho_{E(2)}(r), \quad \text{with} \quad \varrho_{E(2)}(r) = \int \mathrm{d}\boldsymbol{r}'\, \varrho_E(|\boldsymbol{r}' - \boldsymbol{r}|)\, \varrho_E(\boldsymbol{r}'),$$

$$\equiv \frac{48}{\pi} \int_0^\infty \frac{\mathrm{d}Q}{Q^4} \left[G_E^2(Q^2) - 1 + \tfrac{1}{3} R_E^2\, Q^2 \right];$$

charge radius

CORRELATION OF CHARGE AND FRIAR RADII

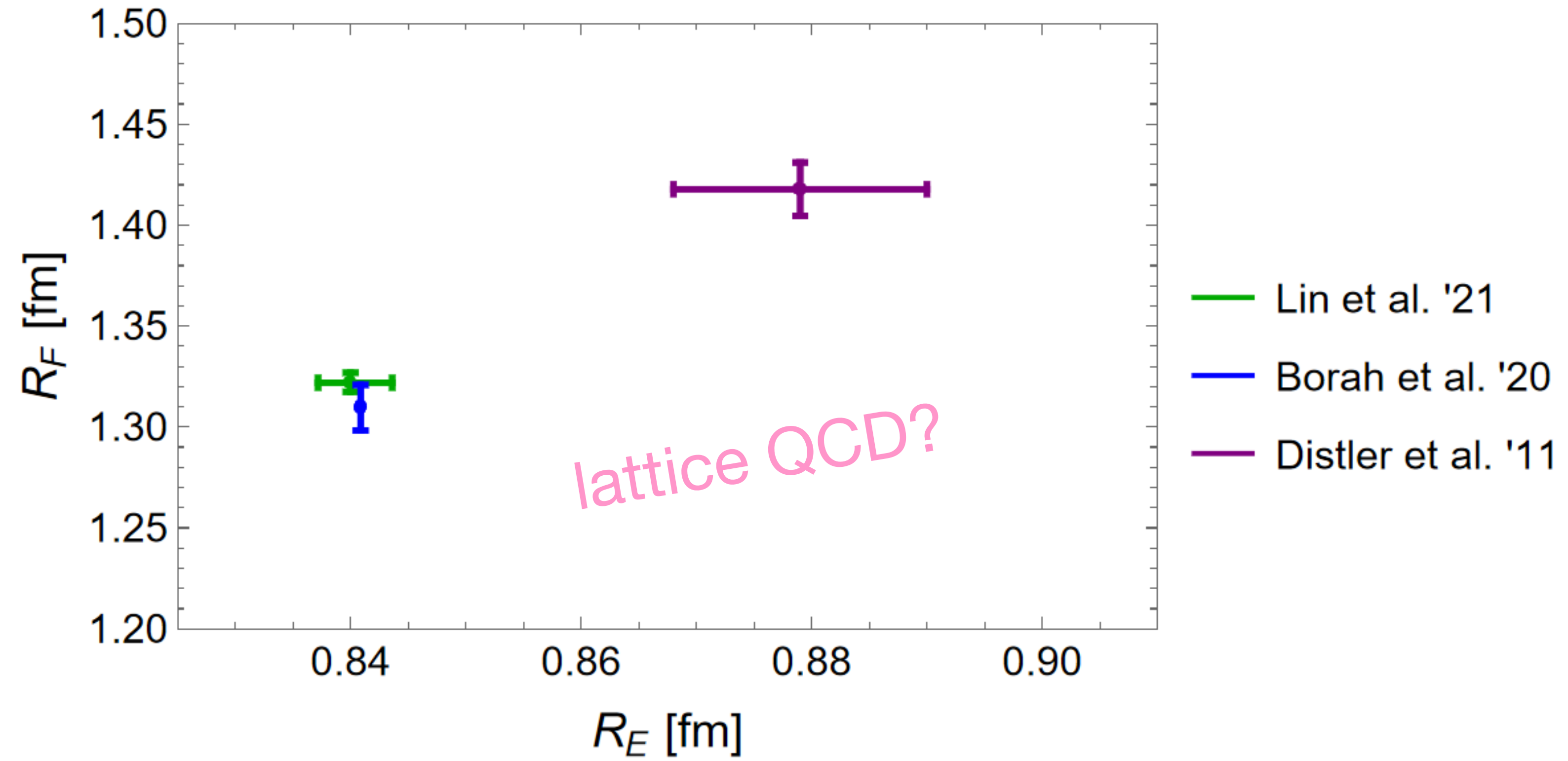

Friar radius or 3rd Zemach moment

$$R_{\mathrm{F}} = \sqrt[3]{\langle r^3 \rangle_{E(2)}},$$

$$\langle r^3 \rangle_{E(2)} \equiv \int \mathrm{d}\boldsymbol{r}\, r^3\, \varrho_{E(2)}(r), \quad \text{with} \quad \varrho_{E(2)}(r) = \int \mathrm{d}\boldsymbol{r'}\, \varrho_E(|\boldsymbol{r'} - \boldsymbol{r}|)\, \varrho_E(\boldsymbol{r'}),$$

$$\equiv \frac{48}{\pi} \int_0^\infty \frac{\mathrm{d}Q}{Q^4} \left[G_E^2(Q^2) - 1 + \tfrac{1}{3} R_E^2 Q^2 \right];$$

charge radius

FRIAR RADIUS IN μH LAMB SHIFT

- Elastic TPE splits into Friar radius + recoil part

Table 1 **Forward 2γ-exchange contributions to the $2S$ shift in muonic hydrogen (μeV)**

Reference	$E_{2S}^{(\mathrm{subt})}$	$E_{2S}^{(\mathrm{inel})}$	$E_{2S}^{(\mathrm{pol})}$	$E_{2S}^{(\mathrm{el})}$	$E_{2S}^{(2\gamma)}$
Data-driven dispersive evaluation					
Pachucki 1999 (75)	1.9	−13.9	−12(2)	−23.2(1.0)	−35.2(2.2)
Martynenko 2006 (76)	2.3	−16.1	−13.8(2.9)		
Carlson et al. 2011 (77)	5.3(1.9)	−12.7(5)	−7.4(2.0)		
Birse & McGovern 2012 (78)	4.2(1.0)	−12.7(5)	−8.5(1.1)	−24.7(1.6)	−33(2)
Gorchtein et al. 2013 (79)[a]	−2.3(4.6)	−13.0(6)	−15.3(4.6)	−24.5(1.2)	−39.8(4.8)
Hill & Paz 2017 (80)					−30(13)
Tomalak 2019 (81)	2.3(1.3)		−10.3(1.4)	−18.6(1.6)	−29.0(2.1)
Leading-order baryon chiral perturbation theory					
Alarcón et al. 2014 (82)			$-9.6^{+1.4}_{-2.9}$		
Lensky et al. 2018 (83)[b]	$3.5^{+0.5}_{-1.9}$	−12.1(1.8)	$-8.6^{+1.3}_{-5.2}$		
Lattice QCD					
Fu et al. 2022 (84)					−37.4(4.9)

FRIAR RADIUS IN μH LAMB SHIFT

- Elastic TPE splits into Friar radius + recoil part

compare to future exp.
uncertainty ~ 0.4 μeV

Table 1 Forward 2γ-exchange contributions to the 2S shift in muonic hydrogen (μeV)

Reference	$E_{2S}^{(subt)}$	$E_{2S}^{(inel)}$	$E_{2S}^{(pol)}$	$E_{2S}^{(el)}$	$E_{2S}^{(2\gamma)}$
Data-driven dispersive evaluation					
Pachucki 1999 (75)	1.9	−13.9	−12(2)	−23.2(1.0)	−35.2(2.2)
Martynenko 2006 (76)	2.3	−16.1	−13.8(2.9)		
Carlson et al. 2011 (77)	5.3(1.9)	−12.7(5)	−7.4(2.0)		
Birse & McGovern 2012 (78)	4.2(1.0)	−12.7(5)	−8.5(1.1)	−24.7(1.6)	−33(2)
Gorchtein et al. 2013 (79)[a]	−2.3(4.6)	−13.0(6)	−15.3(4.6)	−24.5(1.2)	−39.8(4.8)
Hill & Paz 2017 (80)					−30(13)
Tomalak 2019 (81)	2.3(1.3)		−10.3(1.4)	−18.6(1.6)	−29.0(2.1)
Leading-order baryon chiral perturbation theory					
Alarcón et al. 2014 (82)			$-9.6^{+1.4}_{-2.9}$		
Lensky et al. 2018 (83)[b]	$3.5^{+0.5}_{-1.9}$	−12.1(1.8)	$-8.6^{+1.3}_{-5.2}$		
Lattice QCD					
Fu et al. 2022 (84)					−37.4(4.9)

FRIAR RADIUS IN μH LAMB SHIFT

- Elastic TPE splits into Friar radius + recoil part
  - Recoil is small for μH ~ 0.03(5) μeV [Karshenboim et al., PRD 91 (2015) 073003]

compare to future exp.
uncertainty ~ 0.4 μeV

Table 1 **Forward 2γ-exchange contributions to the 2S shift in muonic hydrogen (μeV)**

Reference	$E_{2S}^{(\mathrm{subt})}$	$E_{2S}^{(\mathrm{inel})}$	$E_{2S}^{(\mathrm{pol})}$	$E_{2S}^{(\mathrm{el})}$	$E_{2S}^{(2\gamma)}$
Data-driven dispersive evaluation					
Pachucki 1999 (75)	1.9	−13.9	−12(2)	−23.2(1.0)	−35.2(2.2)
Martynenko 2006 (76)	2.3	−16.1	−13.8(2.9)		
Carlson et al. 2011 (77)	5.3(1.9)	−12.7(5)	−7.4(2.0)		
Birse & McGovern 2012 (78)	4.2(1.0)	−12.7(5)	−8.5(1.1)	−24.7(1.6)	−33(2)
Gorchtein et al. 2013 (79)[a]	−2.3(4.6)	−13.0(6)	−15.3(4.6)	−24.5(1.2)	−39.8(4.8)
Hill & Paz 2017 (80)					−30(13)
Tomalak 2019 (81)	2.3(1.3)		−10.3(1.4)	−18.6(1.6)	−29.0(2.1)
Leading-order baryon chiral perturbation theory					
Alarcón et al. 2014 (82)			$-9.6^{+1.4}_{-2.9}$		
Lensky et al. 2018 (83)[b]	$3.5^{+0.5}_{-1.9}$	−12.1(1.8)	$-8.6^{+1.3}_{-5.2}$		
Lattice QCD					
Fu et al. 2022 (84)					−37.4(4.9)

FRIAR RADIUS IN μH LAMB SHIFT

- Elastic TPE splits into Friar radius + recoil part
  - Recoil is small for μH ~ 0.03(5) μeV [Karshenboim et al., PRD 91 (2015) 073003]
  - $E_{2S}^{\mathrm{el}} = -21.1(2)$ μeV based on $R_F^3 = 2.310(26)$ fm^3 [Lin et al. (2022), PRL]

compare to future exp.
uncertainty ~ 0.4 μeV

Table 1 Forward 2γ-exchange contributions to the 2S shift in muonic hydrogen (μeV)

Reference	$E_{2S}^{(\mathrm{subt})}$	$E_{2S}^{(\mathrm{inel})}$	$E_{2S}^{(\mathrm{pol})}$	$E_{2S}^{(\mathrm{el})}$	$E_{2S}^{(2\gamma)}$
Data-driven dispersive evaluation					
Pachucki 1999 (75)	1.9	−13.9	−12(2)	−23.2(1.0)	−35.2(2.2)
Martynenko 2006 (76)	2.3	−16.1	−13.8(2.9)		
Carlson et al. 2011 (77)	5.3(1.9)	−12.7(5)	−7.4(2.0)		
Birse & McGovern 2012 (78)	4.2(1.0)	−12.7(5)	−8.5(1.1)	−24.7(1.6)	−33(2)
Gorchtein et al. 2013 (79)[a]	−2.3(4.6)	−13.0(6)	−15.3(4.6)	−24.5(1.2)	−39.8(4.8)
Hill & Paz 2017 (80)					−30(13)
Tomalak 2019 (81)	2.3(1.3)		−10.3(1.4)	−18.6(1.6)	−29.0(2.1)
Leading-order baryon chiral perturbation theory					
Alarcón et al. 2014 (82)			$-9.6^{+1.4}_{-2.9}$		
Lensky et al. 2018 (83)[b]	$3.5^{+0.5}_{-1.9}$	−12.1(1.8)	$-8.6^{+1.3}_{-5.2}$		
Lattice QCD					
Fu et al. 2022 (84)					−37.4(4.9)

FRIAR RADIUS IN μH LAMB SHIFT

- Elastic TPE splits into Friar radius + recoil part
  - Recoil is small for μH ~ 0.03(5) μeV [Karshenboim et al., PRD 91 (2015) 073003]
  - $E^{\mathrm{el}}_{2S} = -21.1(2)$ μeV based on $R^3_F = 2.310(26)$ fm^3 [Lin et al. (2022), PRL]
- Aim: self-consistent extraction of from spectroscopy [Karshenboim, PRD 90 (2014) 053012]

compare to future exp. uncertainty ~ 0.4 μeV

Table 1 Forward 2γ-exchange contributions to the 2S shift in muonic hydrogen (μeV)

Reference	$E^{(\mathrm{subt})}_{2S}$	$E^{(\mathrm{inel})}_{2S}$	$E^{(\mathrm{pol})}_{2S}$	$E^{(\mathrm{el})}_{2S}$	$E^{(2\gamma)}_{2S}$
Data-driven dispersive evaluation					
Pachucki 1999 (75)	1.9	−13.9	−12(2)	−23.2(1.0)	−35.2(2.2)
Martynenko 2006 (76)	2.3	−16.1	−13.8(2.9)		
Carlson et al. 2011 (77)	5.3(1.9)	−12.7(5)	−7.4(2.0)		
Birse & McGovern 2012 (78)	4.2(1.0)	−12.7(5)	−8.5(1.1)	−24.7(1.6)	−33(2)
Gorchtein et al. 2013 (79)[a]	−2.3(4.6)	−13.0(6)	−15.3(4.6)	−24.5(1.2)	−39.8(4.8)
Hill & Paz 2017 (80)					−30(13)
Tomalak 2019 (81)	2.3(1.3)		−10.3(1.4)	−18.6(1.6)	−29.0(2.1)
Leading-order baryon chiral perturbation theory					
Alarcón et al. 2014 (82)			$-9.6^{+1.4}_{-2.9}$		
Lensky et al. 2018 (83)[b]	$3.5^{+0.5}_{-1.9}$	−12.1(1.8)	$-8.6^{+1.3}_{-5.2}$		
Lattice QCD					
Fu et al. 2022 (84)					−37.4(4.9)

← used Karshenboim 2014

DEUTERON CHARGE FORM FACTOR

V. Lensky, A. Hiller Blin, V. Pascalutsa, Phys. Rev. C **104** (2021) 054003

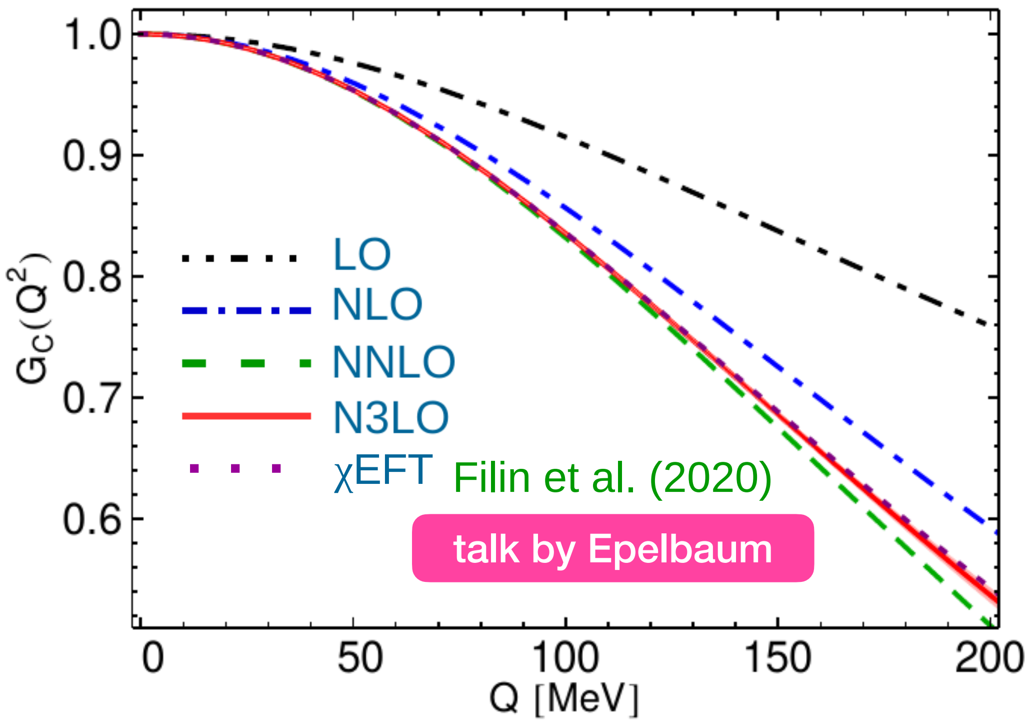

- Agreement of chiral and pionless EFT at N3LO
- Pionless EFT evaluation contains only one unknown low-energy constant l_1 of a longitudinal photon coupling to two nucleons

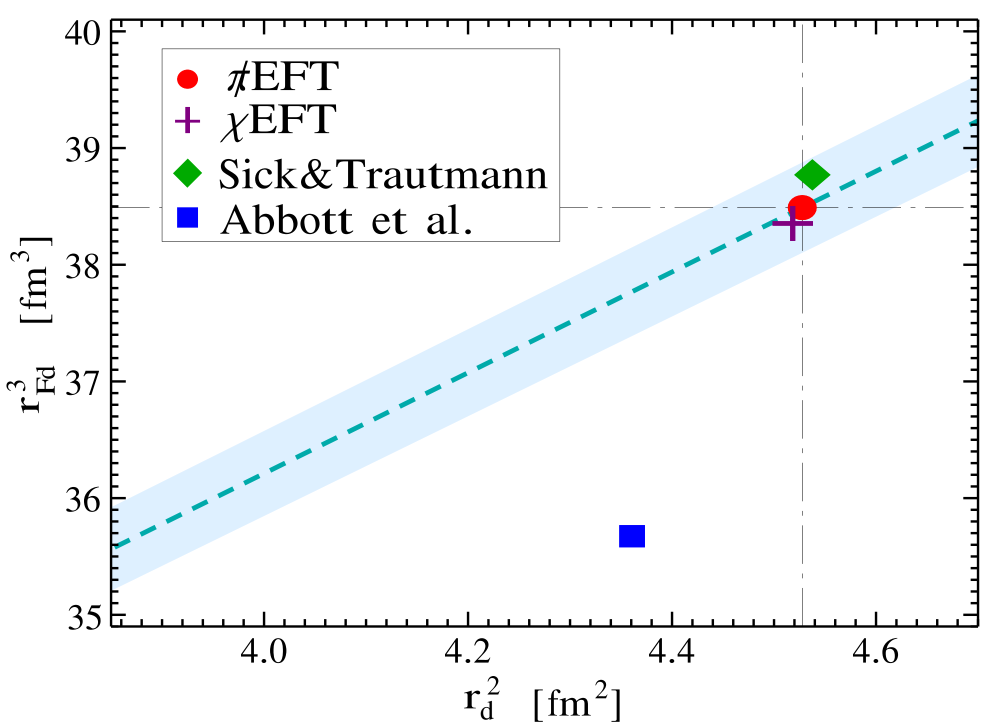

- Use r_d and r_{Fd} correlation to test low-Q properties of form factor parametrisations
- Abbott parametrisation gives different radii

Thank you for your attention!

LOWER BOUND

Lower bound on the proton charge radius from electron scattering data

Franziska Hagelstein [a], Vladimir Pascalutsa [b,*]

[a] Albert Einstein Center for Fundamental Physics, Institute for Theoretical Physics, University of Bern, Sidlerstrasse 5, CH-3012 Bern, Switzerland
[b] Institut für Kernphysik and Cluster of Excellence PRISMA, Johannes Gutenberg Universität Mainz, D-55128 Mainz, Germany

ARTICLE INFO

Article history:
Received 1 January 2019
Received in revised form 18 July 2019
Accepted 30 July 2019
Available online 1 August 2019
Editor: V. Metag

Keywords:
Charge radius
Proton size
Form factors
Charge distribution
Electron scattering

ABSTRACT

The proton charge-radius determinations from the electromagnetic form-factor measurements in electron-proton (*ep*) scattering require an extrapolation to zero momentum transfer ($Q^2 = 0$) which is prone to model-dependent assumptions. We show that the data at finite momentum transfer can be used to establish a rigorous lower bound on the proton charge radius, while bypassing the model-dependent assumptions that go into the fitting and extrapolation of the *ep* data. The near-future precise *ep* experiments at very low Q^2, such as PRad, are expected to set a stringent lower bound on the proton radius.

Disclaimer: "For illustrative purposes, we have made a tentative determination of the lower bound on the proton charge radius from the available data in the region of Q^2 below 0.02 GeV^2. … our uncertainty estimate is only indicative and should be taken with caution. The treatment of systematic errors, most notably the normalization uncertainty, is rather involved in this particular experiment and entangled with the radius extraction."

RMS CHARGE RADIUS

- RMS charge radius: $R_E^2 = -6\,\frac{\mathrm{d}\,G_E(Q^2)}{\mathrm{d}Q^2}\Big|_{Q^2=0} = 4\pi\int_0^\infty \mathrm{d}r\, r^4\,\rho_E(r)$
- $G_E(Q^2) = 4\pi\int_0^\infty \mathrm{d}r\, r^2\, j_0(Qr)\,\rho_E(r)$ with the spherically symmetric charge density $\rho_E(r)$ and the spherical Bessel function $j_0(x) = \frac{\sin x}{x}$
  - $G_E(Q^2)$ and $\rho_E(r)$ are Lorentz-invariant quantities
- Taylor expansion, $G_E(Q^2) = 1 - Q^2\,\langle r^2\rangle_E/6 + Q^4\,\langle r^4\rangle_E/120 + \ldots$, convergence radius is limited by the onset of the pion-production branch cut at $Q^2 \ll 4m_\pi^2 \sim 0.08\,\mathrm{GeV}^2$
  - Dispersive fits and z-expansion take singularities into account

EVALUATION OF THE LOWER BOUND

Lower-bound function: $R_E^2(Q^2) = -\dfrac{6}{Q^2}\log G_E(Q^2)$

- Each data point gives a lower bound — statistical average is used for a more accurate value
- Data below $Q^2 < 0.02\,\mathrm{GeV}^2$ away from pion-production branch cut
- Lower cut at $Q_0^2 \sim 0.01\,\mathrm{GeV}^2$
  - Assume a small normalization error ϵ, such that $G_E^{(\mathrm{exp})} = (1+\epsilon)\,G_E$
  - Lower-bound function observed in experiment: $R_E^{2(\mathrm{exp})}(Q^2) = R_E^2(Q^2) - \dfrac{6}{Q^2}\ln(1+\epsilon)$
    - Lower bound is preserved, $R_E^{2(\mathrm{exp})}(Q^2) \leq R_E^2(Q^2)$, if $\epsilon > 0$
    - Lower bound is violated, $R_E^{2(\mathrm{exp})}(Q^2) \nleq R_E^2(Q^2)$ for $Q^2 < Q_0^2$, if $\epsilon < 0$
  - Estimate lower cut with $\epsilon = -0.001$ and $Q_0^2 = \sqrt{\dfrac{-6\ln(1+\epsilon)}{\langle r^4\rangle_E/20 - R_E^4/12}}$

NORMALIZATION UNCERTAINTY

- Normalization of FF data is in general more complicated:
  - MAMI data have 31 (fitted) normalization parameters
  - Different fit of normalization parameters can generate a shift of the data
- Assume a highly-correlated systematic normalization uncertainty:
  - Averaging a dataset $A_i \pm \sigma_i \pm \Delta$ with correlated systematic error Δ, is equivalent to averaging the dataset $A_i \pm \sigma_i'$ with $\sigma_i' = \sigma_i \left(1 + \Delta^2 \sum_j 1/\sigma_j^2\right)^{1/2}$
  - $\Delta = 0.001$ leads to $\sigma_i' \sim 4.5\,\sigma_i$
- Alternatively one can study subsets where the normalization is an overall factor
- Proper error evaluation should use the covariance matrix established in the experimental analysis

DERIVATION OF THE LOWER BOUND

Lower-bound function: $R_E^2(Q^2) = -\frac{6}{Q^2}\log G_E(Q^2)$

DERIVATION OF THE LOWER BOUND

Lower-bound function: $R_E^2(Q^2) = -\dfrac{6}{Q^2} \log G_E(Q^2)$

- $R_E^2(Q^2) \geq 0$, since $G_E(Q^2) \leq 1$

DERIVATION OF THE LOWER BOUND

Lower-bound function: $R_E^2(Q^2) = -\frac{6}{Q^2}\log G_E(Q^2)$

- $R_E^2(Q^2) \geq 0$, since $G_E(Q^2) \leq 1$

Show that $G_E(Q^2) \leq 1$ for $Q^2 \geq 0$:

- $G_E(Q^2) = F_1(Q^2) - \frac{Q^2}{4M^2} F_2(Q^2)$
- $F_2(Q^2) \geq 0$ (empirically known, e.g., $F_2(0) = \kappa$)
- $F_1(Q^2) \leq 1$ follows from positive definiteness of the transverse charge density $\rho_\perp(b) \geq 0$ — since $F_1(0) - F_1(Q^2) = 2\pi \int_0^\infty \mathrm{d}b\, b\, \left[1 - J_0(Qb)\right] \rho_\perp(b) > 0$ with the cylindrical Bessel function $J_0(x) \leq 1$

DERIVATION OF THE LOWER BOUND

Lower-bound function: $R_E^2(Q^2) = -\dfrac{6}{Q^2} \log G_E(Q^2)$

- $R_E^2(Q^2) \geq 0$, since $G_E(Q^2) \leq 1$
- $R_E^2(Q^2)$ falls with increasing Q^2, if G_E falls not faster than by a power law

DERIVATION OF THE LOWER BOUND

Lower-bound function: $R_E^2(Q^2) = -\dfrac{6}{Q^2} \log G_E(Q^2)$

- $R_E^2(Q^2) \geq 0$, since $G_E(Q^2) \leq 1$
- $R_E^2(Q^2)$ falls with increasing Q^2, if G_E falls not faster than by a power law
- $R_E^2(Q^2)$ is monotonic in the space-like region
  - Unsubtracted dispersion relation: $R_E^2(Q^2) = \dfrac{1}{\pi}\displaystyle\int_{4m_pi^2}^{\infty} \mathrm{d}t\, \frac{\mathrm{Im}\, R_E^2(t)}{t+Q^2}$, with

$\mathrm{Im} R_E^2(t) = \dfrac{6\,\varphi_E(t)}{t}$ and $\varphi(t) \geq 0$ is the phase defined through

$G_E(t) = |G_E(t)|\, e^{i\varphi(t)}$

DERIVATION OF THE LOWER BOUND

Lower-bound function: $R_E^2(Q^2) = -\frac{6}{Q^2}\log G_E(Q^2)$

- $R_E^2(Q^2) \geq 0$, since $G_E(Q^2) \leq 1$
- $R_E^2(Q^2)$ falls with increasing Q^2, if G_E falls not faster than by a power law
- $R_E^2(Q^2)$ is monotonic in the space-like region
  - Unsubtracted dispersion relation: $R_E^2(Q^2) = \frac{1}{\pi}\int_{4m_pi^2}^{\infty} \mathrm{d}t\, \frac{\mathrm{Im}\, R_E^2(t)}{t+Q^2}$, with $\mathrm{Im} R_E^2(t) = \frac{6\,\varphi_E(t)}{t}$ and $\varphi(t) \geq 0$ is the phase defined through $G_E(t) = |G_E(t)|\, e^{i\varphi(t)}$
- Limit equals the proton radius: $\lim\limits_{Q^2\to 0} R_E^2(Q^2) = -6\,\frac{G_E'(Q^2)}{G_E(Q^2)}\Big|_{Q^2=0} = R_E^2$

HYPERFINE SPLITTING

Theory: QED, ChPT, data-driven dispersion relations, ab-initio few-nucleon theories

Experiment: HFS in μH, μHe$^+$, …

Testing the theory

- discriminate between theory predictions for polarizability effect
  - disentangle R_Z & polarizability effect by combining HFS in H & μH
- test HFS theory
  - combining HFS in H & μH with theory prediction for polarizability effect
- test nuclear theories

Interpreting the exp.

extract E^{TPE}, $E^{\text{pol.}}$ or R_Z

Guiding the exp.

find narrow 1S HFS transitions with the help of full theory predictions: QED, weak, finite size, polarizability

Determine fundamental constants

Zemach radius R_Z

Input for data-driven evaluations

form factors, structure functions, polarizabilities

Spectroscopy of ordinary atoms (H, He$^+$)

Electron and Compton Scattering

PLITTING

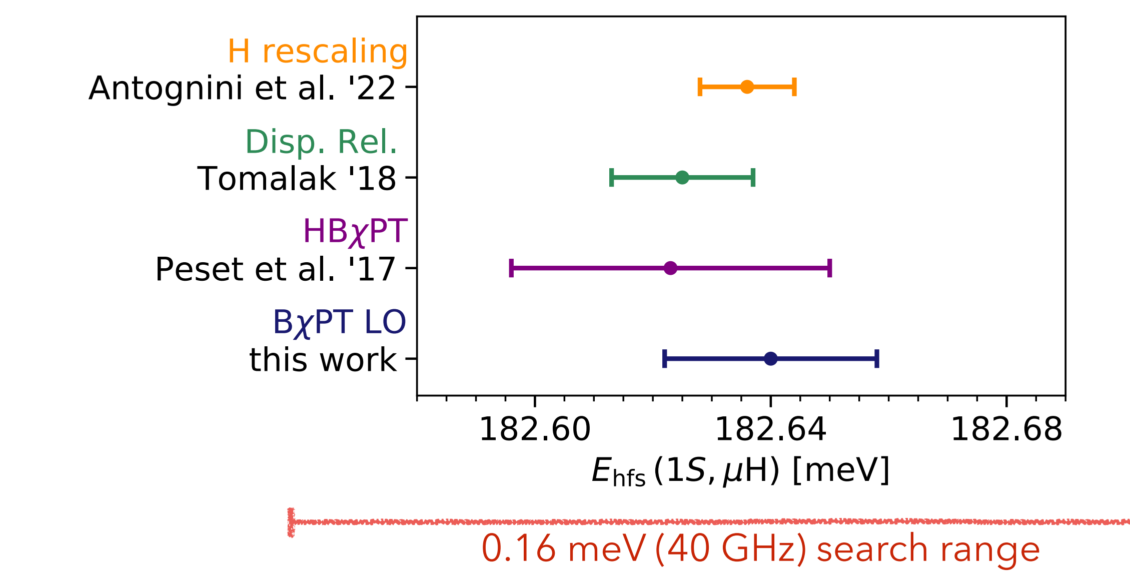

Predictions for the 1S HFS in μH are driven by the 1S HFS in H

A. Antognini, FH, V. Pascalutsa, Ann. Rev. Nucl. Part. **72** (2022)

Experiment: HFS in μH, μHe$^+$, …

Guiding the exp.

find narrow 1S HFS transitions with the help of full theory predictions: QED, weak, finite size, polarizability

Interpreting the exp.

extract $E^{\rm TPE}$, $E^{\rm pol.}$ or R_Z

Input for data-driven evaluations

form factors, structure functions, polarizabilities

esting the theory

inate between theory predictions for polarizability effect

- disentangle R_Z & polarizability effect by combining HFS in H & μH

- test HFS theory
  - combining HFS in H & μH with theory prediction for polarizability effect
- test nuclear theories

Determine fundamental constants

Zemach radius R_Z

Spectroscopy of ordinary atoms (H, He$^+$)

Electron and Compton Scattering

HYPERFINE SPLITTING

The hyperfine splitting of μH (theory update):

A. Antognini, FH, V. Pascalutsa, Ann. Rev. Nucl. Part. **72** (2022)

$$E_{1S\text{-hfs}} = \Big[\underbrace{182.443}_{E_F} \underbrace{+1.350(7)}_{\text{QED+weak}} \underbrace{+0.004}_{\text{hVP}} \underbrace{-1.30653(17)\left(\frac{r_{Zp}}{\text{fm}}\right) + E_F\left(1.01656(4)\,\Delta_{\text{recoil}} + 1.00402\,\Delta_{\text{pol}}\right)}_{2\gamma \text{ incl. radiative corr.}}\Big]\,\text{meV}$$

Guiding the exp.

find narrow 1S HFS transitions with the help of full theory predictions: QED, weak, finite size, polarizability

Interpreting the exp.

extract E^{TPE}, $E^{\text{pol.}}$ or R_Z

Input for data-driven evaluations

form factors, structure functions, polarizabilities

- discriminate between theory predictions for polarizability effect
    - disentangle R_Z & polarizability effect by combining HFS in H & μH
- test HFS theory
    - combining HFS in H & μH with theory prediction for polarizability effect
- test nuclear theories

Determine fundamental constants

Zemach radius R_Z

Spectroscopy of ordinary atoms (H, He^+)

Electron and Compton Scattering

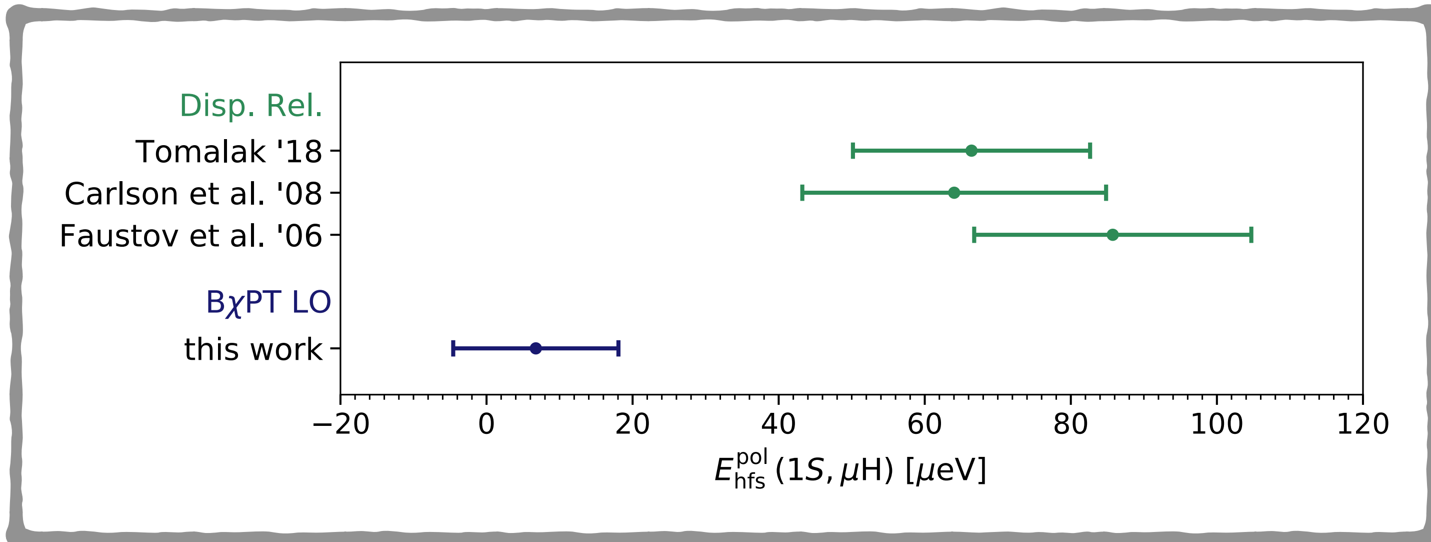

PLITTING

Experiment: HFS in μH, μHe$^+$, …

Testing the theory

- **discriminate between theory predictions for polarizability effect**
  - disentangle R_Z & polarizability effect by combining HFS in H & μH
- test HFS theory
  - combining HFS in H & μH with theory prediction for polarizability effect
- test nuclear theories

Determine fundamental constants

Zemach radius R_Z

Interpreting the exp.

extract E^{TPE}, $E^{\mathrm{pol.}}$ or R_Z

Guiding the exp.

find narrow 1S HFS transitions with the help of full theory predictions: QED, weak, finite size, polarizability

Input for data-driven evaluations

form factors, structure functions, polarizabilities

Spectroscopy of ordinary atoms (H, He$^+$)

Electron and Compton Scattering

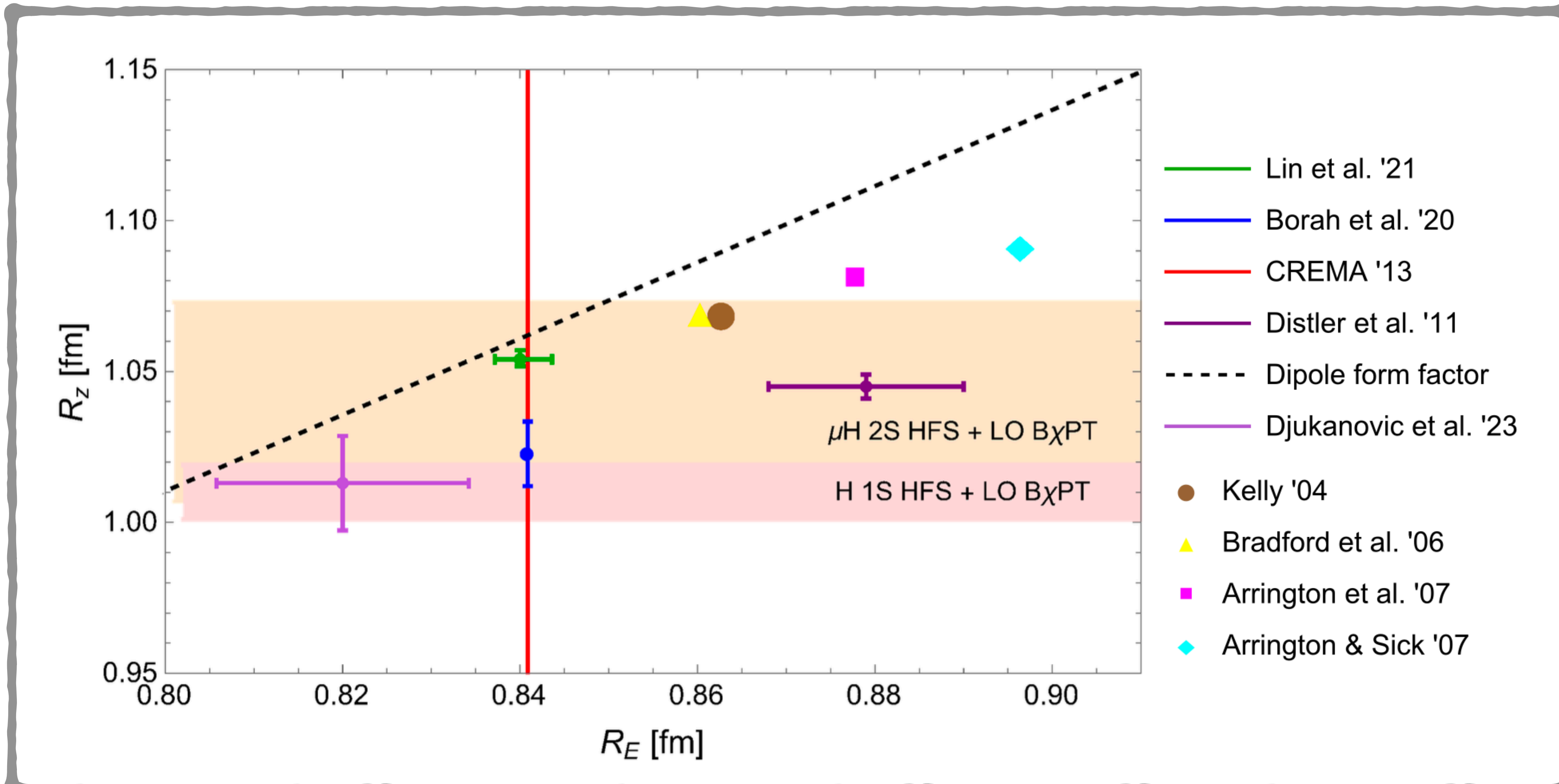

, μHe$^+$, …

Determine fundamental constants

Zemach radius R_Z

transitions with the help of full theory predictions: QED, weak, finite size, polarizability

Input for data-driven evaluations
form factors, structure functions, polarizabilities

combining HFS in H & μH
- test HFS theory
  - combining HFS in H & μH with theory prediction for polarizability effect
- test nuclear theories

Spectroscopy of ordinary atoms (H, He$^+$)

Electron and Compton Scattering

POLARIZABILITY EFFECT FROM BCHPT

- LO BChPT result is compatible with zero
  - Contributions from σ_{LT} and σ_{TT} are sizeable and largely cancel each other

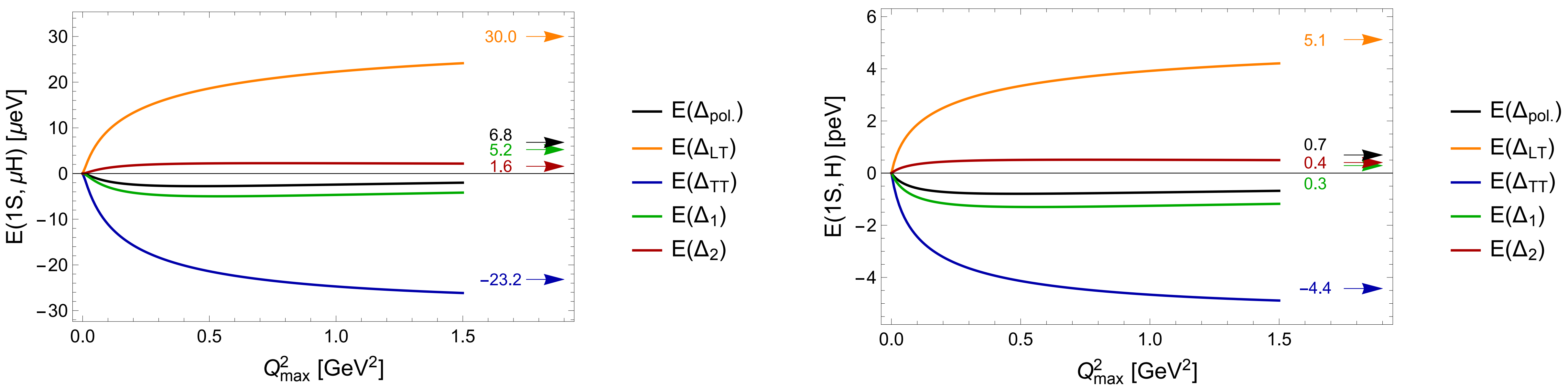

- Are the data-driven evaluations/uncertainties affected by cancelations?
- Scaling with lepton mass of the lepton-proton bound state

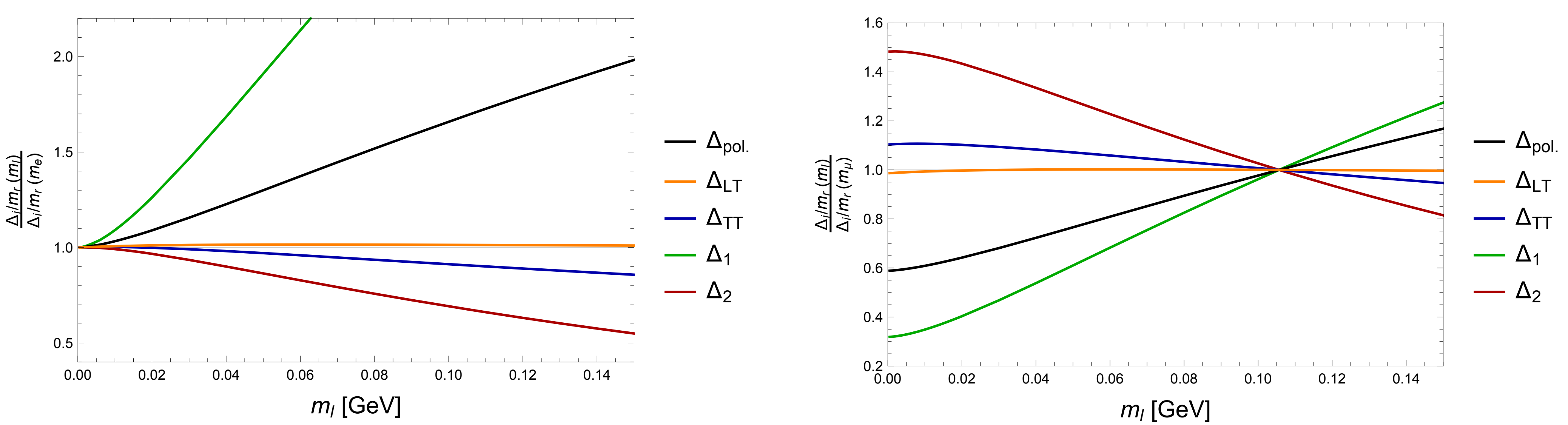

DATA-DRIVEN EVALUATION

- Empirical information on spin structure functions from JLab Spin Physics Programme

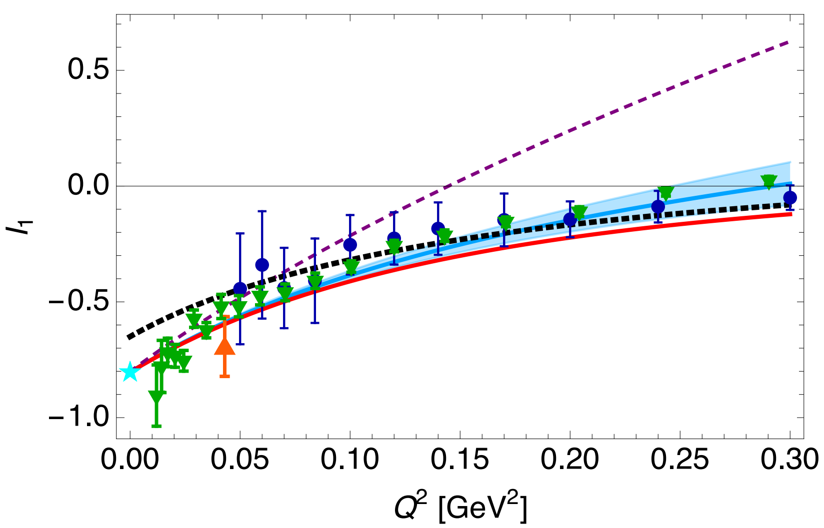

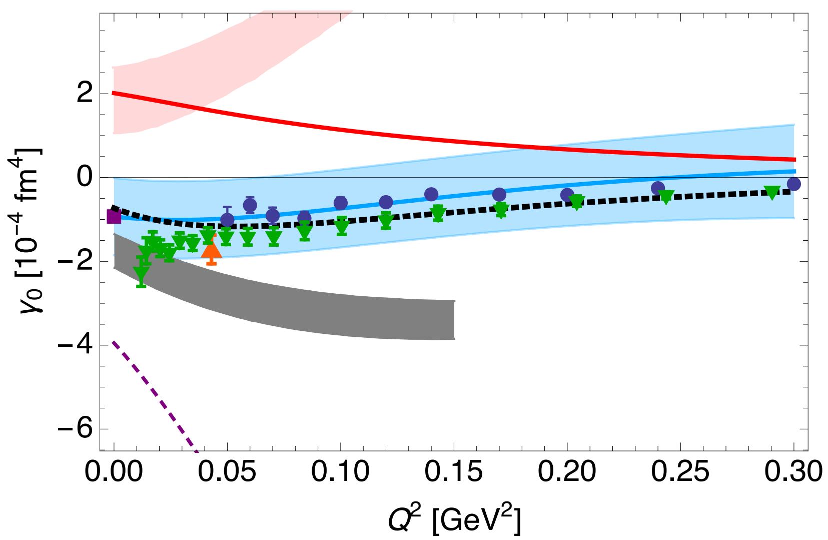

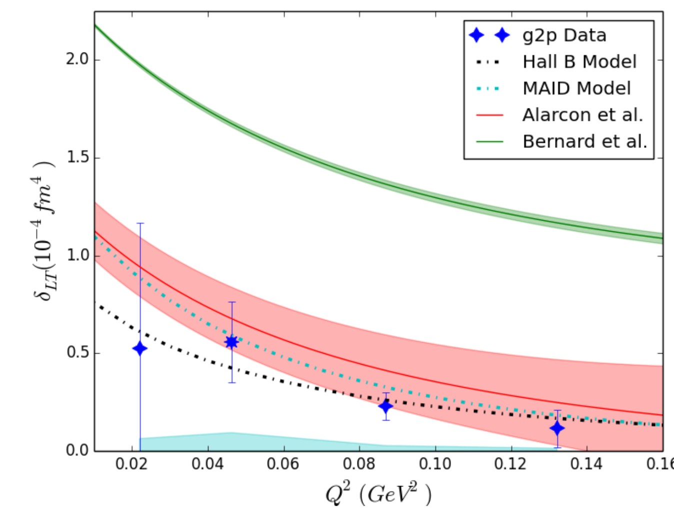

- Low-Q region is very important → cancelation between $I_1(Q^2)$ and $F_2(Q^2)$

$$\delta_1(\text{H}) \sim \left(\underbrace{-\frac{3}{4}\kappa^2 r^2_{\text{Pauli}}}_{\to -2.19} + \underbrace{18M^2 c_{1B}}_{\to 3.54}\right) Q^2_{\max} = 1.35(90),$$

$$\delta_1(\mu\text{H}) \sim \left[\underbrace{-\frac{1}{3}\kappa^2 r^2_{\text{Pauli}}}_{\to -1.45} + \underbrace{8M^2 c_1}_{\to 2.13} \underbrace{-\frac{M^2}{3\alpha}\gamma_0}_{\to 0.18}\right] \int_0^{Q^2_{\max}} \mathrm{d}Q^2 \beta_1(\tau_\mu) = 0.86(69)$$